



**LEYDIANE DE OLIVEIRA PEREIRA**

**PRODUCTION OF MAGNETIC PHOTOCATALYSTS AND  
THEIR APPLICATION IN PHOTOCATALYTIC REACTIONS**

**LAVRAS-MG**

**2019**

**LEYDIANE DE OLIVEIRA PEREIRA**

**PRODUCTION OF MAGNETIC PHOTOCATALYSTS AND THEIR APPLICATION  
IN PHOTOCATALYTIC REACTIONS**

Tese apresentada à  
Universidade Federal de  
Lavras, como parte das  
exigências do Programa de  
Pós-Graduação em  
Agroquímica, para a obtenção  
do título de Doutora.

Prof. Dr. Fabiano Magalhães  
Orientador  
Prof. Dr. Jonas Leal Neto  
Co-orientador  
Profª. Dra. Iara do Rosário Guimarães Carvalho  
Co-orientadora

**LAVRAS-MG**

**2019**

**Ficha catalográfica elaborada pelo Sistema de Geração de Ficha Catalográfica da Biblioteca  
Universitária da UFLA, com dados informados pelo(a) próprio(a) autor(a).**

Pereira, Leydiane de Oliveira.

Production of magnetic photocatalysts and their application in  
photocatalytic reactions / Leydiane de Oliveira Pereira. - 2019.

84 p. : il.

Orientador(a): Fabiano Magalhães.

Coorientador(a): Iara do Rosário Guimarães Carvalho, Jonas  
Leal Neto.

Tese (doutorado) - Universidade Federal de Lavras, 2019.

Bibliografia.

1. Fotocatalisadores magnéticos. 2. Sacarose. 3. Carvão  
ativado. I. Magalhães, Fabiano. II. Carvalho, Iara do Rosário  
Guimarães. III. Neto, Jonas Leal. IV. Título.

**LEYDIANE DE OLIVEIRA PEREIRA**

**PRODUÇÃO DE FOTOCATALISADORES MAGNÉTICOS E SUA APLICAÇÃO EM  
REAÇÕES FOTOCATALÍTICAS**

**PRODUCTION OF MAGNETIC PHOTOCATALYSTS AND THEIR APPLICATION  
IN PHOTOCATALYTIC REACTIONS**

Tese apresentada à  
Universidade Federal de  
Lavras, como parte das  
exigências do Programa de  
Pós-Graduação em  
Agroquímica, para a obtenção  
do título de Doutora.

APROVADA em 29 de março de 2019.

Dra. Juliana Cristina Tristão	UFV
Dr. Márcio Pozzobon Pedroso	UFLA
Dra. Maria Lucia Bianchi	UFLA
Dr. Mário César Guerreiro	UFLA

Prof. Dr. Fabiano Magalhães  
Orientador  
Prof. Dr. Jonas Leal Neto  
Co-orientador  
Profa. Dra. Iara do Rosário Guimarães Carvalho  
Co-orientadora

**LAVRAS-MG**

**2019**

*To my mother for love, encouragement, and example.*

I DEDICATE

## ACKNOWLEDGEMENTS

Firstly, I would like to thank Jesus for being my constant friend and for allowing me to win this dream, always giving me strength and discernment for the best choices.

To my mother, for always encouraging me to study and for giving me all the conditions to finish this stage.

To my father for, the prayers and presence at this stage.

To my dear stepfather, André, for the support and help, giving me conditions to stay on this path.

To my brother, Yan, for cheering moments of my life with sweetness.

To my supervisor and friend Prof. Fabiano, for many years of knowledge, always with patience, support, and trust. I will be eternally grateful for all the teaching and friendship.

To Alan, for the companionship, encouragement, advices, and for always believing in me, making my days happier.

To my lab friends, Evanise, Camila, Kassiana, Cris, Pedro, Lara, Mayara, and Samantha, who made this walk lighter and more cheerful, and for helping me at all times. In particular, I thank Isabela, for helping me in the accomplishment of this work.

To my dear Bic Júnior student, Luana, who contributed to the realization of the experiments, always working with good will and joy, and who cultivated in me a sweet friendship and eternal gratitude.

To my dear professors of the Department of Chemistry, who have accompanied me since graduation and have contributed in a very significant way to my professional and personal growth, and for the valuable contributions with this work, in particular, Iara, Malu, Jaqueline, Graça, and Jonas.

I would like to thank my thesis committee members for all of their guidance, Juliana Tristão, Mario C. Guerreiro, Márcio Pozzobon and Maria L. Bianch.

To my heart sister, Nathália, for being always by my side, supporting me and giving me strength to face the battles of life, and for always guaranteeing my smiles.

To all my friends, who make my walk of life lighter and happier, especially, Juliana, and Raphael.

The NEPE family, who since from the beginning welcomed me with a lot of tenderness, replenishing my energies to face the obstacles of life.

To my dear evangelizers, Michelle and Simone, for love and hospitality.

To the professors Luiz Carlos Alves Oliveira (UFMG), Rochel Monteiro Lago (UFMG), Eduardo Tonon de Almeida (Unifal-MG), Antonio Carlos Doriguetto (Unifal-MG), Adelir Aparecida Saczk (UFLA), Luiz Roberto Guimarães Guilherme (UFLA), for making available equipment and laboratories to carry out the analyzes for characterization of the samples.

To the friends and technicians who helped me in carrying out the analyzes, especially, Ricardo, Sara, Lidiane and Franciane.

To the University of Lavras, to the Department of Chemistry, CAPQ and, in particular, to the post-graduation program Agroquímica, for the opportunity.

To CNPq for the grant of the Doctorate scholarship FAPEMIG, and CAPES.

To the Laboratory of Crystallography and to the Interdisciplinary Chemistry Laboratory of UNIFAL, and to the Group of Environmental Technologies of UFMG, for analyzes.

Finally, to all who have contributed in some way to the execution of this work, my sincere thanks.

This study was financed in part by the Coordenação de Aperfeiçoamento de Pessoal de Nível Superior – Brasil (CAPES) – Finance Code 001.

*“Science is Love that investigates.”*

André Luiz



## RESUMO

Diversos estudos têm sido realizados para a degradação eficiente de contaminantes orgânicos recalcitrantes presentes em efluentes industriais. A fotocatalise heterogênea surge como uma boa alternativa para o tratamento destes efluentes. O semicondutor mais utilizado na fotocatalise é o  $\text{TiO}_2$  P25 devido sua alta eficiência e outras vantagens. No entanto, uma de suas limitações é o pequeno tamanho de suas partículas, fazendo com que sua separação do efluente tratado seja difícil. Para contornar este problema, uma alternativa é associar este semicondutor com uma fase magnética, onde o fotocatalisador pode ser facilmente separado do efluente tratado pela ação de um campo magnético. Diversos autores relatam que é necessária uma camada para evitar o contato físico do  $\text{TiO}_2$  e o ferro, uma vez que o contato destes pode reduzir a atividade fotocatalítica. Sendo assim, neste trabalho foram obtidos os fotocatalisadores magnéticos, Ti/Fe/AC e Ti/C/Fe, onde  $\text{TiO}_2$ -P25 (Ti) foi imobilizado na superfície de dois suportes distintos: (i) Fe/AC – partículas de  $\text{Fe}_3\text{O}_4$  disperso na superfície de carvão ativado comercial (AC) e ii) C/Fe – partículas de  $\text{Fe}_3\text{O}_4$  e  $\text{Fe}_3\text{C}$  revestidas com carvão (C) (configuração core-shell) obtido a partir da decomposição térmica da sacarose. Estes fotocatalisadores foram obtidos com os seguintes teores de  $\text{TiO}_2$ : 20, 40 e 60%, caracterizados e utilizados para degradação do preto remazol 5 (RB5), acetaminofeno e fenol na presença de radiação UV. Os resultados obtidos foram divididos em dois artigos. O primeiro apresenta os resultados obtidos com os fotocatalisadores 20, 40 e 60Ti/Fe/AC (os números indicam o teor de  $\text{TiO}_2$ ) para a degradação do corante preto remazol (RB5). Os resultados de caracterização comprovaram que as partículas de  $\text{TiO}_2$  estão presentes na superfície do suporte Fe/AC, e que este é constituído de magnetita, carbono amorfo e grafítico. Medidas de área superficial BET mostraram uma redução de 283 a 165  $\text{m}^2\text{g}^{-1}$  com o aumento de  $\text{TiO}_2$  suportado. Os testes de sedimentação mostraram que após 30 minutos na presença de campo magnético, a turbidez da mistura fotocatalisador/água reduziu até 93%. A eficiência fotocatalítica dos materiais obtidos aumentou com o teor de  $\text{TiO}_2$ , chegando a reduzir 95% de sua coloração e 90% do carbono orgânico total. No segundo artigo os resultados de caracterização dos fotocatalisadores 20, 40 e 60Ti/C/Fe comprovaram a formação das fases magnéticas,  $\text{Fe}_3\text{C}$  e  $\text{Fe}_3\text{O}_4$ , as quais estão revestidas por carvão amorfo e grafítico. Imagens de microscopia eletrônica de varredura mostraram que partículas de  $\text{TiO}_2$  também estão na superfície do C/Fe. A cinética de sedimentação dos fotocatalisadores mostrou eficiência de 76 a 89 % em apenas 30 minutos na presença de campo magnético, enquanto os testes com  $\text{TiO}_2$  não foram significativos. Os fotocatalisadores apresentaram alta capacidade para degradação do RB5, acetaminofeno e fenol em solução aquosa, sendo que a amostra 60Ti/C/Fe degradou 99, 77, 90% destes três contaminantes, respectivamente. Ao comparar os fotocatalisadores 60Ti/Fe/AC e o 60Ti/C/Fe, nota-se que estes descoloriram 95 e 99% do corante BR5, respectivamente, comprovando que ambos materiais apresentaram boa eficiência fotocatalítica. Sendo assim, pode-se concluir que todos os materiais preparados neste trabalho apresentaram excelente eficiência fotocatalítica, grande facilidade na separação do meio reacional, o que simplifica sua aplicação e reduz custos operacionais. Estes fatores indicam o alto potencial destes materiais para aplicação em maiores escalas.

**Palavras-chave:** Fotocatalisador magnético. Sacarose.  $\text{TiO}_2$ . Degradação. Carvão Ativado.

## ABSTRACT

Many studies have been carried out to assess the efficient degradation of recalcitrant organic contaminants present in industrial effluents. Heterogeneous photocatalysis appears as a good alternative for the treatment of these effluents. The most used semiconductor in photocatalysis is TiO<sub>2</sub> P25, due to its high efficiency and other advantages. However, one of its limitations is the small size of its particles, making difficult its separation from the treated effluent. To overcome this problem, an alternative is to associate this semiconductor with a magnetic phase, where the photocatalyst can be easily separated from the treated effluent by the action of a magnetic field. Several authors reported that a layer is needed to avoid the physical contact of TiO<sub>2</sub> and iron, since the contact of these can reduce the photocatalytic activity. In this study, Ti/Fe/AC and Ti/C/Fe, where TiO<sub>2</sub>-P25 (Ti) was immobilized on the surface of two different substrates: (i) Fe/AC - Fe<sub>3</sub>O<sub>4</sub> particles dispersed on the surface of commercial activated carbon (AC) and ii) Fe/C - Fe<sub>3</sub>O<sub>4</sub> and Fe<sub>3</sub>C particles coated with charcoal (C) (core-shell configuration), which was obtained from thermal decomposition of sucrose. These photocatalysts were obtained with the following TiO<sub>2</sub> contents: 20, 40, and 60%, characterized and used for the degradation of remazol black 5 (RB5), acetaminophen, and phenol in the presence of UV radiation. The results obtained were divided into two articles. The first one presents the results obtained with the photocatalysts 20, 40, and 60Ti/Fe/AC (the numbers indicate the TiO<sub>2</sub> content) for the degradation of black remazol dye (RB5). The characterization results showed that TiO<sub>2</sub> particles are present on the surface of the Fe/AC support, and that it consists of magnetite, amorphous carbon, and graphite. BET surface area reduced from 283 to 165 m<sup>2</sup> g<sup>-1</sup>, with the increase of TiO<sub>2</sub> supported. The sedimentation tests showed that after 30 minutes in the presence of magnetic field, the turbidity of the photocatalyst/water mixture reduced up to 93%. The photocatalytic efficiency of the obtained materials increased with the TiO<sub>2</sub> content, reducing 95% of its coloration and 90% of the total organic carbon. In the second article, the characterization results of the photocatalysts 20, 40, and 60Ti/C/Fe proved the formation of the magnetic phases, Fe<sub>3</sub>C and Fe<sub>3</sub>O<sub>4</sub>, which are coated with amorphous and graphitic charcoal. Scanning electron microscopy images showed that TiO<sub>2</sub> particles are also present on the C/Fe surface. The sedimentation kinetics of the photocatalysts showed efficiency of 76 to 89% in only 30 minutes in the presence of magnetic field, while the TiO<sub>2</sub> tests were not significant. The photocatalysts showed high capacity for degradation of RB5, acetaminophen, and phenol in aqueous solution, and the 60Ti/Fe/C sample degraded 99, 77, and 90% of these three contaminants, respectively. Comparing the 60Ti/Fe/AC and 60Ti/C/Fe photocatalysts, they discolored 95 and 99% of the BR5 dye, respectively, proving that both materials showed good photocatalytic efficiency. Thus, it can be concluded that all materials prepared in this work presented excellent photocatalytic efficiency and great ease in the separation of the reaction medium, which simplifies its application and reduces operational costs. These factors indicate the high potential of these materials for large-scale applications.

**Keywords:** Magnetic photocatalyst. Sucrose. TiO<sub>2</sub>. Degradation. Activated carbon.

## SUMMARY

<b>FIRST PART</b> .....	<b>1</b>
<b>1 INTRODUCTION</b> .....	<b>1</b>
<b>2 LITERATURE REVIEW</b> .....	<b>2</b>
<b>2.1 Environmental Pollution</b> .....	<b>2</b>
<b>2.2 Dyes</b> .....	<b>2</b>
<b>2.3 Acetaminophen</b> .....	<b>5</b>
<b>2.4 Phenol</b> .....	<b>6</b>
<b>2.5 Conventional Treatments</b> .....	<b>7</b>
<b>2.6 Advanced oxidation process</b> .....	<b>7</b>
<b>2.6.1 Fenton</b> .....	<b>8</b>
<b>2.6.2 Ozonolysis</b> .....	<b>9</b>
<b>2.6.3 Photolysis</b> .....	<b>9</b>
<b>2.6.4 Photocatalysis</b> .....	<b>10</b>
<b>2.6.5 TiO<sub>2</sub> applied to photocatalysis</b> .....	<b>11</b>
<b>3 FINAL CONSIDERATIONS</b> .....	<b>14</b>
<b>4 REFERENCES</b> .....	<b>15</b>
<b>SECOND PART</b> .....	<b>24</b>
<b>ARTICLE 1</b> .....	<b>24</b>
<b>ARTICLE 2</b> .....	<b>47</b>

## FIRST PART

### 1 INTRODUCTION

Currently, a serious problem of society is the pollution of water by industrial effluents, contaminating it with a variety of organic and inorganic compounds that are recalcitrant to the environment (AKHTAR et al., 2016).

An alternative that has been investigated is the treatment of these effluents using photocatalysis, which is a very efficient technique for the degradation of organic contaminants. Photocatalysis is based on the generation of hydroxyl radicals through the activation of a semiconductor, in which these radicals can mineralize a variety of organic compounds environment (SOPHA et al., 2018).

Among the studied semiconductors, TiO<sub>2</sub> has been highlighted due to its high efficiency, low cost, non-toxicity, and chemical, thermal, and mechanical stability (LUO et al., 2015). However, it is difficult to separate this oxide from the treated effluent (BORGES et al., 2016).

Several studies in the literature investigate the following alternatives to simplify and/or facilitate the process of separation of the treated solution. They are: (i) immobilizing TiO<sub>2</sub> on the walls of the photoreactor (MANASSERO; SATUF; ALFANO, 2017); (ii) impregnating the glass surface with TiO<sub>2</sub> (SUN et al., 2016); (iii) obtaining floating photocatalysts by the impregnation of TiO<sub>2</sub> on the surface of low density supports (less than 1 g cm<sup>-3</sup>), (MAGALHÃES; MOURA; LAGO, 2011) and (iv) obtaining magnetic photocatalysts (NADIMI et al., 2018; WEI; WANG, 2018; SHI et al., 2018; LI; WU, 2017). The latter can be separated from the reaction medium by the simple application of a magnetic field and, subsequently, the photocatalyst can be reused. In this way, the separation step of the effluent catalyst is simplified, which normally involves the use of centrifuges, filtrations, and/or addition of chemical reagents, such as flocculants. These steps increase operating costs for effluent treatment. On the other hand, the magnetic photocatalyst can be simply and quickly separated from the medium. This type of material can be obtained by the immobilization of TiO<sub>2</sub> particles on the magnetic support surface.

Several magnetic holders can be used (eg.: Fe, FeO, Fe<sub>3</sub>O<sub>4</sub>, Fe<sub>3</sub>C, and δ-FeOOH) to obtain magnetic photocatalysts. In this work, magnetite, which is abundant in nature and of low cost, was used as magnetic holder.

Thus, in this work, two magnetic supports were prepared and used to obtain the magnetic photocatalysts. A support was prepared by coating magnetite with a layer of carbon obtained

from the sucrose, forming the magnetic support (C/Fe). The other support was produced using activated carbon impregnated with magnetite (Fe/AC). On the surface of these materials, TiO<sub>2</sub> particles were added, and two types of magnetic photocatalysts were obtained: Ti/C/Fe and Ti/Fe/AC.

## **2 LITERATURE REVIEW**

### **2.1 Environmental Pollution**

One of the main challenges to sustaining modern society is obtaining quality water resources for various uses. The need for wastewater treatment has increased in recent decades as a way to protect the environment as well as human health (CARDOSO; BESSEGATO; BOLDRIN ZANONI, 2016; ESCUDERO et al., 2017).

Industrial effluent contains a wide variety of organic and inorganic contaminants. Some of these pollutants are toxic and recalcitrant, persisting in the environment and posing a lifelong threat (AKHTAR et al., 2016; ARAÚJO et al., 2016).

Dyes, phenols, and acetaminophen are organic and recalcitrant pollutants commonly found in the environment due to the disposal of effluents from different industries. Due to the presence of aromatic compounds, these contaminants may cause adverse effects on human health and the environment, when found in environmental (SUN et al., 2018; ŽUR et al., 2018).

The textile dye, reactive black 5 (BR5), phenol, and acetaminophen, were chosen as contaminant models for this study. According to several authors, conventional wastewater treatment plants are not totally effective in removing these pollutants present in the aqueous medium. Thus, to avoid the accumulation of these compounds in the environment, several research groups use photocatalysis to mineralize these contaminants or even to form compounds that are less toxic than the initials (PERIYASAMY; MUTHUCHAMY, 2018; IQBAL; NISAR, 2015; EKKA et al., 2018).

### **2.2 Dyes**

Dyes are organic compounds with a complex aromatic molecular structure that can bring color to other materials (CARDOSO et al., 2011). Dye molecules have two main components: chromophores, which are responsible for the color production, and auxochromes, which, in

addition to complementing the chromophore, make the molecule soluble in water and increase affinity with tissues (EL BOURAIE; EL DIN, 2016).

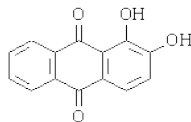
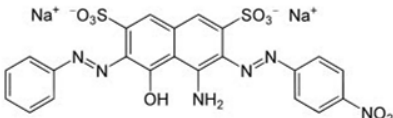
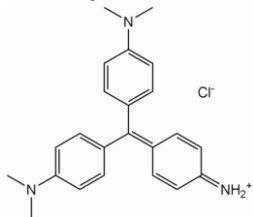
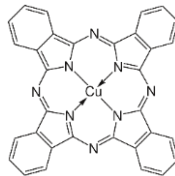
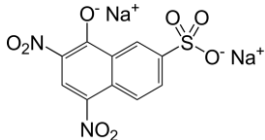
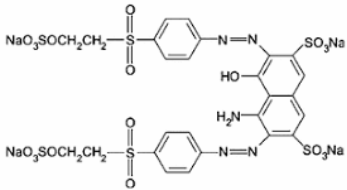
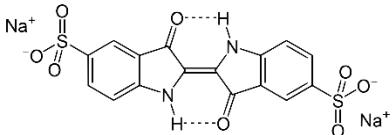
However, the complex molecular structures of dyes make them more stable and difficult to biodegrade (CARDOSO et al., 2011). Therefore, dyes represent a serious environmental hazard because when discarded in the water body, in addition to causing cosmetic problems leaving the water colored, they can block the penetration of sunlight and the dissolution of oxygen that is essential for aquatic life (KHOSRAVI; AZIZIAN, 2014).

Dyes can be classified according to their chemical structure or their method of application. The classification by application is the main system adopted by the International Color Index due to the complexity of the chemical structures present in the dyes (HERBST; HUNGER, 2002). Table 1 shows the classes of dyes used in the textile industry according to their application methods and the name of the chemical structures present in each class.

Nearly 45% of all textile dyes produced annually belong to the reactive class, as it is widely used for the staining of cellulose and viscose fibers. Reactive dyes have been identified as problematic compounds in textile wastewater, since they are found in higher concentrations than other classes of dyes and cannot be easily removed by conventional treatment systems such as physical and biological treatments (AKSU; AKIN, 2010).

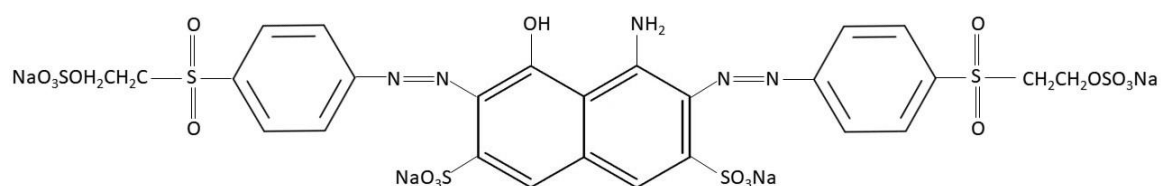
Reactive dyes form covalent bonds with textile fibers and are generally based on azo chromophores combined with different types of chemical structures present in the reactive class. Azo reactive dyes are characterized by the presence of one or more azo groups (-N=N-), presenting a bright color and excellent color stability. Approximately 60 to 70% of the dyes used in the textile industries are those containing the azo chemical structure (SAHEL et al., 2007).

Table 1 - Classes of dyes according to their application methods and the name of the structures present in each class.

Class	Function present	Example of dyes
Acid	Azo (including metallized), anthraquinone, triphenylmethane, azine, xanthene, nitro and nitrous.	<b>Alizarin</b>
		
Azoic	Azo.	<b>Starch black</b>
		
Basic	Cyanine, diphenylmethane, triarylmethane, azo, azine, xanthene, acridine, oxazine, and anthraquinone.	<b>Methyl violet 2B</b>
		
Directs	Azo, phthalocyanine, stilbene, and oxazine.	<b>Phthalocyanine BN blue</b>
		
Dispersive	Azo, anthraquinone, nitro, and benzodifuranone.	<b>Yellow Naphthol S</b>
		
Reactive	Azo, anthraquinone, phthalocyanine, formazan, oxazine, and basic.	<b>Black Remazol 5</b>
		
Vat dyes	Anthraquinone (including polycyclic quinones) and indigoids.	<b>Indigo Carmine</b>
		

Reactive Black 5 or Black Remazol BR5 (Color Index: 20505) stands out among the azo reactive dyes. It is one of the most common synthetic dyes in the textile industry, being the most used for coloring cotton and other fibers (EL BOURAIE; EL DIN, 2016). BR5 was selected as the model compound in this work. Figure 1 shows the structure of the BR5.

Figure 1 - Structure of the dye BR5.

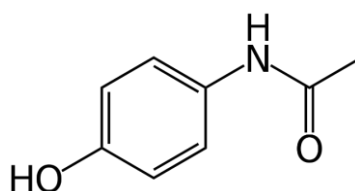


The treatment of effluents from the textile industry to completely remove dyes is a challenging task that has received a lot of attention in recent years, since many dyes are difficult to degrade because of their complex and stable structure. Various methods have been applied for discoloration of textile dyes and conventional systems are considered inefficient in the removal of these dyes (IQBAL; NISAR, 2015).

### 2.3 Acetaminophen

Acetaminophen (N-acetyl-4-aminophenol) is the active principle of analgesic paracetamol, which is an antipyretic drug, which is widely used in treatment to relieve muscle pain, chronic pain from cancer, pain due to tension headache and migraine headache, toothache, back pain, neuralgia, joint pain, and fever in adults and children (PERIYASAMY; MUTHUCHAMY, 2018; WANGFUENKANAGUL; CHAILAPAKUL, 2002; JAGANNATHAN; GRIESER; ASHOKKUMAR, 2013; ŽUR et al., 2018). Figure 2 shows the structure of the acetaminophen.

Figure 2 - Structure of the acetaminophen.





Since paracetamol is a widely used product, it is constantly released into industrial pharmaceutical effluents, excreta, and hospital waste. As a consequence, the environmental contamination by paracetamol occurs, being found in several environmental matrices, such as drink water, soil, and sediments (JAGANNATHAN; GRIESER; ASHOKKUMAR, 2013; ŽUR et al., 2018).

Although the detected concentration of this contaminant ranges from  $\text{ng L}^{-1}$  to  $\mu\text{g L}^{-1}$ , this substance accumulates in the environment, representing a concern since these values may cause a negative effect on living organisms, becoming a threat to environment (ŽUR et al., 2018; PERIYASAMY; MUTHUCHAMY, 2018).

It is necessary to develop new materials and technologies to avoid accumulation of this compound in the environment, since acetaminophen presents a complex molecular structure and conventional treatments of waste water are not efficient for their complete degradation (HERNÁNDEZ et al., 2018). Therefore, several research groups have used the advanced oxidative processes to treat industrial effluents containing paracetamol (PERIYASAMY; MUTHUCHAMY, 2018).

## 2.4 Phenol

Phenol is a white to colorless solid with a characteristic odor. Phenolic compounds are widely used in organic synthesis and in different industries, including petroleum refining, paints, pesticides, plastics, fertilizers, dyes, surfactants, explosives, and rubbers, among others. (DUAN et al., 2018; RAZA et al., 2018). Therefore, these compounds are discarded in wastewater, and due to their high solubility in water ( $8.28 \text{ g } 100 \text{ mL}^{-1}$ ), they can persist in high concentration in aquatic environments (DUAN et al., 2018).

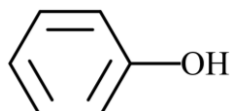
Phenol has low biodegradability which can harm aquatic organisms as well as human health. Phenol-containing wastewater can contaminate drinking water sources, and even at low concentration ( $5 \mu\text{g g}^{-1}$ ), it can cause odor and unpleasant taste (MAO et al., 2019; WANG; YU, 2013).

In addition, effluents contaminated with phenol can be carcinogenic, teratogenic, and mutagenic, influencing the reproduction and growth of aquatic species (EKKA et al., 2018).

Considering the threat caused by phenol, its complete degradation becomes an important task for researchers. To avoid depreciation of water quality and risks to public health, industrial effluents containing phenol must be treated before being released into the environment (SABLE et al., 2018).

Phenol has a benzene ring that (Figure 3) is difficult to be degraded in smaller inorganic molecules using common methods. In addition, during its oxidation, hydroquinone and benzoquinone are formed; those compounds present toxicities superior to those of phenol itself (EKKA et al., 2018; LIU et al., 2013).

Figure 3- Structure of the phenol.



Thus, an efficient degradation method is required to mineralize this contaminant, and advanced oxidative processes appear as a good alternative.

## 2.5 Conventional Treatments

Several methods for the treatment of textile effluents have been presented in the literature, and are generally divided into chemical, physical, and biological processes.

Physical methods such as sedimentation, decantation, filtration, and adsorption are widely used; however, they generate solid waste that requires further treatment (CARDOSO; BESSEGATO; BOLDRIN ZANONI, 2016). Biological processes, which include aerobic, anaerobic, and combinations of these two, are generally slower, requiring large areas of storage; however, they are not always efficient at removing full color (MALPASS et al., 2007). Chemical processes are generally simpler in their application and most of them rely on the formation of an oxidizing agent (CARDOSO; BESSEGATO; BOLDRIN ZANONI, 2016).

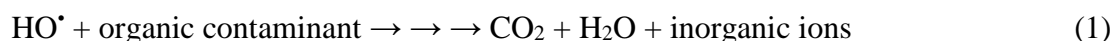
According to Kunz e Peralta-Zamora (2002), the most used process in the textile industry is the precipitation-coagulation, followed by the biological process with activated sludge. This system removes approximately 80% of the dyes. However, due to the high content of dyes adsorbed in the sludge, it is not possible to reuse them, generating a secondary residue.

Thus, advanced oxidative processes (AOPs) appear as a promising approach for the treatment of textile effluents, since they can mineralize the organic contaminant, forming CO<sub>2</sub>, H<sub>2</sub>O, and inorganic ions.

## 2.6 Advanced oxidation process

Advanced oxidation process (AOPs), which are considered clean technologies for the treatment of polluted waters, are based on the production of hydroxyl radicals (HO<sup>•</sup>). The

process is highly reactive ( $E^0 = 2.80V$ ) and slightly selective species, which have the capacity to mineralize a variety of organic compounds, obtaining  $CO_2$ ,  $H_2O$ , and inorganic ions as final products (Equation 1) (RIBEIRO et al., 2015; TOKUMURA et al., 2016).



AOPs include a number of efficient technologies for treating water, which can apply ultraviolet (UV) radiation, ozone ( $O_3$ ), hydrogen peroxide ( $H_2O_2$ ), and iron, among others. Some of the most typical AOPs are the process of Ozonolysis, Photolysis, Fenton, and Photocatalysis (RIBEIRO et al., 2015).

### 2.6.1 Fenton

The Fenton process consists of the combination of iron (II) salts with hydrogen peroxide, resulting in the generation of hydroxyl radicals that can react with the organic contaminant (Equation 2), (SANTOS-JUANES et al., 2017).



It is important to note that this reaction occurs at acidic pH to avoid the precipitation of iron as hydroxide, and, consequently, decrease the production of  $HO^\bullet$ .

Then,  $Fe^{3+}$  can be reduced to  $Fe^{2+}$  by reaction with  $H_2O_2$ , according to Equations 3, 4, and 5 (NÚÑEZ; GARCÍA-HORTAL; TORRADES, 2007).



In order to increase the rate of reduction of  $Fe^{3+}$  to  $Fe^{2+}$ , UV radiation is used together with the Fenton reaction, which is known as the Photo-Fenton process (Equation 6) (SUBRAMANIAN; MADRAS, 2016).



At the end of the treatment using the Fenton reaction, it is necessary to neutralize the reaction mixture, which has an acidic pH. Due to the presence of iron in the solution, raising the pH causes the formation of iron hydroxides, which precipitate, forming sludge (ROBINSON et al., 2001).

The need to add base to the treated effluent after the Fenton reactions, and the step of separating the sludge with subsequent treatment and/or final disposal, increases the costs of the Fenton process.

### 2.6.2 Ozonolysis

Ozone is a triatomic and non-linear molecule. It is a powerful oxidizing agent ( $E^0 = 2.07$  V), which can oxidize a variety of organic compounds through the formation of hydroxyl radicals that can react with the organic contaminant (BARRERA-MARTÍNEZ et al., 2016; SZPYRKOWICZ; JUZZOLINO; KAUL, 2001).

According to Muthujumar and Selvakumar (2004), the decomposition of ozone and hydroxyl radical production begins at slightly basic pH, as the pH increases the ozone stability decreases. The mechanism of radical production was proposed by Rice (1997) (Equations 7 to 11):



The efficiency of the ozonation process can be improved with the use of  $\text{H}_2\text{O}_2$ , since it accelerates the production of hydroxyl radicals, according to Equation 12 (TISA; ABDUL RAMAN; WAN DAUD, 2014).



Ozonation has the advantage that it does not require the addition of chemicals and it can also be used in aqueous solvents, with no residue formation at the end of the process, such as sludge as in the Fenton process (PUNZI et al., 2015). However, besides the high cost for the production of ozone, it is not possible to carry out its storage due to its high instability, being necessary its "*in situ*" generation (KUNZ et al., 1999).

### 2.6.3 Photolysis

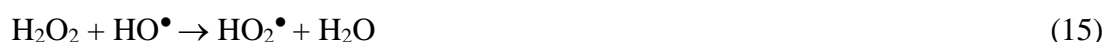
According to Lima and colleagues (2016) the formation of the hydroxyl radical occurs from the homolytic breakdown of  $\text{H}_2\text{O}_2$  with the incidence of UV radiation, forming 2 mol of  $\text{HO}^\bullet$  for each mol of  $\text{H}_2\text{O}_2$ , as shown in Equation 13.



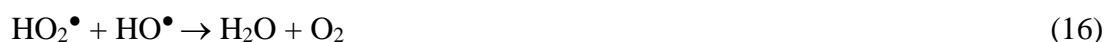
After the formation of the hydroxyl radical, there are several possibilities of reaction. If  $\text{HO}^\bullet$  is at high concentrations, they may recombine and re-form  $\text{H}_2\text{O}_2$  (Eq. 14).



Hydroperoxyl radical formation may occur if hydrogen peroxide is present in high concentration (Eq. 15).



$\text{HO}^\bullet$  can also react with  $\text{HO}_2^\bullet$ , forming  $\text{H}_2\text{O}$ , (Eq. 16).



In order for the photolysis reaction to be satisfactory, a study of the hydrogen peroxide concentration must be carried out, since it can consume the hydroxyl radicals reducing the efficiency of organic matter degradation (COSTA et al., 2010; MELO et al., 2009).

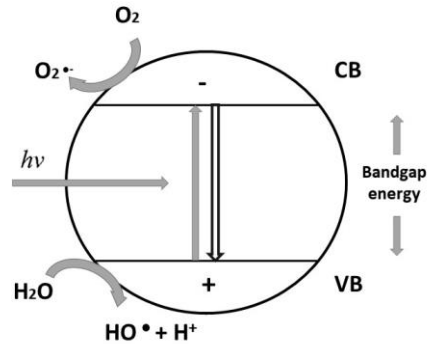
Among the AOPs, photocatalysis stands out as it is considered a promising process of green chemistry and an environmentally benign treatment technology for a series of pollutants.

#### 2.6.4 Photocatalysis

The main advantage of heterogeneous photocatalysis is its potential for the incorporation of solar energy, in which the environmental degradation process acquires significant additional value. Photodegradation of effluent pollutants using sunlight can make it an economically viable process, in particular for large-scale aqueous phase applications (BORGES et al., 2016; PRIETO-RODRIGUEZ et al., 2012).

Heterogeneous photocatalysis is based on the activation of a semiconductor by UV radiation. By absorbing photons with energy higher than the bandgap energy of the semiconductor, the electrons ( $e^-$ ) of the valence band (VB) are excited to the conduction band (CB), generating an electro/vacant pair ( $e^-/h^+$ ). The VB acquires a positive potential, being able to react with the water and to produce  $\text{HO}^\bullet$ , since the electron present in the CB can reduce the  $\text{O}_2$  adsorbed on the surface of the semiconductor forming superoxide radicals ( $\text{O}_2^{\bullet-}$ ). The generated radicals can oxidize the organic contaminant, promoting its mineralization (ÂNGELO et al., 2016; SALGADO et al., 2009; JARDIM, 1998). Figure 4 shows a simplified form the photocatalytic process with the formation of the  $e^-/h^+$  pair and the radical species.

Figure 4 - Representative scheme of photocatalysis in a particle of a semiconductor.



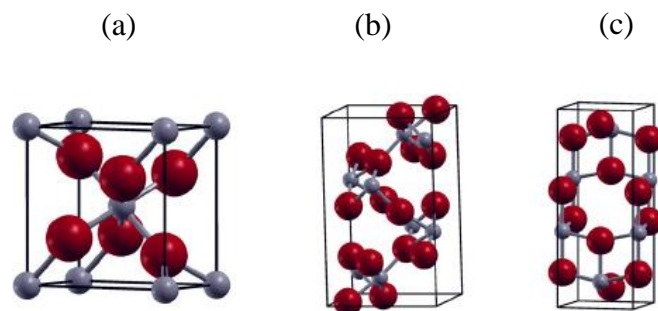
Source: Adapted from Nogueira and Jardim (1998).

Several semiconductors (eg.:  $\text{TiO}_2$ ,  $\text{ZnO}$ ,  $\text{V}_2\text{O}_5$ , and  $\text{WO}_3$ ) have been widely studied as photocatalysts. However,  $\text{TiO}_2$  has been outstanding due to its high photocatalytic efficiency, low cost, non-toxicity, and chemical and thermal stability (LUO et al., 2015; WANG et al., 2015).

### 2.6.5 $\text{TiO}_2$ applied to photocatalysis

$\text{TiO}_2$  exists in three different naturally occurring crystalline forms: anatase, brookite and rutile (Figure 5).

Figure 5 - Unit cells of rutile.



Subtitle: (a), brookite (b), and anatase (c) structures of  $\text{TiO}_2$ .

Source: Esch, Gadaczek and Bredow (2014)

According to Ohno and colleagues (2001), TiO<sub>2</sub> P25, which has 80% of the anatase form and 20% of the rutile form, presents greater photoactivity. The higher efficiency of the anatase phase can be explained by the lower recombination speed of the e<sup>-</sup>/h<sup>+</sup> pair, due to the higher band gap energy (3.2 eV for anatase, 3.0 eV for rutile, and 3.2 eV for brookite) (MURGOLO et al., 2017).

Despite the advantages of TiO<sub>2</sub>, one of its limitations is the small size of its particles, which makes the decantation, recovery, and reuse difficult and expensive. Furthermore, if TiO<sub>2</sub> is not efficiently recovered, it can cause secondary pollution of the treated effluent (BORGES et al., 2016; XIN et al., 2014).

One way around this problem is the use of supported photocatalysts to avoid the loss of photocatalysts and additional treatments such as filtration and centrifugation. Several materials have been studied as support for TiO<sub>2</sub>, such as glass, activated carbon, silica, and polymeric materials. The immobilization of TiO<sub>2</sub> to suitable carriers decreases their loss in photocatalytic degradation processes and increases their recycling over several successive cycles (AYOUBI-FEIZ et al., 2014).

Glass is widely used as a support for TiO<sub>2</sub> due to its high transparency to UV radiation, and good adhesion to TiO<sub>2</sub>. Additionally, it does not interfere with its catalytic activity, presenting high temperature resistance, low cost, and resistance to corrosive environments. TiO<sub>2</sub> can be fixed in various glass materials, such as (BOUARIOUA; ZERDAOUI, 2017), glass fibers and pearls (SUN et al., 2016; PHAM; LEE, 2015; SHEN et al., 2012), glass cylinder (GELOVER; MONDRAGÓN; JIMÉNEZ, 2004), and in reactor walls (MENDES et al., 2009). However, when TiO<sub>2</sub> is immobilized in the wall of reactors, slides, and glass fibers, there is a reduction in its surface area, which, consequently, reduces its efficiency (NOORJAHAN et al., 2003).

Another alternative to overcome this problem is to associate TiO<sub>2</sub> with a magnetic part, where the photocatalyst can be removed from the treated effluent only by the action of a magnetic field (LI et al., 2015; WILSON et al., 2017).

TiO<sub>2</sub> directly supported on iron oxides has already been synthesized, forming TiO<sub>2</sub>/Fe<sub>3</sub>O<sub>4</sub>, where the magnetic core was used to facilitate the separation of the photocatalyst, and the external coating of titanium oxide was useful for the degradation of organic contaminants (STEFAN et al., 2016; XIN et al., 2014).

Authors reported that a layer is required to coat the surface of the iron particles to protect the magnetic core from possible contamination and prevent chemical dissolution or degradation of the iron oxides (LI et al., 2015; LIU et al., 2011; WILSON et al., 2017).

Iron oxides have already been immobilized on polymers such as chitosan (CHEN et al., 2012) and methyl methacrylate (CHEN et al., 2009). However, these may be vulnerable to photodegradation, since a study using TiO<sub>2</sub> has already been carried out with the aim of degrading polymers (ALLEN; BULLEN; MCKELLAR, 1977).

Authors have already synthesized a silicon coated iron support with TiO<sub>2</sub> on their surface, forming the TiO<sub>2</sub>/SiO<sub>2</sub>/Fe<sub>3</sub>O<sub>4</sub> composites (LI et al., 2016; RUZMANOVA; STOLLER; CHIANESE, 2013; WILSON et al., 2017). Another alternative would be to use charcoal as a carrier.

One of the factors that affect the decomposition of organic compounds is the adsorption of these pollutants on the surface of the photocatalyst. The semiconductor TiO<sub>2</sub> P25 is characterized by a relatively small surface area, which is around 50 to 55 m<sup>2</sup> g<sup>-1</sup>. Increasing the surface area of TiO<sub>2</sub> makes the process more effective (LI et al., 2016; CZECH et al., 2015).

In the literature, there are studies where the authors used charcoal to coat the magnetic particles present in the photocatalyst. They used iron chloride as source of iron, styrene or glucose polymer as carbon source, and titanium oxide or titanium dioxide as TiO<sub>2</sub> source for the formation of the TiO<sub>2</sub>/C/Fe<sub>3</sub>O<sub>4</sub> photocatalyst by hydrothermal or solvothermic methods (ZHANG et al., 2015; LIU et al., 2014; JHANG et al., 2019).

A similar study was carried out by our research group, where red mud (RM) and tar (C) were used as source of iron and charcoal, respectively, forming the magnetic support C/RM, and TiO<sub>2</sub> was inserted on its surface. However, these materials presented low surface area, adsorbing only 4% of the Black Remazol 5 dye (PEREIRA et al., 2019).

Therefore, the objective of this study is the synthesis of photocatalysts obtained from iron nitrate, sucrose or activated carbon, and TiO<sub>2</sub>, as a source of magnetite, charcoal, and TiO<sub>2</sub>, respectively, using a simple and different methodology of studies found in the literature. These materials aim to improve the separation, adsorption and degradation capacities of organic pollutants.

Activated carbon (AC) is widely used as a commercial adsorbent and catalyst support because of its stability, mechanical strength, and high surface area (FU et al., 2015). By using AC as a support for iron oxide, it also increases the surface area of the material, which can adsorb the molecules of contaminants on its surface, causing it to be near to the generated



radicals, resulting in the acceleration of the photocatalytic reactions (LI et al., 2015; LIU et al., 2011; HU et al., 2013).

In addition to activated carbon, another alternative support is the carbon obtained from sucrose. Authors reported that the preparation of carbon from renewable resources presents high carbon yield. Sucrose is a widely available product and has been reported by several authors as being an excellent source of carbon materials with mesoporous structure (JANA; FIERRO; CELZARD, 2013; LEZANSKA et al., 2015).

Thus, this work utilized sucrose and AC as the carbon source for the synthesis of the magnetic media, C/Fe and Fe/AC, respectively. TiO<sub>2</sub> particles were added on the surface of these substrates to obtain the Ti/C/Fe and Ti/Fe/AC magnetic photocatalysts with different TiO<sub>2</sub> contents (20, 40 and 60% w/w). These materials were characterized by X-ray diffraction XRD, Thermal Analysis (TG), X-Ray Fluorescence (XRF), Raman spectroscopy, Specific surface area (SSA), magnetic properties by VSM, Diffuse reflectance spectroscopy (DRX) and Scanning electron microscope (SEM). The photocatalytic activity of the prepared photocatalysts was investigated with reactions for the discoloration of BR5 dye and/or phenol and/or acetaminophen under UV radiation of 51 W.

### 3 FINAL CONSIDERATIONS

Due to the high demand of industrial activities, a large amount of effluent is generated, contaminating the environment and endangering human health. Within a very broad spectrum of compounds that the industries use and do not properly treat, three contaminants models were chosen to assess the efficiency of the materials prepared in this work: dye BR5, acetaminophen, and phenol. To investigate the treatment of these pollutants, photocatalysis was chosen, using TiO<sub>2</sub> as the semiconductor since it stands out for its many advantages, among them its high efficiency, low cost and non-toxicity. However, TiO<sub>2</sub> presents difficulty in being separated from the treated solution, and to overcome this problem, this work proposes the synthesis of magnetic photocatalysts, which can be separated from the contaminated effluent simply and quickly with the aid of a magnet. Thus, magnetic photocatalysts based on TiO<sub>2</sub>, charcoal and iron oxide were prepared. Iron nitrate, commercial activated charcoal or sucrose were used as sources of iron and charcoal. Fe<sub>3</sub>O<sub>4</sub> was obtained due to its magnetic property and the charcoal was used to disperse or coat the iron oxide. The magnetic photocatalysts were prepared with different percentages of TiO<sub>2</sub> (20, 40 and 60%) and the results showed that these materials have similar

photocatalytic activities for the degradation of BR5, these materials are easily separated in the reaction medium and have high photocatalytic efficiency for the degradation of black remazol, acetaminophen, and phenol. In this way, it can be affirmed that the magnetic photocatalysts obtained in this work have great potential to be applied in a scale up.

#### 4 REFERENCES

ADOLFO, G.; MARTINEZ, L. Síntese de nanopartículas magnéticas com elevada magnetização de saturação e estabilidade química. 2013.

AHMED, S. et al. Heterogeneous photocatalytic degradation of phenols in wastewater : A review on current status and developments. **DES**, v. 261, n. 1–2, p. 3–18, 2010.

AIDIL, M. et al. Fabrication of TiO<sub>2</sub>-graphene photocatalyst by direct chemical vapor deposition and its anti-fouling property. **Materials Chemistry and Physics**, v. 198, p. 42–48, 2017.

AKHTAR, M. F. et al. Textile industrial effluent induces mutagenicity and oxidative DNA damage and exploits oxidative stress biomarkers in rats. **Environmental Toxicology and Pharmacology**, v. 41, p. 180–186, 2016.

AL-HAMDI, A. M. et al. Applied Surface Science Efficient photocatalytic degradation of phenol in aqueous solution by SnO<sub>2</sub>:Sb nanoparticles. **Applied Surface Science**, v. 370, p. 229–236, 2016.

ALLEN, N. S.; BULLEN, D. J.; MCKELLAR, J. F. Photo-oxidation of commercial polyethylene containing titanium dioxide (rutile)/ antioxidant systems. **Journal of Materials Science**, v. 12, n. 7, p. 1320–1324, 1977.

AMORIM, C. C. et al. Chemosphere Use of tar pitch as a binding and reductant of BFD waste to produce reactive materials for environmental applications. **Chemosphere**, v. 109, p. 143–149, 2014.

ÂNGELO, J. et al. Characterization of TiO<sub>2</sub>-based semiconductors for photocatalysis by electrochemical impedance spectroscopy. **Applied Surface Science**, v. 387, p. 183–189, 2016.

ARABATZIS, I. M. et al. Preparation, characterization and photocatalytic activity of nanocrystalline thin film TiO<sub>2</sub> catalysts towards 3,5-dichlorophenol degradation. **Journal of Photochemistry and Photobiology A: Chemistry**, v. 149, n. 1–3, p. 237–245, 2002.

ARDISSON, J. C. T. F. G. DE M. R. M. L. J. D. Controlled formation of reactive Fe particles dispersed in a carbon matrix active for the oxidation of aqueous contaminants with H<sub>2</sub>O<sub>2</sub>. **Environ Sci Pollut Res**, v. 22, p. 856–863, 2015.

AYOUBI-FEIZ, B. et al. Preparation and application of  $\alpha$ -Fe<sub>2</sub>O<sub>3</sub>/TiO<sub>2</sub>/activated charcoal plate nanocomposite as an electrode for electrosorption-assisted visible light photoelectrocatalytic process. **Journal of Molecular Catalysis A: Chemical**, v. 395, p. 440–448, 2014.

AZUWA, M. et al. Photodegradation of phenol by N-Doped TiO<sub>2</sub> anatase / rutile nanorods assembled microsphere under UV and visible light irradiation. **Materials Chemistry and**

**Physics**, v. 162, p. 113–123, 2015.

BARRERA-MARTÍNEZ, I. et al. Ozonolysis of alkaline lignin and sugarcane bagasse: Structural changes and their effect on saccharification. **Biomass and Bioenergy**, v. 94, p. 167–172, 2016.

BILAL, M. et al. Toxicological Assessment and UV / TiO<sub>2</sub> -Based Induced Degradation Profile of Reactive Black 5 Dye. **Environmental Management**, v. 61, p. 171–180, 2018.

BORGES, M. E. et al. Photocatalysis with solar energy: Sunlight-responsive photocatalyst based on TiO<sub>2</sub> loaded on a natural material for wastewater treatment. **Solar Energy**, v. 135, p. 527–535, 2016.

BOUARIOUA, A.; ZERDAOUI, M. Photocatalytic activities of TiO<sub>2</sub> layers immobilized on glass substrates by dip-coating technique toward the decolorization of methyl orange as a model organic pollutant. **Journal of Environmental Chemical Engineering**, v. 5, n. 2, p. 1565–1574, 2017.

CARDOSO, J. C.; BESSEGATO, G. G.; BOLDRIN ZANONI, M. V. Efficiency comparison of ozonation, photolysis, photocatalysis and photoelectrocatalysis methods in real textile wastewater decolorization. **Water Research**, v. 98, p. 39–46, 2016.

CARDOSO, N. F. et al. Removal of remazol black B textile dye from aqueous solution by adsorption. **Desalination**, v. 269, n. 1–3, p. 92–103, 2011.

CHEN, A. et al. Novel thiourea-modified magnetic ion-imprinted chitosan/TiO<sub>2</sub> composite for simultaneous removal of cadmium and 2,4-dichlorophenol. **Chemical Engineering Journal**, v. 191, p. 85–94, 2012.

CHEN, Y. H. et al. Photocatalytic degradation of p-phenylenediamine with TiO<sub>2</sub>-coated magnetic PMMA microspheres in an aqueous solution. **Journal of Hazardous Materials**, v. 163, n. 2–3, p. 973–981, 2009.

CHOI, K. et al. Enhanced photocatalytic degradation of tri-chlorophenol by Fe<sub>3</sub>O<sub>4</sub> @ TiO<sub>2</sub> @ Au photocatalyst under visible-light. **Ceramics International**, n. July, p. 0–1, 2018.

COSTA, R. C. C. et al. Controlled reduction of red mud waste to produce active systems for environmental applications: heterogeneous Fenton reaction and reduction of Cr(VI). **Chemosphere**, v. 78, n. 9, p. 1116–20, fev. 2010.

CZECH, B. et al. MWCNT-TiO<sub>2</sub>-SiO<sub>2</sub> nanocomposites possessing the photocatalytic activity in UVA and UVC. **Applied Catalysis B: Environmental**, v. 162, p. 564–572, 2015.

DARJA MAUČEC, ANDRAŽ ŠULIGOJ, ALENKA RISTIĆ, GORAN DRAŽIĆ, ALBIN PINTAR, N. N. T. Titania versus zinc oxide nanoparticles on mesoporous silica supports as photocatalysts for removal of dyes from wastewater at neutral pH. **Catalysis Today**, v. 310, n. February 2017, p. 32–41, 2018.

DUAN, W. et al. Ecotoxicity of phenol and cresols to aquatic organisms: A review. **Ecotoxicology and Environmental Safety**, v. 157, n. April, p. 441–456, 2018.

EKKA, B. et al. Synthesis of hydroxyapatite-zirconia nanocomposite through sonochemical route: A potential catalyst for degradation of phenolic compounds. **Journal of Environmental Chemical Engineering**, v. 6, n. 5, p. 6504–6515, 2018.

EL BOURAIIE, M.; EL DIN, W. S. Biodegradation of Reactive Black 5 by *Aeromonas hydrophila* strain isolated from dye-contaminated textile wastewater. **Sustainable Environment Research**, v. 26, n. 5, p. 209–216, 2016.

ESCH, T. R.; GADACZEK, I.; BREDOW, T. Surface structures and thermodynamics of low-index of rutile, brookite and anatase - A comparative DFT study. **Applied Surface Science**, v. 288, n. October, p. 275–287, 2014.

ESCUADERO, C. J. et al. Performance of electrochemical oxidation and photocatalysis in terms of kinetics and energy consumption. New insights into the p-cresol degradation. **Journal of Environmental Management**, v. 195, p. 117–124, 2017.

FILIPPO, E. et al. Efficient, Green Non-Aqueous Microwave-Assisted Synthesis of Anatase TiO<sub>2</sub> and Pt Loaded TiO<sub>2</sub> Nanorods with High Photocatalytic Performance. **Nanomaterials and Nanotechnology**, v. 5, p. 31, 2015.

FU, X. et al. Improved performance of surface functionalized TiO<sub>2</sub>/activated carbon for adsorption-photocatalytic reduction of Cr(VI) in aqueous solution. **Materials Science in Semiconductor Processing**, v. 39, p. 362–370, 2015.

FUJISHIMA, A.; RAO, T. N.; TRYK, D. A. Titanium dioxide photocatalysis. **Journal of Photochemistry and Photobiology C: Photochemistry Reviews**, v. 1, n. March, p. 1–21, 2000.

GELOVER, S.; MONDRAGÓN, P.; JIMÉNEZ, A. Titanium dioxide sol-gel deposited over glass and its application as a photocatalyst for water decontamination. **Journal of Photochemistry and Photobiology A: Chemistry**, v. 165, n. 1–3, p. 241–246, 2004.

HABIBI-YANGJEH, A.; MOUSAVI, M.; NAKATA, K. Journal of Photochemistry & Photobiology A: Chemistry Boosting visible-light photocatalytic performance of g-C<sub>3</sub>N<sub>4</sub>/Fe<sub>3</sub>O<sub>4</sub> anchored with CoMoO<sub>4</sub> nanoparticles: Novel magnetically recoverable photocatalysts. **Journal of Photochemistry & Photobiology, A: Chemistry**, v. 368, n. July 2018, p. 120–136, 2019.

HERNÁNDEZ, R. et al. Microwave-assisted sol-gel synthesis of an Au-TiO<sub>2</sub> photoanode for the advanced oxidation of paracetamol as model pharmaceutical pollutant. **Electrochemistry Communications**, v. 96, n. August, p. 42–46, 2018.

HU, Y. et al. Carbon-coated CdS petalous nanostructures with enhanced photostability and photocatalytic activity. **Angewandte Chemie - International Edition**, v. 52, n. 21, p. 5636–5639, 2013.

HUNGER, K. **Industrial Dyes**. [s.l: s.n.].

IDE, Y.; KOIKE, Y.; OGAWA, M. Journal of Colloid and Interface Science Molecular selective photocatalysis by TiO<sub>2</sub> / nanoporous silica core / shell particulates. **Journal of Colloid And Interface Science**, v. 358, n. 1, p. 245–251, 2011.

IQBAL, M.; NISAR, J. Cytotoxicity and mutagenicity evaluation of gamma radiation and hydrogen peroxide treated textile effluents using bioassays. **Journal of Environmental Chemical Engineering**, v. 3, n. 3, p. 1912–1917, 2015.

JAGANNATHAN, M.; GRIESER, F.; ASHOKKUMAR, M. Sonophotocatalytic degradation of paracetamol using TiO<sub>2</sub> and Fe<sup>3+</sup>. **Separation and Purification Technology**, v. 103, p.

114–118, 2013.

**JANA; FIERRO; CELZARD, 2016.** , [s.d.].

JANA, P.; FIERRO, V.; CELZARD, A. Ultralow cost reticulated carbon foams from household cleaning pad wastes. **Carbon**, v. 62, p. 517–520, 2013.

JARDIM, R. F. P. N. E W. F. A FOTOCATÁLISE HETEROGÊNEA E SUA APLICAÇÃO AMBIENTAL Raquel F. P. Nogueira e Wilson F. Jardim. **Química Nova**, v. 2, n. 1, p. 69–72, 1998.

JHANG, J. et al. Microporous and Mesoporous Materials A new porous structure with dispersed nano-TiO<sub>2</sub> in a three-dimensional carbon skeleton for achieving high photocatalytic activity. **Microporous and Mesoporous Materials**, v. 276, n. July 2018, p. 62–67, 2019.

JING WANG, GUOXIONG WANG, SHU MIAO, XIAOLE JIANG, JIAYUAN LI, X. B. Synthesis of Fe / Fe<sub>3</sub>C nanoparticles encapsulated in nitrogen-doped carbon with single-source molecular precursor for the oxygen reduction reaction. **Carbon**, v. 75, p. 381–389, 2014.

KADRIYE OZLEM HAMALOGLU, EBRU SAG, AYKUT BILIR, A. T. Monodisperse-porous titania microspheres and their gold decorated forms as new photocatalysts for dye degradation in batch fashion. **Materials Chemistry and Physics**, v. 207, p. 359–366, 2018.

KHOSRAVI, M.; AZIZIAN, S. Journal of Industrial and Engineering Chemistry Adsorption of anionic dyes from aqueous solution by iron oxide nanospheres. **Journal of Industrial and Engineering Chemistry**, v. 20, n. 4, p. 2561–2567, 2014.

KOVALEVSKIY, N. S. et al. Analysis of air photocatalytic purification using a total hazard index : Effect of the composite TiO<sub>2</sub> / zeolite photocatalyst. **Journal of Hazardous Materials journal**, v. 358, n. April, p. 302–309, 2018.

KRÝSA, J. et al. Composite photocatalysts based on TiO<sub>2</sub> – carbon for air pollutant removal : Aspects of adsorption. **Catalysis Today journal**, n. August, 2018.

KUNZ, A. et al. Construção e otimização de um sistema para produção e aplicação de ozônio em escala de laboratório. **Química Nova**, v. 22, n. 3, p. 425–428, 1999.

KUNZ, A.; PERALTA-ZAMORA, P. Revisão. v. 25, n. 1, p. 78–82, 2002.

**LEZANSKA et al.** , [s.d.].

LI, D. et al. Convenient synthesis of magnetically recyclable Fe<sub>3</sub>O<sub>4</sub>@C@CdS photocatalysts by depositing CdS nanocrystals on carbonized ferrocene. **Journal of Alloys and Compounds**, v. 646, p. 978–982, 2015.

LI, H. et al. Journal of Physics and Chemistry of Solids Preparation of phenol-formaldehyde resin-coupled TiO<sub>2</sub> and study of photocatalytic activity during phenol degradation under sunlight. **Journal of Physical and Chemistry of Solids**, v. 122, n. June, p. 25–30, 2018a.

LI, M. et al. Synergetic effect between adsorption and photodegradation on nanostructured TiO<sub>2</sub> / activated carbon fiber felt porous composites for toluene removal. **Journal of Hazardous Materials**, v. 333, p. 88–98, 2017.

LI, Q. et al. Microporous and Mesoporous Materials Preparation and enhanced photocatalytic performance of a novel photocatalyst : Hollow network Fe<sub>3</sub>O<sub>4</sub> / mesoporous SiO<sub>2</sub> / TiO<sub>2</sub> (

FST ) composite microspheres. **Microporous and Mesoporous Materials**, v. 265, n. November 2017, p. 18–25, 2018b.

LI, W.; WU, H. Sodium citrate functionalized reusable Fe<sub>3</sub>O<sub>4</sub> @ TiO<sub>2</sub> photocatalyst for water purification. **Chemical Physics Letters**, v. 686, p. 178–182, 2017.

LI, Y. et al. Photocatalytic oxidation of small molecule hydrocarbons over Pt/TiO<sub>2</sub> nanocatalysts. **RSC Advances**, v. 6, n. 4, p. 2760–2767, 2016.

LIMA, L. B. DE et al. Degradation of organic contaminants in effluents — synthetic and from the textile industry — by Fenton , photocatalysis , and H<sub>2</sub>O<sub>2</sub> photolysis. **Environmental Science and Pollution Research**, 2016.

LIU, G. et al. Applied Catalysis B: Environmental Yolk – shell structured Fe<sub>3</sub>O<sub>4</sub> @ C @ F-TiO<sub>2</sub> microspheres with surface fluorinated as recyclable visible-light driven photocatalysts. “**Applied Catalysis B, Environmental**”, v. 150–151, p. 515–522, 2014.

LIU, X. et al. Performance and mechanism into TiO<sub>2</sub> / Zeolite composites for sulfadiazine adsorption and photodegradation. **Chemical Engineering Journal**, v. 350, n. February, p. 131–147, 2018.

LIU, Y. et al. Magnetic-field induced formation of 1D Fe<sub>3</sub>O<sub>4</sub>/C/CdS coaxial nanochains as highly efficient and reusable photocatalysts for water treatment. **Journal of Materials Chemistry**, v. 21, n. 45, p. 18359–18364, 2011.

LIU, Y. et al. Degradation and mineralization mechanism of phenol by BiPO<sub>4</sub> photocatalysis assisted with H<sub>2</sub>O<sub>2</sub>. **Applied Catalysis B: Environmental**, v. 142–143, p. 561–567, 2013.

LUO, L. et al. Hydrothermal synthesis of fluorinated anatase TiO<sub>2</sub>/reduced graphene oxide nanocomposites and their photocatalytic degradation of bisphenol A. **Applied Surface Science**, v. 353, p. 469–479, 2015.

MAGALHÃES, F. et al. Novel highly reactive and regenerable carbon/iron composites prepared from tar and hematite for the reduction of Cr(VI) contaminant. **Journal of Hazardous Materials**, v. 165, n. 1–3, p. 1016–1022, 2009a.

MAGALHÃES, F. et al. Novel highly reactive and regenerable carbon / iron composites prepared from tar and hematite for the reduction of Cr ( VI ) contaminant. **Journal of Hazardous Materials**, v. 165, p. 1016–1022, 2009b.

MAGALHÃES, F.; MOURA, F. C. C.; LAGO, R. M. TiO<sub>2</sub>/LDPE composites: A new floating photocatalyst for solar degradation of organic contaminants. **Desalination**, v. 276, n. 1–3, p. 266–271, 2011.

MALPASS, G. R. P. et al. Decolorisation of real textile waste using electrochemical techniques: Effect of the chloride concentration. **Water Research**, v. 41, n. 13, p. 2969–2977, 2007.

MANASSERO, A.; SATUF, M. L.; ALFANO, O. M. Photocatalytic reactors with suspended and immobilized TiO<sub>2</sub> : Comparative efficiency evaluation. **Chemical Engineering Journal**, v. 326, p. 29–36, 2017.

MAO, D. et al. Size tunable Bi<sub>3</sub>O<sub>4</sub>Br hierarchical hollow spheres assembled with {0 0 1}-facets exposed nanosheets for robust photocatalysis against phenolic pollutants. **Journal of Catalysis**, v. 369, p. 209–221, 2019.

- MARTINS, A. C. et al. Sol-gel synthesis of new TiO<sub>2</sub> / activated carbon photocatalyst and its application for degradation of tetracycline. **Ceramics International**, v. 43, n. 5, p. 4411–4418, 2017.
- MOCTEZUMA, E. et al. Photocatalytic degradation of paracetamol : Intermediates and total reaction mechanism. **Journal of Hazardous Materials**, v. 243, p. 130–138, 2012.
- MURGOLO, S. et al. A new supported TiO<sub>2</sub> film deposited on stainless steel for the photocatalytic degradation of contaminants of emerging concern. **Chemical Engineering Journal**, v. 318, p. 103–111, 2017.
- NADIMI, M. et al. Photodegradation of Methylene Blue by a ternary magnetic TiO<sub>2</sub> / Fe<sub>3</sub>O<sub>4</sub> / Graphene oxide nanocomposite under visible light. **Materials Chemistry and Physics**, 2018.
- NEGHI, N.; KUMAR, M.; BURKHALOV, D. Synthesis and application of stable , reusable TiO<sub>2</sub> polymeric composites for photocatalytic removal of metronidazole : Removal kinetics and density functional analysis. **Chemical Engineering Journal**, v. 359, n. August 2018, p. 963–975, 2019.
- NOORJAHAN, M. et al. Photocatalytic degradation of H-acid over a novel TiO<sub>2</sub> thin film fixed bed reactor and in aqueous suspensions. **Journal of Photochemistry and Photobiology A: Chemistry**, v. 156, n. 1–3, p. 179–187, 2003.
- NORHARYATI, W. et al. Journal of Photochemistry & Photobiology A: Chemistry Photocatalytic degradation of phenol over visible light active ZnO / Ag<sub>2</sub>CO<sub>3</sub> / Ag<sub>2</sub>O nanocomposites heterojunction. **Journal of Photochemistry & Photobiology A: Chemistry**, v. 364, n. June, p. 602–612, 2018.
- NÚÑEZ, L.; GARCÍA-HORTAL, J. A.; TORRADES, F. Study of kinetic parameters related to the decolourization and mineralization of reactive dyes from textile dyeing using Fenton and photo-Fenton processes. **Dyes and Pigments**, v. 75, n. 3, p. 647–652, 2007.
- O, T. F. et al. Journal of Photochemistry and Photobiology A: Chemistry Photocatalytic degradation of paracetamol over magnetic fl ower-like. **“Journal of Photochemistry & Photobiology, A: Chemistry”**, v. 347, p. 186–198, 2017.
- OHNO, T. et al. Morphology of a TiO<sub>2</sub> Photocatalyst ( Degussa , P-25 ) Consisting of Anatase and Rutile Crystalline Phases. **Journal of Catalysis** **203**, v. 203, p. 82–86, 2001.
- PEREIRA, L. D. O. et al. Journal of Environmental Chemical Engineering Magnetic photocatalysts from industrial residues and TiO<sub>2</sub> for the degradation of organic contaminants. **Journal of Environmental Chemical Engineering**, v. 7, n. 1, p. 102826, 2019.
- PERIYASAMY, S.; MUTHUCHAMY, M. Electrochemical oxidation of paracetamol in water by graphite anode: Effect of pH, electrolyte concentration and current density. **Journal of Environmental Chemical Engineering**, n. June, p. 1–10, 2018.
- PHAM, T. D.; LEE, B. K. Disinfection of Staphylococcus aureus in indoor aerosols using Cu-TiO<sub>2</sub> deposited on glass fiber under visible light irradiation. **Journal of Photochemistry and Photobiology A: Chemistry**, v. 307–308, p. 16–22, 2015.
- PHONGAMWONG, T. et al. Novel visible-light-sensitized Chl-Mg/P25 catalysts for photocatalytic degradation of rhodamine B. **Applied Catalysis B: Environmental**, v. 207, p.

326–334, 2017.

PIPI, A.; BYZYNSKI, G.; RUOTOLO, L. Photocatalytic Activity and RNO Dye Degradation of Nitrogen-doped TiO<sub>2</sub> Prepared by Ionothermal Synthesis. **Materials Research**, v. 20, n. 3, p. 628–638, 2017.

PRIETO-RODRIGUEZ, L. et al. Optimization of mild solar TiO<sub>2</sub> photocatalysis as a tertiary treatment for municipal wastewater treatment plant effluents. **Applied Catalysis B: Environmental**, v. 128, p. 119–125, 2012.

PUNTES-CÁRDENAS, J. et al. Simultaneous decolorization and detoxification of black reactive 5 using TiO<sub>2</sub> deposited over borosilicate glass. **Univ. Sci.**, v. 17, p. 53–63, 2012.

PUNZI, M. et al. Combined anaerobic-ozonation process for treatment of textile wastewater: Removal of acute toxicity and mutagenicity. **Journal of Hazardous Materials**, v. 292, p. 52–60, 2015.

RAZA, W. et al. Removal of phenolic compounds from industrial waste water based on membrane-based technologies. **Journal of Industrial and Engineering Chemistry**, 2018.

REAÇÕES, E. M. et al. Artigo. v. 36, n. 9, p. 1332–1337, 2013.

RIBEIRO, A. R. et al. An overview on the advanced oxidation processes applied for the treatment of water pollutants defined in the recently launched Directive 2013/39/EU. **Environment International**, v. 75, p. 33–51, 2015.

RIMOLDI, L. et al. Applied Surface Science The role played by different TiO<sub>2</sub> features on the photocatalytic degradation of paracetamol. **Applied Surface Science**, v. 424, p. 198–205, 2017.

ROBINSON, T. et al. Remediation of dyes in textile e,uent a critical review on current.pdf. **Bioresource Technology**, v. 77, p. 247–255, 2001.

RUZMANOVA, Y.; STOLLER, M.; CHIANESE, A. Photocatalytic Treatment of Olive Mill Wastewater by Magnetic Core Titanium Dioxide Nanoparticles. **CHEMICAL ENGINEERING TRANSACTIONS**, v. 32, n. 2009, p. 2269–2274, 2013.

SABLE, S. S. et al. Catalytic oxidative degradation of phenol using iron oxide promoted sulfonated-ZrO<sub>2</sub> by Advanced Oxidation Processes (AOPs). **Journal of the Taiwan Institute of Chemical Engineers**, v. 91, p. 434–440, 2018.

SAHEL, K. et al. Photocatalytic decolorization of Remazol Black 5 (RB5) and Procion Red MX-5B-Isotherm of adsorption, kinetic of decolorization and mineralization. **Applied Catalysis B: Environmental**, v. 77, n. 1–2, p. 100–109, 2007.

SALGADO, B. C. B. et al. Descoloração de efluentes aquosos sintéticos e têxtil contendo corantes índigo e azo via processos Fenton e foto-assistidos (UV e UV/H<sub>2</sub>O<sub>2</sub>). **Engenharia Sanitaria e Ambiental**, v. 14, n. 1, p. 1–8, 2009.

SÁNCHEZ-RODRÍGUEZ, D. et al. Journal of Environmental Chemical Engineering Photocatalytic properties of BiOCl-TiO<sub>2</sub> composites for phenol photodegradation. **Journal of Environmental Chemical Engineering**, v. 6, n. 2, p. 1601–1612, 2018.

SANTOS-JUANES, L. et al. Combining ZVI reduction with photo-Fenton process for the removal of persistent pollutants. **Chemical Engineering Journal**, v. 310, p. 484–490, 2017.



SHEN, C. et al. Facile synthesis and photocatalytic properties of TiO<sub>2</sub> nanoparticles supported on porous glass beads. **Chemical Engineering Journal**, v. 209, p. 478–485, 2012.

SHI, L. et al. Recyclable photo-thermal conversion and purification systems via Fe<sub>3</sub>O<sub>4</sub>@TiO<sub>2</sub> nanoparticles. **Energy Conversion and Management**, v. 171, n. June, p. 272–278, 2018.

SOPHA, H. et al. Electrochemistry Communications Scaling up anodic TiO<sub>2</sub> nanotube layers for gas phase photocatalysis. **Electrochemistry Communications**, v. 97, n. October, p. 91–95, 2018.

STEFAN, M. et al. Magnetic recoverable Fe<sub>3</sub>O<sub>4</sub>-TiO<sub>2</sub>:Eu composite nanoparticles with enhanced photocatalytic activity. **Applied Surface Science**, v. 390, p. 248–259, 2016.

SUBRAMANIAN, G.; MADRAS, G. Introducing saccharic acid as an efficient iron chelate to enhance photo-Fenton degradation of organic contaminants. **Water Research**, v. 104, p. 168–177, 2016.

SUN, J. et al. Insight into the mechanism of adsorption of phenol and resorcinol on activated carbons with different oxidation degrees. **Colloids and Surfaces A: Physicochemical and Engineering Aspects**, 2018.

SUN, P. et al. Photocatalyst of organic pollutants decomposition: TiO<sub>2</sub>/glass fiber cloth composites. **Catalysis Today**, v. 274, p. 2–7, 2016.

SZCZEPANIK, B. Applied Clay Science Photocatalytic degradation of organic contaminants over clay-TiO<sub>2</sub> nanocomposites : A review. **Applied Clay Science**, v. 141, p. 227–239, 2017.

SZPYRKOWICZ, L.; JUZZOLINO, C.; KAUL, S. N. A comparative study on oxidation of disperse dyes by electrochemical process, ozone, hypochlorite and fenton reagent. **Water Research**, v. 35, n. 9, p. 2129–2136, 2001.

THOMMES, M. et al. Physisorption of gases, with special reference to the evaluation of surface area and pore size distribution ( IUPAC Technical Report ). **Pure Appl. Chem.**, v. 87, p. 1051–1069, 2015.

TISA, F.; ABDUL RAMAN, A. A.; WAN DAUD, W. M. A. Applicability of fluidized bed reactor in recalcitrant compound degradation through advanced oxidation processes: A review. **Journal of Environmental Management**, v. 146, p. 260–275, 2014.

TOKUMURA, M. et al. Comprehensive study on effects of water matrices on removal of pharmaceuticals by three different kinds of advanced oxidation processes. **Chemosphere**, v. 159, p. 317–325, 2016.

WANG, H. et al. Analysis of TiO<sub>2</sub> photocatalysis in a pulsed discharge system for phenol degradation. **Journal of Electrostatics**, v. 67, n. 6, p. 886–889, 2009.

WANG, R. C.; YU, C. W. Phenol degradation under visible light irradiation in the continuous system of photocatalysis and sonolysis. **Ultrasonics Sonochemistry**, v. 20, n. 1, p. 553–564, 2013.

WANG, X. et al. Facile synthesis and magnetic properties of Fe<sub>3</sub>C/C nanoparticles via a sol-gel process. **Dyes and Pigments**, v. 112, p. 305–310, 2015.

WANG, X. et al. Science of the Total Environment Novel photocatalytic system Fe-complex /

TiO<sub>2</sub> for efficient degradation of phenol and norfl oxacin in water. v. 656, p. 1010–1020, 2019.

WANGFUENKANAGUL, N.; CHAILAPAKUL, O. Electrochemical analysis of D-penicillamine using a borondoped diamond thin film electrode applied to flow injection system. **Talanta**, v. 58, n. 6, p. 1213–1219, 2002.

WEI, X.; WANG, H. Preparation of magnetic g-C<sub>3</sub>N<sub>4</sub> / Fe<sub>3</sub>O<sub>4</sub> / TiO<sub>2</sub> photocatalyst for visible light photocatalytic application. **Journal of Alloys and Compounds**, v. 763, p. 844–853, 2018.

WILSON, M. et al. Magnetic recyclable microcomposite silica-steel core with TiO<sub>2</sub>nanocomposite shell photocatalysts for sustainable water purification. **Colloids and Surfaces A: Physicochemical and Engineering Aspects**, v. 523, p. 27–37, 2017.

WU, M. et al. Molybdenum disulfide ( MoS<sub>2</sub> ) as a co-catalyst for photocatalytic degradation of organic contaminants : A review. **Process Safety and Environmental Protection**, v. 118, p. 40–58, 2018.

XIN, T. et al. A facile approach for the synthesis of magnetic separable Fe<sub>3</sub>O<sub>4</sub>@TiO<sub>2</sub>, core-shell nanocomposites as highly recyclable photocatalysts. **Applied Surface Science**, v. 288, p. 51–59, 2014.

YANG, X. et al. Chinese Journal of Chemical Engineering Doping effects on the electro-degradation of phenol on doped titanium suboxide anodes. **Chinese Journal of Chemical Engineering**, v. 26, n. 4, p. 830–837, 2018.

ZHANG, Q. et al. Study on enhanced photocatalytic activity of magnetically recoverable Fe<sub>3</sub>O<sub>4</sub>@C@TiO<sub>2</sub> nanocomposites with core-shell nanostructure. **Optical Materials**, v. 46, p. 52–58, 2015.

ZHANG, W. et al. Kinetics of heterogeneous photocatalytic degradation of rhodamine B by TiO<sub>2</sub> -coated activated carbon : Roles of TiO<sub>2</sub> content and light intensity. **Desalination**, v. 266, p. 40–45, 2011.

ŽUR, J. et al. Paracetamol – toxicity and microbial utilization. Pseudomonas moorei KB4 as a case study for exploring degradation pathway. **Chemosphere**, v. 206, p. 192–202, 2018.

## SECOND PART

### ARTICLE 1

#### **Preparation of magnetic photocatalysts from TiO<sub>2</sub>, activated carbon and iron nitrate for environmental remediation**

**Manuscript submitted to Journal of Photochemistry and Photobiology**

Impact factor: 2.891

Qualis Capes (Ciências Agrárias): B1

**Leydiane de Oliveira Pereira<sup>a</sup>, Isabela Marques Sales<sup>a</sup>, Luana Pereira Zampiere<sup>a</sup>, Sara Silveira Vieira<sup>b</sup>, Iara do Rosário Guimarães<sup>a</sup>, Fabiano Magalhães<sup>a,\*</sup>**

<sup>a</sup> Department of Chemistry, Federal University of Lavras, 37200-000 Lavras - MG, Brazil

<sup>b</sup> Department of Chemistry, Federal University of Minas Gerais, 31270-901 Belo Horizonte – MG, Brazil

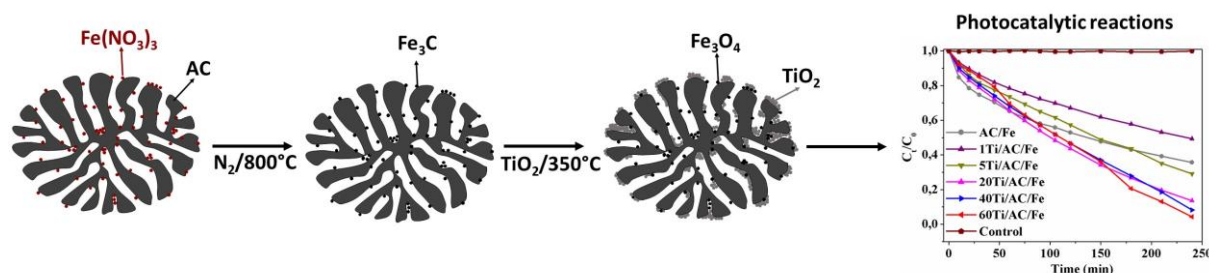
E-mail address: leydi.13@hotmail.com (Leydiane de Oliveira Pereira)

#### **Abstract**

In this study different magnetic photocatalysts were prepared. Activated carbon (AC) and iron nitrate were used for the preparation of a magnetic support (Fe/AC). Different TiO<sub>2</sub> contents were supported on the surface of Fe/AC to obtain the photocatalyst Ti/Fe/AC. Results obtained by XRD showed that the photocatalysts have Fe<sub>3</sub>O<sub>4</sub>, which confers magnetic property. The presence of carbon and TiO<sub>2</sub> was confirmed by Raman and XRD. Scanning Electron Microscopy images showed clusters of TiO<sub>2</sub> particles on the surface of Fe/AC. Results of X-ray fluorescence allowed the obtention of the levels of carbon, iron and titanium in the photocatalysts, which followed the expected trend. The results of reactions carried out in the presence of ultraviolet radiation showed that the magnetic photocatalysts removed from 50 to 96% of color ratio of Reactive Black (RB) in aqueous medium. The best efficiency for removal of total organic carbon (TOC) reached 90%. Sedimentation kinetics tests performed in the presence of magnetic field showed that nearly 92% of the photocatalysts could be rapidly separated from the aqueous medium, while pure TiO<sub>2</sub> does not sediment efficiently. Results for the recovery and reuse of the photocatalysts for four consecutive reactions showed that they can be separated from the reaction medium in a simple and fast way, without significant losses of photocatalytic efficiency. These results showed that the prepared magnetic photocatalysts have excellent photocatalytic activity and can be easily recovered and reused, which implies the reduction of costs and increases the potential for scale up application.

**Keywords:** Magnetic photocatalyst; TiO<sub>2</sub>; Activated carbon.

## Graphical Abstract



## 1. Introduction

Over the last years studies on eliminating organic pollutants through photocatalytic degradation have been conducted [1,2]. Photocatalysis, which combines low input demands and an environmentally acceptable process, represents a very efficient and low pollutant method. Its principle involves the activation of a solar or artificial radiation semi-conductor, generating hydroxyl radicals that can oxidize the organic contaminant and produce  $\text{CO}_2$  and  $\text{H}_2\text{O}$  as main products [3].

Titanium dioxide ( $\text{TiO}_2$ ) is the most used semi-conductor in photocatalytic reactions due to its high efficiency, low cost, non-toxicity, and chemical, thermal and mechanic stability [4,5,6]. However, despite these advantages,  $\text{TiO}_2$  presents technical limitations, such as the low dimension of its particles, which makes recovery and reuse more difficult with the need to use expensive separation processes to treat the effluent. Moreover, if  $\text{TiO}_2$  is not efficiently recovered, it could cause secondary pollution of the medium that is receiving the treatment [7,8]. A way of overcoming this problem is supporting the photocatalyst on a matrix with elevated superficial area, in which the particle dimension does not keep conventional processes, such as filtration and centrifugation, from preventing the material recovery and its posterior use. The elevated surface area of the composite ought to act as a support that guarantees elevated photocatalyst dispersion and optimization of the active sites in radiation-mediated processes [9]. In this scenario, several compounds have been studied to be used as support to  $\text{TiO}_2$ , such as glass [10,11], activated carbon [12,13], silica [14,15], zeolite [16,8] and polymeric materials [17,18]. Immobilization of  $\text{TiO}_2$  on proper supports decreases its loss in photocatalytic degradation processes and increases the possibility of recycling and reuse [15]. Another alternative to overcome this problem is associating  $\text{TiO}_2$  with a magnetic phase, where the photocatalyst can be removed from the treated effluent by the action of a magnetic field [19,20,21].

Titanium dioxide supported directly on iron oxides have been synthesized, forming  $\text{TiO}_2/\text{Fe}_3\text{O}_4$ , where the magnetic core was used to make separation from the photocatalyst easier, and the external coating of  $\text{TiO}_2$  was used for organic contaminant degradation [22,1]. Studies have reported that one layer is necessary to coat the surface of iron particles in order to protect the magnetic core from eventual contamination and to avoid the occurrence of chemical dissolution or degradation of iron oxides [23,19,20,21]. Authors have synthesized a silica-coated iron magnetic support with  $\text{TiO}_2$  on its surface, forming the composites  $\text{TiO}_2/\text{SiO}_2/\text{Fe}_3\text{O}_4$  [24,25,21].

Another alternative would be using activated carbon as a support. Activated carbon is broadly used as commercial adsorbent and support for catalysts due to its stability, mechanical resistance, and elevated superficial area [26]. In addition to protecting  $\text{Fe}_3\text{O}_4$ , activated carbon has the positive effect of decomposing organic compounds in the presence of  $\text{TiO}_2$ . Some authors have reported this synergetic effect, which can be attributed to better adsorption of pollutants on the surface of the photocatalyst, making them close to the radicals generated in the acceleration of photocatalytic reactions [19,5,8].

The semi-conductor  $\text{TiO}_2$  P25 is characterized by a relatively small surface area around 50 to 55  $\text{m}^2 \text{g}^{-1}$ . Increasing the superficial area of  $\text{TiO}_2$  makes the process more effective, considering that photocatalytic reactions occur mainly on the surface of the composites [27,25]. Therefore, combining an adsorbent phase with photocatalysts to remove organic pollutants from contaminated medium has many advantages: (i) the adsorbent concentrates the contaminants on the surface of the photocatalyst, increasing photocatalytic efficiency; (ii) the pollutants are degraded and the adsorbent is regenerated; and (iii) suspended powder  $\text{TiO}_2$  particles agglomerates more than the  $\text{TiO}_2$  supported on the adsorbent [28].

Therefore, in this study, new types of photocatalysts were prepared (identified as Ti/Fe/AC) by the dispersion of iron oxide on the surface and within the pores of activated carbon, forming the magnetic support. These materials aim at improving separation abilities, adsorption and degradation of organic pollutants.

## **2. Material and methods**

### **2.1 Synthesis of Fe/AC composites**

The synthesis of the magnetic support was based on the methodology of Tristão et al. [29], where 1.4  $\text{mol L}^{-1}$   $\text{Fe}_3(\text{NO}_3)_3 \cdot 9\text{H}_2\text{O}$  aqueous solution (Synth, PA) was mixed with 92%

(w/w) of commercial activated carbon (AC) (Synth, PA). The mixture was magnetically stirred for 2 hours and part of the solvent was evaporated at 80 °C for 2 hours. The material was thermally treated at 800 °C in inert atmosphere (N<sub>2</sub>, 10 °C min<sup>-1</sup>) for one hour, using a tubular furnace. The iron content added to the AC was 8% (w/w).

## 2.2 Magnetic photocatalysts preparation

The procedure used to support TiO<sub>2</sub> on the Fe/AC composite surface was based on Arabatzis et al. [30], with modifications. For the synthesis of the photocatalyst named 20Ti/Fe/AC, 0.2 g of TiO<sub>2</sub> (Degussa) were added to water containing 0.1 mL of acetylacetone (Neon, PA), forming a viscous paste. This paste was slowly diluted with 1.2 mL of water to reduce viscosity. Then, one drop of Triton X-100 (Synth) was added to the paste and mixed with 0.8 g of Fe/AC. The materials containing a mixture of the composite (Fe/AC) with TiO<sub>2</sub> were dried at 100 °C for 20 minutes and thermally treated at 350 °C for 30 minutes in tubular furnace with oxidizing atmosphere (synthetic air, 10 °C min<sup>-1</sup>). The magnetic photocatalysts were prepared with 1, 5, 20, 40, and 60% of TiO<sub>2</sub> (w/w) and named as following: 1Ti/Fe/AC, 5Ti/Fe/AC, 20Ti/Fe/AC, 40Ti/Fe/AC and 60Ti/Fe/AC, in which the number indicates the content of TiO<sub>2</sub>. Table 1 shows the denomination of each material and the respective amounts of Fe, AC, and TiO<sub>2</sub> used in the preparation of the magnetic photocatalysts.

**Table 1.** Magnetic photocatalysts and amounts of Fe, AC, and TiO<sub>2</sub> used in their preparation.

Magnetic photocatalyst	Fe content (g)	AC content (g) Thermal treatment at 800°C/N <sub>2</sub>	TiO <sub>2</sub> Content (g) Thermal treatment at 350°C/Synthetic Air
1Ti/Fe/AC	0.079	0.911	0.010
5Ti/Fe/AC	0.076	0.874	0.050
20Ti/Fe/AC	0.064	0.736	0.200
40Ti/Fe/AC	0.048	0.552	0.400
60Ti/Fe/AC	0.032	0.368	0.600

## 2.3 Characterization of magnetic photocatalysts

X-Ray Diffraction (XRD) analysis was performed in a Rigaku equipment, model Ultima IV, with Cu K  $\alpha = 1.54051 \text{ \AA}$ . Scans were performed between the angles  $15^\circ < 2\theta < 80^\circ$  with speed of  $4^\circ \text{ min}^{-1}$ . The average crystallite size was calculated using the Scherrer equation ( $d =$

$k\lambda/\beta\cos\theta$ ), where  $d$  is the crystal size (nm),  $\lambda$  is the wavelength of the incident beam (nm),  $\beta$  is the width a Half height of the most intense peak and  $\theta$  is the Bragg angle. The structure of the carbonaceous material in the composites was analyzed on a Raman spectrometer (Senterra Bruker) coupled to an optical microscope (OLYMPUS BX51). Samples were excited by laser at wavelength of 633 nm, with a potency of 0.2 mW. The number of conditions was 10 and the integration time was 10 seconds. Thermal analysis (TG) and differential thermal analysis (DTA) were performed in a Shimadzu equipment. Analyses were conducted with temperature ranging from 30 °C to 900 °C, with heating rate of 10 °C min<sup>-1</sup>, under synthetic air atmosphere (10 mL min<sup>-1</sup>). Elemental quantitative chemical analysis was detected by total reflection X-ray fluorescence spectrometry (S2 PICOFOX - Bruker). Scanning electron microscopy (SEM) analyses were performed using a LEO EVO 40XVP (Carl Zeiss SMT) equipment at 25 kV in order to study the morphology of the materials. Powder samples were fixed on double-sided carbon tape. Specific superficial areas were analyzed by adsorption and desorption of N<sub>2</sub> at 77 K using a Autosorb1-MP Quantachrome equipment. Samples were degassed at 200 °C for 24 hours before the analyses. A radiation analysis was performed to obtain the solid electron transition energy. The magnetic properties of the produced composites were measured using a vibrational sample magnetometer (VSM) (model EV9, Microsense) at room temperature under a magnetic field ranging from -20000 to 20000 Oe.

#### **2.4 Remazol Black dye removal study**

Two tests were performed to evaluate the efficiencies of the photocatalysts to remove Reactive Black dye (RB): (i) adsorption capacity and (ii) photocatalytic degradation tests. The adsorption tests were performed in the dark with constant magnetic stirring, where 60 mg of each photocatalyst was added to 200 mL of 40 mg L<sup>-1</sup> RB dye solution pH 5. At different time intervals, aliquots of the RB solution were collected and the supernatant was separated from the catalyst using either a magnet or centrifugation (1500 rpm for 3 minutes). Adsorption kinetics was accompanied by discoloration of RB supernatant solution using a visible UV spectrophotometer, where the variation of the intensity of the highest absorption band (598 nm) was monitored. The photocatalytic reactions, as well as the degradation kinetics (dye discoloration), were performed under the same experimental conditions of the adsorption tests. For this, a reactor equipped with low-pressure mercury lamp with emission spectrum at 254 nm (30W - Philips,  $I = 1.20 \text{ mW cm}^{-2}$ ) was used. The germicidal lamp was placed in the reactor's upper part at a distance of approximately 20 cm from the dye solution, and the radiation

incidence area was 13 cm of diameter. Before initiating the photocatalytic reactions, the remazol black dye solution was kept in the dark in contact with each catalyst for 1 h for adsorption. The efficiency of the photocatalysts to mineralize RB was evaluated at the end of the reactions by the reduction of total organic carbon (TOC). The TOC measurements were performed using a Shimadzu TOC – VCPH equipment, in which the analyzed supernatant was separated from the photocatalyst by centrifugation and filtration.

## **2.5 Sedimentation kinetics of the photocatalysts**

For sedimentation tests, 2 mg of magnetic photocatalyst or TiO<sub>2</sub> and 10 mL of distilled water were added in the sample holder, and the turbidity variation was monitored at different time intervals in the presence of a magnetic field (magnet), using a turbidimeter (Hanna Instruments HI 98703).

## **2.6 TiO<sub>2</sub> leaching tests**

The assessment of leachate in the reaction medium was evaluated to verify the removal of TiO<sub>2</sub> from the magnetic photocatalysts. For that, 60 mg of photocatalyst were left in contact with 100 mL of distilled water for 2 hours, under magnetic stirring. Then, the solid composites were separated from water (supernatant) with the aid of a magnet. Next, 100 mL of 80 mg L<sup>-1</sup> RB dye solution were added to the 100 mL of the previously obtained supernatant (the total resulting from 200 mL of 40 mgL<sup>-1</sup> RB solution) and submitted to photocatalytic reaction under the same conditions of the photocatalytic tests described on item 1.4, without the addition of the photocatalysts.

## **2.7 Catalyst recovery and reuse tests**

To verify the magnetic separation and reuse efficiency of the produced composites after the photocatalytic reaction, the material was recovered with the aid of a commercial magnet, washed with distilled water, oven dried at 60 °C, and weighed. Then, it was again put in contact with the dye solution. This procedure was repeated other three times.



### 3. Results and discussion

#### 3.1 Characterization of the materials

##### 2.6.1 3.1.1 X-ray diffraction (XRD)

Fig. 1 presents the diffractogram patterns of the samples of: TiO<sub>2</sub>, AC, Fe/AC and the photocatalysts 20, 40 and 60Ti/Fe/AC.

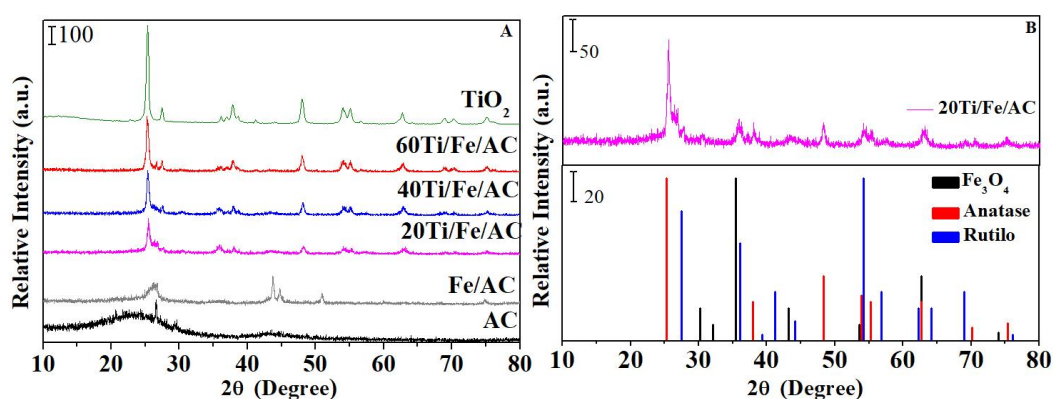


**Fig. 1.** A) Diffractogram of AC, Fe/AC, 20Ti/Fe/AC, 40Ti/Fe/AC, 60Ti/Fe/AC and TiO<sub>2</sub>. B) Expansion of 20Ti/Fe/AC diffractogram and Fe<sub>3</sub>O<sub>4</sub>, anatase and rutile standards.

The extended signals centered at 23° and 43° in the activated carbon diffractogram confirmed the presence of amorphous carbon and the signal at 26° indicated the presence of graphitic carbon (JCPDS, 12-0212). In the Fe/AC diffractogram, there are signals at 51° and 75° that indicated the presence of organized carbon (JCPDS, 43-11004). In this diffractogram, the reflection line referring to Fe<sup>0</sup> (44.2°- JCPDS, 03-1050) formed during the thermal treatment by the Fe<sup>3+</sup> reduction reaction as showed by Eq. 1 can also be observed.



The photocatalysts presented diffraction lines in the stages of anatase (JCPDS, 02-0387) and rutile (JCPDS, 01-1292) of TiO<sub>2</sub> and Fe<sub>3</sub>O<sub>4</sub> (JCPDS, 07-0322). These results show that after supporting TiO<sub>2</sub> on the surface of the composite Fe/AC, Fe<sup>0</sup> was oxidized into Fe<sub>3</sub>O<sub>4</sub>. This can be explained by the presence of O<sub>2</sub> during the thermal treatment at 350°C during the preparation of materials, Eq. 2.



The intensity of the diffraction lines of the anatase and rutile phases increased with the TiO<sub>2</sub> contents in the photocatalysts and the C and Fe<sub>3</sub>O<sub>4</sub> peak intensities decreased. The

presence of Fe<sup>0</sup> and Fe<sub>3</sub>O<sub>4</sub> explains the magnetic activity of the composite Fe/AC and of the photocatalysts, respectively.

According to the results of Fig. 1, the average crystallite size was calculated for the reflection with 100% intensity. The mean diameter was calculated by the Scherrer equation for the anatase phase of TiO<sub>2</sub> at 26°, assuming that the greater the width and half height of the more intense anatase peak, the smaller the crystallites should be. The magnetic photocatalysts 20, 40 and 60Ti/Fe/AC showed a mean crystallite size of 23.9, 24.3 and 27.1 nm, respectively. The higher is the percentage of TiO<sub>2</sub> present in the material, the higher is the anatase crystallite. These values are higher than the pure TiO<sub>2</sub> crystallite (23 nm).

### 1.1.1 3.1.2 X-ray Fluorescence

The percentage of iron and titanium in the materials was estimated by X-Ray fluorescence (XRF) and the content of TiO<sub>2</sub> and C were calculated from these values (Table 2).

**Table 2.** Carbon, iron and titanium contents in materials obtained with AC.

Sample	C (%)	Fe (%)	Ti (%)	TiO <sub>2</sub> (%)
AC/Fe	94.3	5.6	0	0
20Ti/Fe/AC	55.0	8.0	20.2	33.8
40Ti/Fe/AC	48.3	5.6	26.3	43.9
60Ti/Fe/AC	40.3	3.6	32.8	54.7

The contents of TiO<sub>2</sub> found for the photocatalysts 40 and 60Ti/C/Fe are around 44 and 55%, respectively, which is close to the expected values of 40 and 60%. The photocatalyst 20Ti/C/Fe presented TiO<sub>2</sub> and Fe contents higher than expected, with 34 and 8%, respectively. This may have occurred due to carbon oxidation while the photocatalyst was being prepared (Eq. 3), since the sample was heated at 350°C, under oxidizing atmosphere.



Thus, with the reduction of the activated carbon present in the material, the contents of TiO<sub>2</sub> and Fe increased. The contents of Fe and C in the photocatalysts 40 and 60Ti/C/Fe followed the expected trend, considering that the increase in the content of TiO<sub>2</sub> in the photocatalysts leads to a reduction of iron and carbon contents present in the magnetic support.

### 1.1.2 3.1.3 Raman spectroscopy

Raman spectroscopy is an efficient method to analyze the structure of the carbon formed in the material. Fig. 2 shows the Raman spectra obtained for AC, Fe/AC, 20, 40 and 60Ti/Fe/AC.

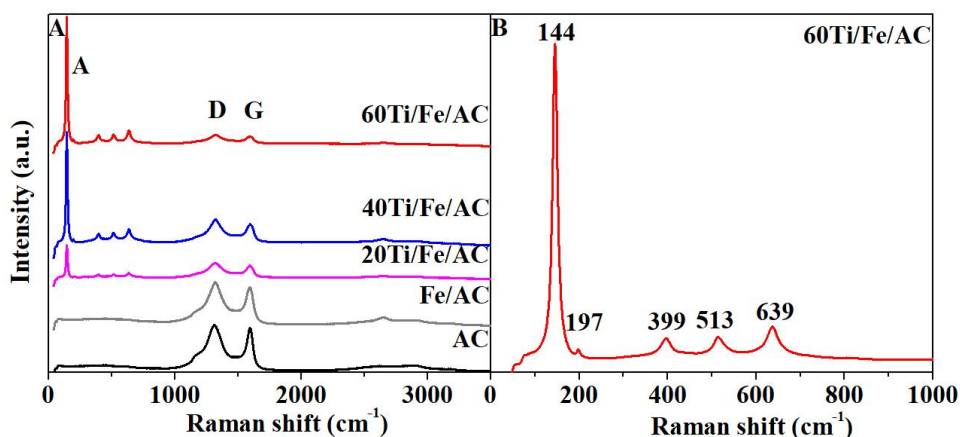


**Fig. 2.** A) Raman spectra obtained for AC, Fe/AC, 20, 40 and 60Ti/Fe/AC. B) Expansion of the Raman spectrum for 60Ti /Fe/AC.

It is observed in Fig. 2 that all materials showed bands in  $1315\text{ cm}^{-1}$  (band D) and  $1596\text{ cm}^{-1}$  (band G), which indicate the presence of amorphous and organized carbon, respectively.

According to Ohsaka, Izumi and Fujiki [31],  $\text{TiO}_2$  anatase phase has six bands in Raman with the largest appearing at  $144\text{ cm}^{-1}$ , followed by other five low-intensity bands at 197, 399, 513, 519 and  $641\text{ cm}^{-1}$ . Rutile has only four bands, located at 143, 236, 447 and  $613\text{ cm}^{-1}$ . It is observed in Fig. 2B that the  $\text{TiO}_2$  anatase phase is present in the photocatalyst because the presented bands are in accordance with the literature. Nevertheless, it was impossible to observe the bands in the rutile phase, once it is presented in smaller amounts in  $\text{TiO}_2$ -P25. Raman spectra did not present signals related to the iron phase due to the low content of this phase in the materials. Table 3 presents the ratios between bands G and D ( $I_G/I_D$ ), A (Anatase) and G ( $I_A/I_G$ ) and A and D ( $I_A/I_D$ ) intensities obtained from Raman spectra.

Intensity ratios from band G to band D ( $I_G/I_D$ ) for AC and Fe/AC are 0.947 and 0.896, respectively. The decrease of the  $I_G/I_D$  ratio suggests that the relative quantity of graphitic carbon decreases after the thermal treatment. It indicates that graphitic carbon reduced  $\text{Fe}^{3+}$  to  $\text{Fe}^0$  during thermal treatment, as presented by equation (1). On the other hand, the  $I_G/I_D$  ratio obtained for the photocatalysts presented similar values.

In the Raman spectra of the photocatalysts 20, 40 and 60Ti/Fe/AC, a band intensity increase is clearly noted at  $144\text{ cm}^{-1}$ , which is related to the increase of  $\text{TiO}_2$  content. This is

confirmed by the increase observed in the values of  $I_A/I_G$  and  $I_A/I_D$  ratios, as presented in Table 3.

**Table 3.** Ratios between bands G and D ( $I_G/I_D$ ), A (Anatase) and G ( $I_A/I_G$ ) and A and D ( $I_A/I_D$ ) intensities obtained from Raman spectra of materials obtained from commercial AC.

Sample	$I_G/I_D$	$I_A/I_G$	$I_A/I_D$
AC	0.947	-	-
Fe/AC	0.896	-	-
20Ti/Fe/AC	0.890	0.669	1.78
40Ti/Fe/AC	0.889	3.71	3.29
60Ti/Fe/AC	0.895	8.45	7.56

### 3.1.4 Thermal Analysis (TG)

Thermal analysis presents mass loss of materials due to temperature variation. Fig. 3 shows the TG and DTA curves obtained from the photocatalysts, the magnetic support and activated carbon in oxidizing atmosphere.

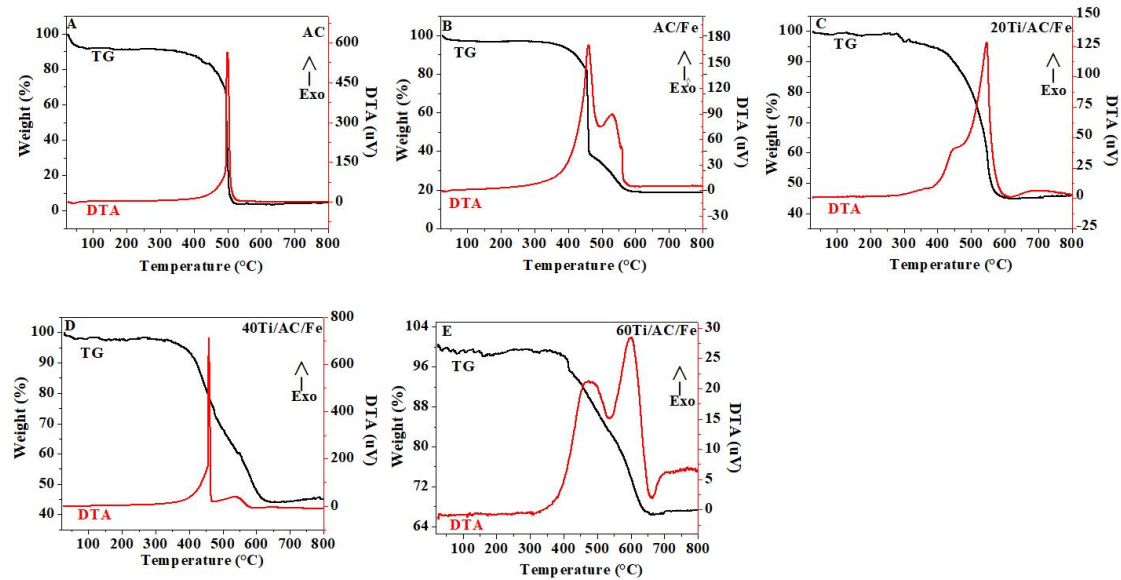
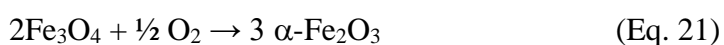


**Fig. 3.** TG and DTA curves obtained from A) AC, B) Fe/AC, C) 20Ti/Fe/AC, D) 40Ti/Fe/AC and E) 60Ti/Fe/AC in oxidizing atmosphere ( $O_2$ ).

A small mass loss around 100 °C related to adsorbed water [11] is observed for all materials. For AC, there is a loss of 89% of mass from 350 to 530 °C, which is related to the

thermal decomposition of the activated carbon (Eq. 3), and it is accompanied by an exothermic effect on the DTA curve (Fig. 3A) [18]. The residual mass is attributed to ash.

Figure 3B shows the TG/DTA curve of the Fe/AC composite characterized by the presence of coal and iron in its composition. The TG-DTA profile of the composite composed of more than one material directly reflects the surface discontinuity of the mixture, causing loss of mass with superimposed exothermic events. These events are related to carbon oxidation around 450 °C, and the second, at higher temperatures (ca 520 °C), is related to the oxidation of the metallic iron and oxidation products (Eqs. 4-6), [32].



For the weight losses from 350 to 650°C of the magnetic photocatalysts, two important considerations must be made:

(i) mass losses for the materials containing 20, 40, and 60% of TiO<sub>2</sub> is 54, 53 and 32%, respectively, which can also be attributed to activated carbon decomposition. The residual in ash, corresponding to the phases of the iron and titanium oxides, increased proportionally to the content of TiO<sub>2</sub>;

(ii) on the other hand, with respect to the definition of the DTA signal, these materials have a broad peak related to the exothermic events of iron and carbon oxidation. This signal reverses the intensity of its maximum point, especially for larger amounts of TiO<sub>2</sub>. The displacement of the exothermic event to higher temperatures present in these materials suggests the formation of more thermostable structures. There appears to be a synergistic behavior between the components that thermally stabilizes both the carbonaceous matrix and the magnetic phases. This phenomenon can be evidenced by the increase in the baseline shown in Fig. 3E, typical for stable alloys with thermal conductivity higher than that exhibited by the starting materials [27].

### 3.1.5 Scanning electron microscopy (SEM)

Scanning electron microscopy was used to investigate the morphology of AC, Fe/AC and the photocatalyst composites, as shown in Fig. 4.

Fig. 4A and B show a fibrous structure with different diameter cavities in various shapes that are inherent to all activated carbons. Micrographies of the composite Fe/AC (Fig. 4C and D) are similar to the images in Fig. 4A and B, showing that after the addition of iron to the AC, there was no significant change in the morphology of the material. In images C and D of Fig.

4, it is not possible to clearly observe the presence of iron on AC surface, which indicates that this material could have been formed inside the AC cavity.

On the other hand, in the images obtained by SEM for the photocatalysts, it is possible to observe that new clumps of particles were deposited on the structure of the carbon matrix, especially that there is a filling of the valleys between the cavities of the material. This new profile displayed by the blocks of Ti/Fe/AC suggests that their cavities are agglomerated with uniformly dispersed  $\text{TiO}_2$  particles. It is also noted that the higher the  $\text{TiO}_2$  percentage used in the synthesis of materials, the more the support will be coated in  $\text{TiO}_2$ .

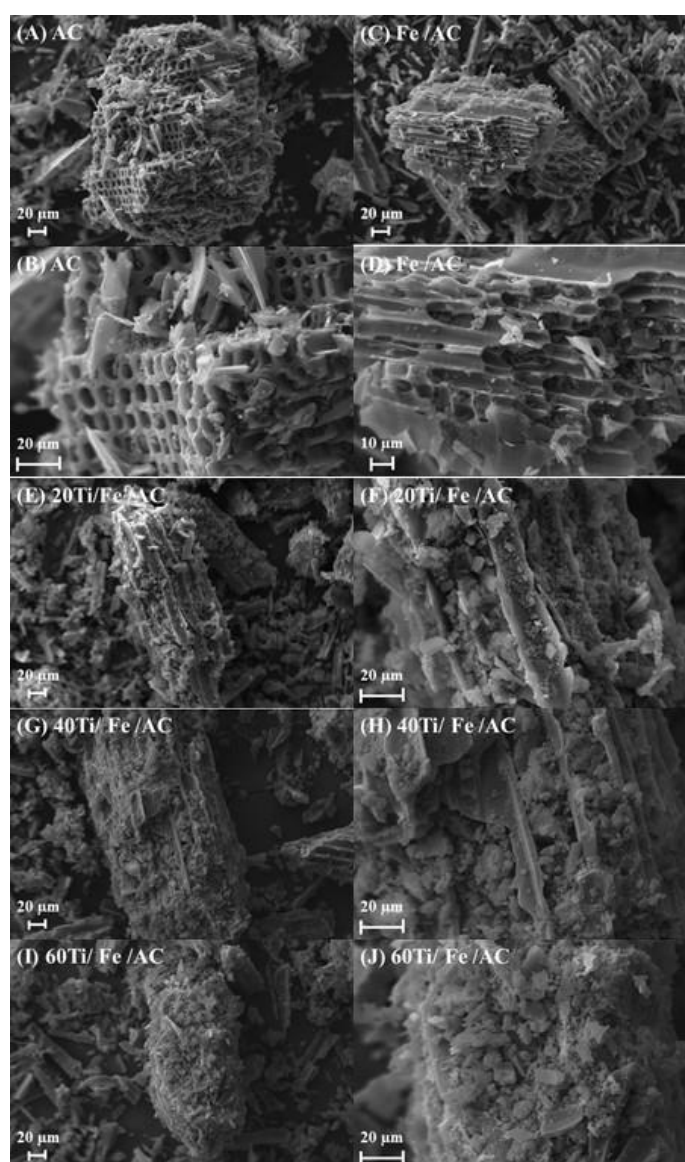


**Fig. 4.** Images obtained by SEM of AC, Fe/AC and photocatalysts (500 and 1500x magnitude).

### 1.1.3 3.1.6 Specific surface area

Table 4 shows the results of the adsorption/desorption isotherms measurements for commercial AC, magnetic support and the photocatalysts 20, 40 and 60Ti/Fe/AC.

**Table 4.** Specific surface area measurements for AC, Fe/AC, TiO<sub>2</sub> and the photocatalysts 20, 40 and 60Ti/Fe/AC.

Sample	Specific surface area (BET) (m <sup>2</sup> g <sup>-1</sup> )
AC	710
Fe/AC	485
20Ti/Fe/AC	283
40Ti/Fe/AC	259
60Ti/Fe/AC	165
TiO <sub>2</sub> P25	65

The activated carbon used in this study presented superficial area equal to 710 m<sup>2</sup> g<sup>-1</sup>, while for the magnetic support Fe/AC this value is 485 m<sup>2</sup> g<sup>-1</sup>. The reduction of the surface area of the carbon phase after impregnation with iron can be explained by the fact that iron occupies part of the pores. In addition, part of the mass that comprises the material is formed by metallic iron, whose specific surface area is intrinsically low. These two added factors certainly caused a decrease in the area of the composite-type material relative to the AC area.

Otherwise, when evaluating the specific surface area of the commercial semiconductor TiO<sub>2</sub>-P25, it can be verified that the oxide exhibits a very compact crystalline structure, which leads to a relatively low area (65 m<sup>2</sup> g<sup>-1</sup>) when compared to others oxides.

For this material with photocatalytic sensitivity, when comparing the superficial areas of the composite magnetic/carbon/materials with TiO<sub>2</sub> P25, it is observed that there has been significant increase, proving the efficiency of incorporating activated carbon with TiO<sub>2</sub>, to increase the superficial area, enabling more catalytic applicability. The superficial areas obtained for the photocatalysts 20, 40 and 60 Ti/Fe/AC were 283, 259 and 164 m<sup>2</sup> g<sup>-1</sup>, respectively. The reduction of the superficial area in comparison with Fe/AC is due the occupation of TiO<sub>2</sub> in the magnetic support pores (Zhang et al., 2014). These results can also be confirmed by SEM, where TiO<sub>2</sub> agglomerations are observed on the surface of Fe/AC pores. Fig. 5 shows the adsorption and desorption isotherms of N<sub>2</sub> for the studied materials.

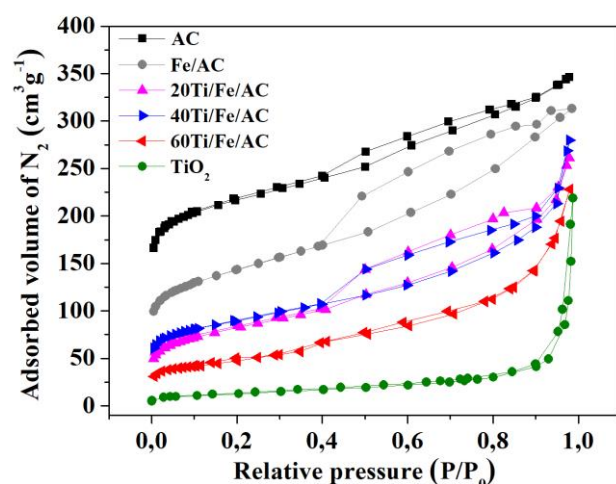


**Fig. 5.** Adsorption and desorption isotherms of  $N_2$  for AC, Fe/AC,  $TiO_2$ , and the photocatalysts 20, 40 and 60Ti/Fe/AC.

Fig. 5 shows the results of the  $N_2$  physisorption analysis for the materials. Together with the specific surface area data, the isotherm profile provides very relevant information about the materials. According to the IUPAC classification, the isotherms of AC, Fe/AC, 20 and 40Ti/Fe/AC are type 4A, which are characteristic of mesoporous materials characterized by desorption hysteresis, with some microporosity. Hysteresis is formed when the desorption curve does not coincide with the adsorption curve of the isotherm, where the bottom line represents the amount of gas adsorbed with increasing pressure, and the line above the amount of desorbed gas. The hysteresis of these materials is of type H4, which refers to non-homogeneous laminar pores that may have interconnectivity. The isotherm profile does not exclude the presence of microporosity, with openings smaller than  $20 \text{ \AA}$  [33].

The isotherm profile of sample 60Ti/Fe/AC has a characteristic similar to the  $TiO_2$  isotherm profile. This can be explained by the fact that this photocatalyst has a higher amount of  $TiO_2$  in its composition than the other materials, which presented type B isotherms that are also characteristic of mesoporous materials, with mesopores of smaller width as compared to materials of type 4A isotherms [33]. The fact that these materials possess mesopores of smaller diameter width can be explained by the smaller amount of iron in mass present of material. Iron may participate in the activation process of AC during the heat treatment and contribute to the formation of mesoporosity. Thus, the higher the percentage of iron in the materials, the greater the tendency in the width of the mean diameter of the pores. Corroborating this data, in the



isotherm for pure  $\text{TiO}_2$ , practically no typical hysteresis signal exists in  $P/P_0$  higher than 0.5, emphasizing the importance of the magnetic phases.

### 3.1.7 Magnetic properties

The magnetic properties of the photocatalysts were investigated using VSM analysis at room temperature, on the magnetic field range from -2000 to 2000 Gauss. The hysteresis cycles of the materials are presented in Fig. 6.

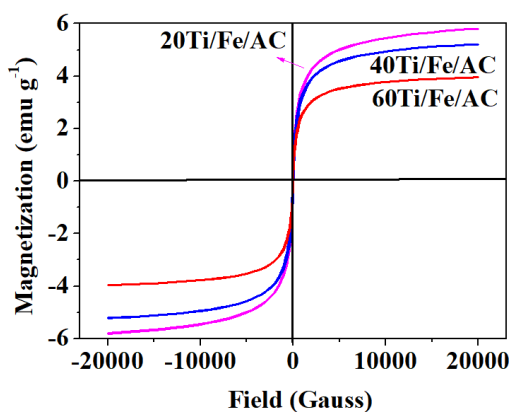


**Fig. 6.** Hysteresis cycles of samples 20, 40 and 60Ti/Fe/AC.

The saturation magnetization values ( $M_s$ ) of the photocatalysts 20, 40 and 60Ti/Fe/AC were 5.8, 5.2 and 4.0  $\text{emu g}^{-1}$ , respectively. The magnetic property of these materials is due to the presence of magnetite, once  $\text{TiO}_2$  and the activated carbon are not magnetic. Thus, the higher the iron percentage in the photocatalyst, the higher the  $M_s$  value.

### 3.2 RB dye adsorption study in the magnetic photocatalysts and photocatalytic tests

Adsorption and photocatalysis with adsorption study for AC, Fe/AC, 1, 5, 20, 40 and 60Ti/Fe/AC and  $\text{TiO}_2$  was conducted and the results are showed in Fig. 7 A and B, respectively.

It is observed in Fig. 7A that  $\text{TiO}_2$  adsorbed only 5% of RB dye after 240 minutes of contact. The magnetic support Fe/AC adsorbed 48% of RB dye. It is noted that the adsorption is faster during the first 60 minutes of contact and, after that, it becomes slower. With 240 minutes of contact between the materials and the RB solution, it was possible to observe adsorptions of 35, 40, 28, 27 and 28% in the photocatalysts 1, 5, 20, 40 and 60Ti/Fe/AC, respectively. These results are expected considering that the higher the percentage of Fe/AC in photocatalysts, the larger the superficial area and higher the adsorption. It is also noted that the photocatalysts 20, 40 and 60Ti/Fe/AC presented very similar adsorption results.

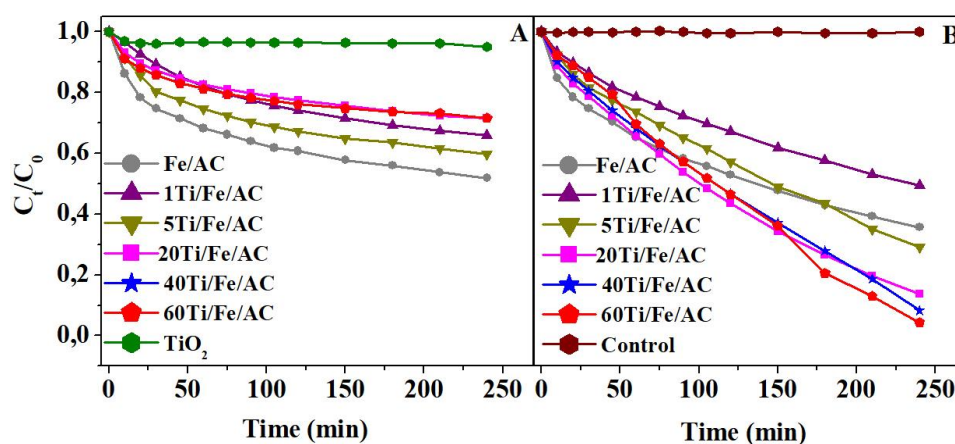


**Fig. 7.** A) Adsorption and B) photocatalysis for Fe/AC, 1, 5, 20, 40 and 60Ti/Fe/AC and TiO<sub>2</sub>.

It is observed in Fig. 7B that there was no significant discoloration in 240 minutes in the control reaction, which is just dye solution in the presence of UV radiation. Thus, it can be concluded that 51-W UV light alone is not enough to discolor the RB and no photolysis reaction at that wavelength is verified.

The results shown in Fig. 7B present a significant part of RB dye discoloration, being 64, 50, 69, 86, 92 and 95% for Fe/AC, 1, 5, 20, 40 and 60Ti/Fe/AC, respectively. However, part of this discoloration is from adsorption and part from photocatalysis. Thus, with the results for adsorption presented in Fig. 7A, it was possible to calculate the percentage of discoloration presented by RB dye solution due to photocatalytic activity of the studied materials. The percentage of discoloration of the RB dye only from photocatalysis was 16, 17, 28, 58, 64 and 67% for the Fe/AC, 1, 5, 20, 40 and 60Ti/Fe/AC, respectively.

It should be noted that Fe/AC presented about 16% RB removal attributed to photocatalysis, showing to be a material with photoactive behavior. According to Velo-Gala et al. [34] activated carbons behave as semiconductor materials, being active in the presence of UV radiation. The photoactive ability of the activated carbon is controversial because it is not a property inherent to the material. However, authors have reported the ability displayed by this material to absorb UV light photons and generate hydroxyl radicals in aqueous medium. However, studies that allow explaining this behavior and proposing mechanisms are still required [35,34].

When comparing the photocatalytic efficiency of 1 and 5Ti/Fe/AC with the other photocatalysts (20, 40 and 60Ti/Fe/AC), it is observed that only 1 and 5% TiO<sub>2</sub> used in the synthesis of these materials were not enough to promote good discoloration by photocatalysis

of the pollutant used in this study. Thus, this study focused only on the photocatalysts 20, 40 and 60Ti/Fe/AC, making the characterization of the other materials unnecessary.

Considering RB discoloration kinetics by photocatalysts 20, 40 and 60Ti/Fe/AC as pseudo-zero order, the reaction rate constants ( $k$ ) were obtained and they are presented in Fig. 8.

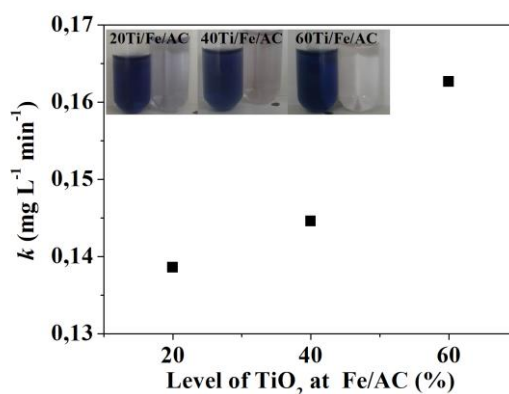


**Fig. 8.** Reaction rate constants obtained for reactions using photocatalysts 20, 40 and 60Ti/C/Fe.

It is noted that the values of the reaction rate constants for the photocatalysts 20, 40 and 60Ti/Fe/AC increased with the content of TiO<sub>2</sub>. The images of RB solutions after photocatalytic reactions within Fig. 8 confirmed the efficiency of photocatalysts, because after 240 minutes of reaction the solutions acquired practically clear aspects.

Dye removal was also accompanied by TOC analysis, where TiO<sub>2</sub>, 20, 40 and 60Ti/Fe/AC photocatalysts removed 88, 21, 71 and 90% of organic matter, respectively. These results show the potential of these materials to wastewater treatment.

Similar photocatalysts were prepared by our research group [36], where TiO<sub>2</sub> P25 was supported on the surface of the composite coal/reduced red mud (C/RM). The photocatalysts obtained presented 36-71% efficiency for discoloration of 40 mgL<sup>-1</sup> remazol black. Considering that the experimental conditions of the photocatalytic reactions used in both studies were very similar, it is perceived that the photocatalysts have near photocatalytic activity.

Hung et al. [37] and Zhang et al. [38] prepared the Fe<sub>3</sub>O<sub>4</sub>/SiO<sub>2</sub>/TiO<sub>2</sub> and Fe<sub>3</sub>O<sub>4</sub>@C@TiO<sub>2</sub> photocatalysts, respectively, and tested the efficiency for 10 mg L<sup>-1</sup> methylene blue degradation, where the concentration of catalyst used was 0.5 mg L<sup>-1</sup>. In the first study, the photocatalyst presented 15% efficiency to degrade methylene blue after 320 minutes of reaction in the presence of sunlight. On the other hand, the photocatalyst Fe<sub>3</sub>O<sub>4</sub>@C@TiO<sub>2</sub> obtained by Zhang et al. [38] degraded 96% of the dye after 8 minutes of reaction using a 500

W medium pressure Hg lamp, which is related to the high power of the lamp used. In the study of Li et al. [39],  $1.25 \text{ mg mL}^{-1}$  of the photocatalyst -  $\text{Fe}_3\text{O}_4/\text{SiO}_2/\text{TiO}_2$  was used to degrade  $50 \text{ mg L}^{-1}$  methyl orange dye in the presence of a 15 W Hg lamp. The authors showed that c.a 93% of the dye was degraded after 120 minutes of reaction. Good results using a lamp of lower power to degrade a more concentrated contaminant were obtained. However, comparing it to the present study, a larger mass of photocatalyst was used and the design of the reactor was not presented.

Thus, it is observed that the experimental conditions used by different authors are distinct, which makes it difficult to make a direct comparison of the photocatalytic efficiency, since it depends on several factors, such as volume of solution, concentration and type of contaminant model, power and type of radiation source, reactor design, reaction time, presence of oxidizing species, mass, morphology, surface area and type of photocatalyst.

### 3.3 Sedimentation kinetics

Fig. 9 presents the sedimentation kinetics of pure  $\text{TiO}_2$  and of the photocatalysts in the presence of a magnet.

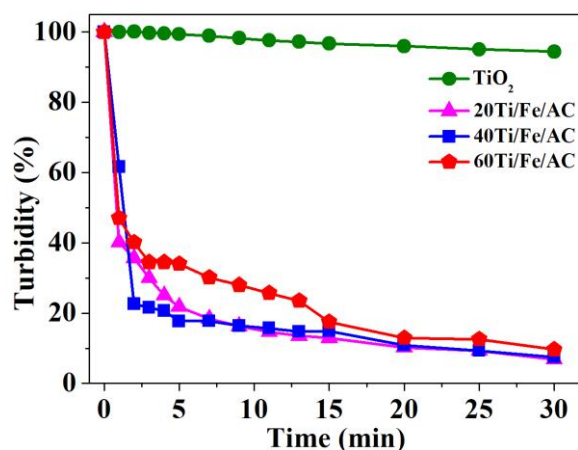


**Fig. 9.**  $\text{TiO}_2$  and magnetic photocatalysts sedimentation kinetics obtained from AC.

It is observed that in the presence of magnetic field, it was possible to sediment 93, 92 and 90% of photocatalysts 20, 40 and 60Ti/Fe/AC, while  $\text{TiO}_2$  presented only 6% of sedimentation during 30 minutes. When comparing this result with the iron percentage obtained by XRF, it is observed that the higher the iron content in the photocatalysts, the easier it

separates from the effluent treated. This is related to the higher magnetization presented by the photocatalysts with higher iron contents, according to results obtained by VSM.

These results confirm the efficiency of incorporating a magnetic phase to the TiO<sub>2</sub>.

### 3.4 Leaching tests

To evaluate if TiO<sub>2</sub> is being leached from the photocatalysts, the materials were submitted to leaching test.

The results show that all materials presented a small percentage of dye discoloration, being 12, 5 and 10% for the photocatalysts 20, 40 and 60Ti/Fe/AC, respectively, indicating that a small portion of TiO<sub>2</sub> was leached.

### 3.5 Photocatalyst recovery and reuse tests

An important factor from the economic point of view is the possibility of recovering and reusing a photocatalyst. Fig. 2S in the Supplementary Material presents the recovery and reuse efficiency of the magnetic photocatalysts. It was possible to recover 67, 50 and 44% of photocatalysts 20, 40 and 60Ti/Fe/AC, respectively, after the fourth reuse reaction. These results are in accordance with those expected, provided that the higher the percentage of iron in these materials, the higher their saturation magnetization and possibility of recovery.

After four successive uses, a reduction of 29, 13 and 0% for photocatalysts 20, 40 and 60Ti/Fe/AC, respectively, was observed in the discoloration efficiency of RB dye. The higher the percentage of TiO<sub>2</sub> in the photocatalyst, the more efficient is the reaction.

## 4. Conclusion

The results obtained for the characterization of Ti/Fe/AC showed that the synthesis of magnetic photocatalysts was efficient, showing the presence of TiO<sub>2</sub>, Fe<sub>3</sub>O<sub>4</sub> and Fe<sup>0</sup> supported on activated carbon surface. All prepared magnetic photocatalysts presented excellent photocatalytic efficiency to discolor RB dye, reducing up to 95% of the color of the solution when using radiation from a 51-W - UV-C lamp. The results of VSM analysis and the magnetic separation tests showed that the magnetization of the photocatalysts increases with the increase in Fe contents and that it is possible to sediment up to 90% of the particles in a few minutes, when a magnetic field is applied. Due to their magnetic and photocatalytic properties, the studied materials presented great efficiency in the tests of recovery and degradation of remazol

black in up to four successive cycles. Thus, these materials present great potential for scale up applications, since they are efficient under UV radiation and easy to be recovered from the effluent treated avoiding additional steps, which may reduce the costs of industrial processes.

## 5. Acknowledgements

The authors gratefully thank UFLA, FAPEMIG, Capes and CNPq for the financial support and the Scanning Electronic Microscopy Laboratory of UFLA, Central of Analysis and Chemical Prospecting of UFLA, Elementary Analysis Laboratories of UNIFAL-MG, Electronic Microscopy Center of the UFMG and for the characterization analyzes.

## 6. References

1. M. Stefan, C. Leostean, O. Pana, D. Toloman, A. Popa, I. Perhaita, M. Senilă, O. Marincaș, L. Barbu-Tudoran. Magnetic recoverable Fe<sub>3</sub>O<sub>4</sub>-TiO<sub>2</sub>:Eu composite nanoparticles with enhanced photocatalytic activity. *Appl. Surf. Sci.* 390, (2016) 248–259. <https://doi.org/http://dx.doi.org/10.1016/j.apsusc.2016.08.084>.
2. P. Dhiman, M. Naushad, K. Mujasam, A. Kumar, G. Sharma, A. A. Ghfar, G. Kumar, M. Singh. Nano Fe x Zn 1 Å x O as a tuneable and efficient photocatalyst for solar powered degradation of bisphenol A from aqueous environment. *J. Clean. Prod.* 165, (2017) 1542–1556. <https://doi.org/http://dx.doi.org/10.1016/j.jclepro.2017.07.245>.
3. J. Wang, Y. Chen, G. Liu, Y. Cao. Synthesis, characterization and photocatalytic activity of inexpensive and non-toxic Fe<sub>2</sub>O<sub>3</sub>-Fe<sub>3</sub>O<sub>4</sub> nano-composites supported by montmorillonite and modified by graphene. *Compos. Part B Eng.* 114, (2017) 211–222. <https://doi.org/http://dx.doi.org/10.1016/j.compositesb.2017.01.055>.
4. F. H. Mustapha, A. A. Jalil, M. Mohamed, S. Triwahyono, N. S. Hassan, N. F. Khusnun, C. N. C. Hitam, A. F. A. Rahman, L. Firmanshah, A. S. Zolkifli, A. New insight into self-modified surfaces with defect-rich rutile TiO<sub>2</sub> as a visible-light-driven photocatalyst. *J. Clean. Prod.* 168, (2017) 1150–1162. <https://doi.org/http://dx.doi.org/10.1016/j.jclepro.2017.09.095>.
5. S. Miaralipour, D. Friedmann, J. Scott, R. Amal. TiO<sub>2</sub>/porous adsorbents: Recent advances and novel applications. *J. Hazard. Mater.* 341, (2018) 404–423. <https://doi.org/http://dx.doi.org/10.1016/j.jhazmat.2017.07.070>.
6. M. Tahir. Photocatalytic carbon dioxide reduction to fuels in continuous flow monolith photoreactor using montmorillonite dispersed Fe/TiO<sub>2</sub> nanocatalyst. *J. Clean. Prod.* 170, (2018) 242–250. <https://doi.org/https://doi.org/10.1016/j.jclepro.2017.09.118>.
7. M. E. Borges, M. Sierra, E. Cuevas, R. D. García, P. Esparza. Photocatalysis with solar energy: Sunlight-responsive photocatalyst based on TiO<sub>2</sub> loaded on a natural material for wastewater treatment. *Sol. Energy* 135, (2016) 527–535. <https://doi.org/http://dx.doi.org/10.1016/j.solener.2016.06.022>.
8. G. Zhang, A. Song, Y. Duan, S. Zheng. Microporous and Mesoporous Materials Enhanced photocatalytic activity of TiO<sub>2</sub>/zeolite composite for abatement of pollutants.

- Microporous Mesoporous Mater. 255, (2018) 61–68.  
<https://doi.org/http://dx.doi.org/10.1016/j.micromeso.2017.07.028>.
9. J. Sun, X. Liu, F. Zhang, J. Zhou, J. Wu, A. Alsaedi, T. Hayat, J. Li. Insight into the mechanism of adsorption of phenol and resorcinol on activated carbons with different oxidation degrees. *Colloids Surfaces A Physicochem. Eng. Asp.* (2018) <https://doi.org/10.1016/j.colsurfa.2018.11.042>.
  10. P. Sun, R. Xue, W. Zhang, I. Zada, Q. Liu, J. Gu, H. Su, Z. Zhang, J. Zhang, D. Zhang. Photocatalyst of organic pollutants decomposition: TiO<sub>2</sub>/glass fiber cloth composites. *Catal. Today* 274, (2016) 2–7.  
<https://doi.org/http://dx.doi.org/10.1016/j.cattod.2016.04.036>.
  11. A. Mavrogiorgou, M. Louloud. Pyrolytic carbon as support matrix for heterogeneous oxidation catalysts: The influence of pyrolytic process on catalytic behavior. *J. Environ. Chem. Eng.* 6, (2018) 1127–1136.  
<https://doi.org/https://doi.org/10.1016/j.jece.2018.01.040>.
  12. F. Wu, W. Liu, J. Qiu, J. Li, W. Zhou, Y. Fang, S. Zhang, X. Li. Applied Surface Science Enhanced photocatalytic degradation and adsorption of methylene blue via TiO<sub>2</sub> nanocrystals supported on graphene-like bamboo charcoal. *Appl. Surf. Sci.* 358, (2015) 425–435. <https://doi.org/http://dx.doi.org/10.1016/j.apsusc.2015.08.161>.
  13. A. C. Martins, A. L. Cazetta, O. Pezoti, J. R. B. Souza, T. Zhang. Sol-gel synthesis of new TiO<sub>2</sub> / activated carbon photocatalyst and its application for degradation of tetracycline. *Ceram. Int.* 43, (2017) 4411–4418.  
<https://doi.org/http://dx.doi.org/10.1016/j.ceramint.2016.12.088>.
  14. S. Landi, J. Carneiro, S. Ferdov, A. M. Fonseca, I. C. Neves, M. Ferreira, P. Parpot, O. S. G. P. Soares, M. F. R. Pereira. Journal of Photochemistry and Photobiology A : Chemistry Photocatalytic degradation of Rhodamine B dye by cotton textile coated. *J. Photochem. Photobiol. A Chem.* 346, (2017) 60–69.  
<https://doi.org/http://dx.doi.org/10.1016/j.jphotochem.2017.05.047>.
  15. N. N. T. Darja Maučec, Andraž Šuligoj, Alenka Ristić, Goran Dražić, Albin Pintar. Titania versus zinc oxide nanoparticles on mesoporous silica supports as photocatalysts for removal of dyes from wastewater at neutral pH. *Catal. Today* 310, (2018) 32–41.  
<https://doi.org/10.1016/j.cattod.2017.05.061>.
  16. N. Setthaya, P. Chindapasirt, S. Yin, K. Pimraksa. TiO<sub>2</sub>-zeolite photocatalysts made of metakaolin and rice husk ash for removal of methylene blue dye. *Powder Technol.* 313, (2017) 417–426. <https://doi.org/http://dx.doi.org/10.1016/j.powtec.2017.01.014>.
  17. Y. H. Chen, Y. Y. Liu, R. H. Lin, F. S. Yen. Photocatalytic degradation of p-phenylenediamine with TiO<sub>2</sub>-coated magnetic PMMA microspheres in an aqueous solution. *J. Hazard. Mater.* 163, (2009) 973–981.  
<https://doi.org/http://dx.doi.org/10.1016/j.jhazmat.2008.07.097>.
  18. P. Benjwal, K. Kamal. Simultaneous photocatalysis and adsorption based removal of inorganic and organic impurities from water by titania/activated carbon/carbonized epoxy nanocomposite. *J. Environ. Chem. Eng.* 3, (2015) 2076–2083.  
<https://doi.org/https://doi.org/10.1016/j.jece.2015.07.009>.

19. D. Li, J. Xie, Y. Zhang, R. Qiao, S. Li, Z. Li. Convenient synthesis of magnetically recyclable  $\text{Fe}_3\text{O}_4@\text{C}@\text{CdS}$  photocatalysts by depositing CdS nanocrystals on carbonized ferrocene. *J. Alloys Compd.* 646, (2015) 978–982. <https://doi.org/http://dx.doi.org/10.1016/j.jallcom.2015.06.075>.
20. C. Chen, D. Jaihindh, S. Hu, Y. Fu. Journal of Photochemistry and Photobiology A : Chemistry Magnetic recyclable photocatalysts of Ni-Cu-Zn ferrite@ $\text{SiO}_2$ @  $\text{TiO}_2$ @Ag and their photocatalytic activities. *J. Photochem. Photobiol. A Chem.* 334, (2017) 74–85. <https://doi.org/http://dx.doi.org/10.1016/j.jphotochem.2016.11.005>.
21. M. Wilson, C. Y. C. Cheng, G. Oswald, R. Srivastava, S. K. Beaumont, J. P. S. Badyal. Magnetic recyclable microcomposite silica-steel core with  $\text{TiO}_2$  nanocomposite shell photocatalysts for sustainable water purification. *Colloids Surfaces A Physicochem. Eng. Asp.* 523, (2017) 27–37. <https://doi.org/http://dx.doi.org/10.1016/j.colsurfa.2017.03.034>.
22. T. Xin, M. Ma, H. Zhang, J. Gu, S. Wang, M. Liu, Q. Zhang. A facile approach for the synthesis of magnetic separable  $\text{Fe}_3\text{O}_4@\text{TiO}_2$ , core-shell nanocomposites as highly recyclable photocatalysts. *Appl. Surf. Sci.* 288, (2014) 51–59. <https://doi.org/http://dx.doi.org/10.1016/j.apsusc.2013.09.108>.
23. Y. Liu, L. Zhou, Y. Hu, C. Guo, H. Qian, F. Zhang, X. W. Lou. Magnetic-field induced formation of 1D  $\text{Fe}_3\text{O}_4/\text{C}/\text{CdS}$  coaxial nanochains as highly efficient and reusable photocatalysts for water treatment. *J. Mater. Chem.* 21, (2011) 18359–18364. <https://doi.org/http://dx.doi.org/10.1039/c1jm13789a>.
24. Y. Ruzmanova, M. Stoller, A. Chianese. Photocatalytic Treatment of Olive Mill Wastewater by Magnetic Core Titanium Dioxide Nanoparticles. *Chem. Eng. Trans.* 32, (2013) 2269–2274.
25. Z. D. Li, H. L. Wang, X. N. Wei, X. Y. Liu, Y. F. Yang, W. F. Jiang. Preparation and photocatalytic performance of magnetic  $\text{Fe}_3\text{O}_4@\text{TiO}_2$  core-shell microspheres supported by silica aerogels from industrial fly ash. *J. Alloys Compd.* 659, (2016) 240–247. <https://doi.org/http://dx.doi.org/10.1016/j.jallcom.2015.10.297>.
26. X. Fu, H. Yang, G. Lu, Y. Tu, J. Wu. Improved performance of surface functionalized  $\text{TiO}_2$ /activated carbon for adsorption-photocatalytic reduction of Cr(VI) in aqueous solution. *Mater. Sci. Semicond. Process.* 39, (2015) 362–370. <https://doi.org/http://dx.doi.org/10.1016/j.mssp.2015.05.034>.
27. P. M. B. Chagas, L. B. Carvalho, A. A. Caetano, F. G. E. Nogueira, D. Corrêa, I. R. Guimarães. Nanostructured oxide stabilized by chitosan: Hybrid composite as an adsorbent for the removal of chromium (VI). *J. Environ. Chem. Eng.* 6, (2018) 1008–1019. <https://doi.org/https://doi.org/10.1016/j.jece.2018.01.026>.
28. J. Miyawaki, T. Shimohara, N. Shirahama, A. Yasutake, M. Yoshikawa, I. Mochida, S.-H. Yoon. Applied Catalysis B : Environmental Removal of  $\text{NO}_x$  from air through cooperation of the  $\text{TiO}_2$  photocatalyst and urea on activated carbon fiber at room temperature. *Applied Catal. B, Environ.* 110, (2011) 273–278. <https://doi.org/http://dx.doi.org/10.1016/j.apcatb.2011.09.012>.
29. J. C. T. F. G. de M. R. M. L. J. D. Ardisson. Controlled formation of reactive Fe particles dispersed in a carbon matrix active for the oxidation of aqueous contaminants with  $\text{H}_2\text{O}_2$ .



- Env. Sci Pollut Res 22, (2015) 856–863. <https://doi.org/10.1007/s11356-014-2554-z>.
30. I. M. Arabatzis, S. Antonaraki, T. Stergiopoulos, A. Hiskia, E. Papaconstantinou, M. C. Bernard, P. Falaras. Preparation, characterization and photocatalytic activity of nanocrystalline thin film TiO<sub>2</sub> catalysts towards 3,5-dichlorophenol degradation. *J. Photochem. Photobiol. A Chem.* 149, (2002) 237–245. [https://doi.org/10.1016/S1010-6030\(01\)00645-1](https://doi.org/10.1016/S1010-6030(01)00645-1).
  31. Ohsaka, T., Izumi, N.F., Fujiki, Y, 1978. Raman spectrum of anatase, TiO<sub>2</sub>. *J. Raman Spectrosc.* 7, 321–324. <https://doi.org/10.1002/jrs.1250070606>.
  32. F. Magalhães, M. C. Pereira, J. D. Fabris, S. E. C. Bottrel, M. T. C. Sansiviero, A. Amaya, N. Tancredi, R. M. Lago. Novel highly reactive and regenerable carbon / iron composites prepared from tar and hematite for the reduction of Cr ( VI ) contaminant. *J. Hazard. Mater.* 165, (2009) 1016–1022. <https://doi.org/10.1016/j.jhazmat.2008.10.087>.
  33. M. Thommes, K. Kaneko, A. V Neimark, J. P. Olivier, F. Rodriguez-reinoso, J. Rouquerol, K. S. W. Sing. Physisorption of gases , with special reference to the evaluation of surface area and pore size distribution ( IUPAC Technical Report ). *Pure Appl. Chem.* 87, (2015) 1051–1069. <https://doi.org/10.1515/pac-2014-1117>.
  34. V.-G. I, L.-P. J.J, M. Sánchez-Polo, J. Rivera-Utrilla. Applied Catalysis B : Environmental Role of activated carbon surface chemistry in its photocatalytic activity and the generation of oxidant radicals under UV or solar radiation. *Appl. Catal. B Environ.* 207, (2017) 412–423. <https://doi.org/http://dx.doi.org/10.1016/j.apcatb.2017.02.028>.
  35. L. F. Velasco, V. Maurino, E. Laurenti, I. M. Fonseca, J. C. Lima, C. O. Ania. Applied Catalysis A : General Photoinduced reactions occurring on activated carbons . A combined photooxidation and ESR study. *Appl. Catal. A, Gen.* 452, (2013) 1–8. <https://doi.org/http://dx.doi.org/10.1016/j.apcata.2012.11.033>.
  36. L. D. O. Pereira, S. G. De Moura, G. C. M. Coelho, L. C. A. Oliveira, E. T. De Almeida, F. Magalhães. Journal of Environmental Chemical Engineering Magnetic photocatalysts from industrial residues and TiO<sub>2</sub> for the degradation of organic contaminants. *J. Environ. Chem. Eng.* 7, (2019) 102826. <https://doi.org/10.1016/j.jece.2018.102826>.
  37. X. Huang, G. Wang, M. Yang, W. Guo, H. Gao. Synthesis of polyaniline-modified Fe<sub>3</sub>O<sub>4</sub>/SiO<sub>2</sub>/TiO<sub>2</sub> composite microspheres and their photocatalytic application. 65, (2011) 2887–2890. <https://doi.org/https://doi.org/10.1016/j.matlet.2011.06.005>.
  38. Q. Zhang, G. Meng, J. Wu, D. Li, Z. Liu. Study on enhanced photocatalytic activity of magnetically recoverable Fe<sub>3</sub>O<sub>4</sub>@C@TiO<sub>2</sub> nanocomposites with core-shell nanostructure. *Opt. Mater. (Amst).* 46, (2015) 52–58. <https://doi.org/10.1016/j.optmat.2015.04.001>.
  39. Q. Li, K. Ma, Z. Ma, Q. Wei, J. Liu, S. Cui, Z. Nie. Microporous and Mesoporous Materials Preparation and enhanced photocatalytic performance of a novel photocatalyst: hollow network Fe<sub>3</sub>O<sub>4</sub>/mesoporous SiO<sub>2</sub>/TiO<sub>2</sub> (FST) composite microspheres. *Microporous Mesoporous Mater.* 265, (2018) 18–25. <https://doi.org/10.1016/j.micromeso.2017.12.012>.

## ARTICLE 2

**Magnetic photocatalysts production and degradation of different organic contaminants**  
**Manuscript submitted to Journal Applied Catalysis B Environmental**

Impact factor: 11.698

Qualis Capes (Ciências Agrárias): A1

**Leydiane de Oliveira Pereira<sup>a</sup>, Luana Pereira Zampiere<sup>a</sup>, Isabela Sales Marques<sup>a</sup>, Iara do Rosario Guimarães<sup>a</sup>, Fabiano Magalhães<sup>a\*</sup>**<sup>a</sup>Department of Chemistry, Federal University of Lavras, 37200-000 Lavras - MG, Brazil

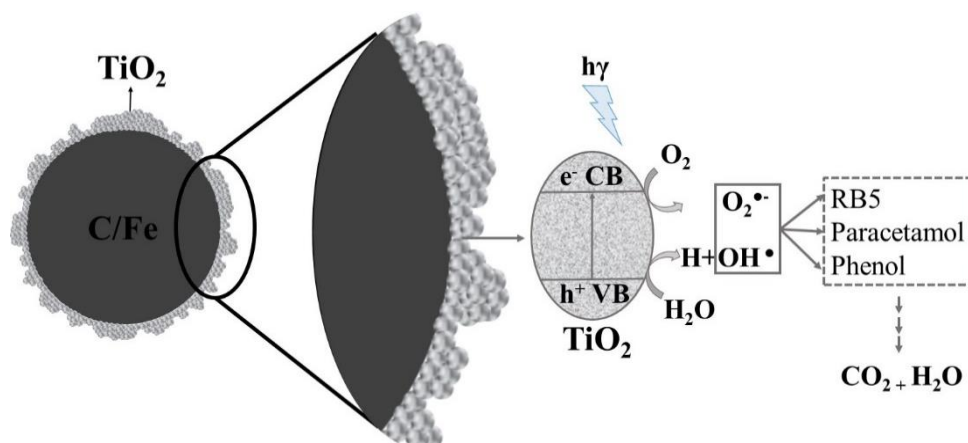
E-mail address: leydi.13@hotmail.com (Leydiane de Oliveira Pereira)

**Abstract**

Ti/C/Fe photocatalysts were prepared by supporting TiO<sub>2</sub> (20, 40 and 60% w/w) on a carbon/iron oxide (C/Fe) magnetic carrier. This support was prepared by using iron nitrate as a source of Fe<sub>3</sub>O<sub>4</sub>/Fe<sub>3</sub>C and sucrose as a source of char. Characterization *via* Raman spectroscopy, X-ray diffractometry, thermal analysis, X-ray fluorescence, scanning electron microscopy and magnetic property analysis by vibrating-sample magnetometry confirmed the presence of TiO<sub>2</sub>, Fe<sub>3</sub>O<sub>4</sub>, Fe<sub>3</sub>C and char in the photocatalysts as well as their magnetic properties. The results of surface specific area analysis showed that the C/Fe support had a surface area of 183 m<sup>2</sup> g<sup>-1</sup> and that this area decreased with an increasing amount of supported TiO<sub>2</sub>, reaching up to 129 m<sup>2</sup> g<sup>-1</sup>. Diffuse reflectance spectroscopy characterization revealed that the photocatalysts showed absorption in the same region of TiO<sub>2</sub> and in the visible light region, resulting in a decrease of bandgap values. The prepared photocatalysts showed high photocatalytic efficiency in degrading and mineralizing the contaminants remazol black (RB5), paracetamol and phenol, and the 60Ti/C/Fe sample showed the best results (99 and 82% reductions in color and total amount of organic carbon of RB5 dye, respectively). Photocatalyst recovery and reuse tests for the discoloring of RB5 showed that after the fourth reaction, the photocatalytic efficiency was reduced by approximately 50%, and the recovery of 70, 54 and 49% of the 20, 40 and 60Ti/C/Fe materials, respectively, was observed. Sedimentation kinetics showed that while only 6% of the pure TiO<sub>2</sub> deposited, up to 89% of the photocatalysts deposited. These results indicate that the photocatalysts present excellent photocatalytic efficiency for different contaminants and can be easily and quickly separated from the reaction medium by magnetic separation.

**Keywords:** Sucrose. Paracetamol. Phenol. Dye

## Graphical Abstract



## Highlights

- TiO<sub>2</sub>, sucrose and iron nitrate were used to prepare photocatalysts.
- RB5, paracetamol and phenol were efficiently degraded by photocatalysts.
- Photocatalysts can be recovered using a magnet and reused in reactions.

## 1. Introduction

Excessive disposal of wastewater containing a number of non-degradable compounds represents a major risk to human health and the ecosystem due to their high toxicity and difficult degradation [1]. Since harmful organic compounds, such as dyes, phenol and paracetamol, are often released into industrial effluents, reducing their generation and finding an efficient treatment method for these effluents are necessary [2,3].

To solve such problems, researchers have proposed the use of photocatalysis, as this is an efficient and environmental friendly method suitable for the removal of organic contaminants present in wastewater [4]. Heterogeneous photocatalysis is based on the use of a semiconductor that in the presence of radiation in aqueous media generates active species that mineralize organic contaminants [5]. The mechanism of photocatalysis using semiconductors is well known and has already been reported in detail in the literature by several authors [6,7,8].

Among the used semiconductors, TiO<sub>2</sub> has attracted considerable interest due to its nontoxicity, low cost, chemical stability and high photocatalytic efficiency [9,10]. However, despite the numerous advantages in the application of TiO<sub>2</sub> to wastewater treatment, there are several limitations. For example, it is difficult to separate TiO<sub>2</sub> from the treated effluent since it forms a stable suspension due to its small particles size, which can cause secondary pollution [11]. Different strategies have been investigated to solve this problem. One of these strategies is to use different materials as a support for TiO<sub>2</sub>, such as glass [12], zeolite [13], activated

carbon [14], silica [15] and polymeric materials [16] or even to immobilize TiO<sub>2</sub> on the wall of reactors [17].

Another alternative is to support TiO<sub>2</sub> on a magnetic matrix. TiO<sub>2</sub> supported directly on materials with magnetic properties have already been prepared (Fe<sub>3</sub>O<sub>4</sub>, SiO<sub>2</sub>@Fe<sub>3</sub>O<sub>4</sub>, δ-Fe<sub>2</sub>O<sub>3</sub>, FeO or Fe) to obtain a magnetic photocatalyst, which enables its simple and fast separation through the use of a magnetic field [2, 9,11,18]. These materials, in addition to being separated and recovered in a simple way, can be reused several times, which results in savings and waste reduction of the unrecovered used catalyst.

The photocatalytic properties of TiO<sub>2</sub> are mainly related to the morphology and size of the particles. The small surface area of the particles causes the low capacity for contaminant adsorption on their surface, which represents another limitation of their use [19]. Since the reactions occur on the photocatalyst surface, the adsorption of an organic contaminant facilitates its degradation. Materials such as clay [4], silica [20], zeolite [21], char [22] have already been used as supports for TiO<sub>2</sub>, aiming to increase the surface area of the final composite.

In this study, a magnetic composite Fe<sub>3</sub>C (C/Fe) will be used as support for TiO<sub>2</sub> to obtain Ti/C/Fe magnetic photocatalysts. The carbon layer surrounding the Ti/C/Fe magnetic photocatalyst core may contribute to an increase in contaminant adsorption, preventing TiO<sub>2</sub> agglomeration in the solution and hindering the recombination of electron-vacancy pairs. The solid-solid interfaces between charcoal and TiO<sub>2</sub> promote charge transfer and spatial separation, protect the magnetic core from possible oxidation or dissolution in the effluent and avoid the reduction of TiO<sub>2</sub> photocatalytic activity due to the interaction of the magnetic core and TiO<sub>2</sub> [18,23,22]. Some authors reported that obtaining carbon from renewable resources, such as sucrose, results in a high yield [24,25].

Thus, this study utilized sucrose as a carbon source to obtain the magnetic support C/Fe, where magnetic particles (Fe<sub>3</sub>O<sub>4</sub> and Fe<sub>3</sub>C) were covered by carbon and their surfaces impregnated with TiO<sub>2</sub> in different proportions (20, 40 and 60% w/w), forming the photocatalysts 20Ti/C/Fe, 40Ti/C/Fe and 60Ti/C/Fe. These materials were characterized by Raman spectroscopy, X-ray diffractometry (XRD), thermal analysis (TGA and DTA), X-ray fluorescence (XRF), scanning electron microscopy (SEM), surface specific area (SSA) analysis, diffuse reflectance spectroscopy (DRS) and magnetic property analysis via vibrating-sample magnetometry (VSM). The photocatalytic activities of the photocatalysts were investigated by studying the degradation of the following contaminant models under UV radiation: remazol black (RB5) textile dye, paracetamol and phenol.

## **2. Material and methods**

### **2.1. Synthesis of photocatalysts**

#### **2.1.1. Synthesis of C/Fe composites**

Synthesis of the magnetic supports (C/Fe) based on sucrose was carried out according to the methodology of Tristão et al. (2015) [26]. Initially, a solution containing 8% iron by mass was prepared from  $\text{Fe}(\text{NO}_3)_3 \cdot 9\text{H}_2\text{O}$  (Synth, PA) in 30 mL of distilled water. The pH of the solution was adjusted to 1 with  $\text{HNO}_3$  (Synth, PA) to prevent iron precipitation. For the addition of 92% by mass of sucrose (Union brand refined sugar), the solution was heated until a dark slurry was formed. Carbonization was performed at  $800^\circ\text{C}$  for two hours in a quartz tube under inert atmosphere ( $\text{N}_2$ ). Char synthesis without iron was also performed following the same procedure.

#### **2.1.2. Coating of composites with $\text{TiO}_2$**

The coating of composites with  $\text{TiO}_2$  was performed based on the methodology of Arabatzis et al. (2002) [27]. For the synthesis of 1 g of the photocatalyst 20Ti/C/Fe, 0.2 g of  $\text{TiO}_2$  (Evonik) were added to 1 mL of water containing 0.1 mL of acetylacetone (Neon, PA), in which a viscous slurry was formed. This slurry was slowly diluted in 1.7 mL of water. Next, one drop of Triton X-100 (Synth) was added to the slurry, which was then mixed with 0.8 g of C/Fe. After drying at  $100^\circ\text{C}$  for 20 minutes, the mixed composite of C/Fe and  $\text{TiO}_2$  was heat treated at  $350^\circ\text{C}$  for 30 minutes in an oxidizing atmosphere ( $10^\circ\text{C min}^{-1}$ ).

Magnetic photocatalysts were prepared with 20, 40 and 60%  $\text{TiO}_2$  (w/w) and denoted as 20Ti/C/Fe, 40Ti/C/Fe and 60Ti/C/Fe, where the number indicates the  $\text{TiO}_2$  contents.

### **2.2. Characterization of the prepared materials**

Raman spectra were acquired by a Raman (Senterra Bruker) spectrometer with a coupled optical microscope (OLYMPUS BX51). XRD analysis was performed on a Rigaku Ultima IV model, with  $\text{Cu K } \alpha = 1.54051 \text{ \AA}$ . Scans were obtained over the angles of  $15 < 2\theta < 80^\circ$  at a speed of  $4^\circ \text{ min}^{-1}$ . Thermogravimetric analysis (TGA) was performed on Shimadzu equipment at a heating rate of  $10^\circ\text{C min}^{-1}$  from  $30^\circ\text{C}$  to  $900^\circ\text{C}$  under synthetic air flow ( $100 \text{ mL min}^{-1}$ ). The contents of the elements were detected by total reflection X-ray fluorescence spectrometry (S2 PICOFOX - Bruker). For the study of the morphology of the materials, SEM analyses were

performed using a LEO EVO 40XVP (Carl Zeiss SMT) at a 25 kV voltage. Powder samples were fixed with double-sided carbon tape. The specific surface areas of the samples were analyzed by adsorption and desorption of N<sub>2</sub> at 77 K using an Autosorb1-MP Quantachrome. Samples were degassed at 200°C for 24 hours prior to analysis. To obtain the electron transition energy of the solid, radiation analysis was performed. Diffuse reflectance spectra in the UV-vis region were obtained on Shimadzu UV-2600 equipment. To treat the data, the analysis results were converted to absorbance following the Kubelka-Munk method to thus calculate the bandgap value. A vibrating-sample magnetometer (model EV9, Microsense) was used to measure the magnetic properties of the photocatalysts under a magnetic field ranging from -20000 to 20000 Oe at room temperature. Total organic carbon (TOC) was analyzed using Shimadzu model TOC-V CPH.

### **2.3. Study of the removal of the model contaminants**

Adsorption tests were conducted with 30 mg of photocatalyst added to 100 mL of aqueous solution of various organic contaminants (RB5: 40 mg L<sup>-1</sup>; paracetamol: 30 mg L<sup>-1</sup> and phenol: 25 mg L<sup>-1</sup>). The solutions were left in the dark under constant stirring, and aliquots were withdrawn at different time intervals. Afterwards, the photocatalyst was removed with the aid of a magnet, and the adsorption tests of model contaminants were monitored using a UV-vis spectrophotometer (Micronal AJX-3000PC) at 598, 243 and 269 nm for the contaminants RB5 (Sigma-Aldrich), paracetamol (Sigma-Aldrich) and phenol (Sigma-Aldrich), respectively. Photocatalytic tests were performed under the same conditions as the adsorption tests. However, the reactions were performed in a reactor equipped with magnetic stirring and a low-pressure mercury lamp with emission at 254 nm (51 W - Philips, I = 1,908 mW cm<sup>-2</sup>). The germicidal lamp was placed in the upper part of the reactor at a distance of approximately 20 cm from the dye solution, and the radiation incidence area was 13 cm in diameter. The degradation kinetics of the studied contaminants were monitored using a UV-vis spectrophotometer (Micronal AJX-3000PC), as previously described. However, phenol degradation and formation of intermediates during photocatalytic reactions were also monitored by HPLC, where the reverse phase column Shimpack ODS C18 and SPDM-20A detector and isocratic method (Methanol: MilliQ water 30:70% v/v) with flow of 1 mL min<sup>-1</sup> temperature of 30 °C were used.

#### 2.4. Sedimentation kinetics

The sedimentation kinetics was determined based on the turbidity reduction by mixing 2 mg of the magnetic photocatalysts or TiO<sub>2</sub> with 10 mL of water. This mixture was placed in the sample port of a homogenized turbidimeter, and in the presence of a magnetic field (magnet). The turbidity variation was monitored over time using a calibrated turbidimeter (HANNA INSTRUMENTS HI 98703)

#### 2.5. Photocatalyst recovery and reuse tests

To evaluate the separation efficiency and photocatalytic activity, a photocatalyst sample was recovered and used in four consecutive RB5 discoloration reactions. In this experiment, the photocatalyst was placed in contact with an RB5 dye solution under the same conditions as those used in the photocatalytic reactions. After 4 hours of reaction, the photocatalyst was separated from the solution with the aid of a magnet. Then, the photocatalyst was washed with distilled water, oven dried and weighed. This procedure was repeated four times in a solution volume proportional to the amount of recovered photocatalyst. From the recovered photocatalyst mass, it was possible to calculate its recovery efficiency.

### 3. Results and discussion

#### 3.1. Characterization of Ti/C/Fe materials

To identify the nature of the carbon formed in the magnetic support C/Fe, it was characterized by Raman spectroscopy. Figure 1 shows the Raman spectrum obtained for the magnetic carrier C/Fe.

The Raman spectrum shows signals in the magnetic media at 216 and 277 cm<sup>-1</sup>, corresponding to Fe<sub>3</sub>C, and the other three bands at 1330, 1584 and 2651 cm<sup>-1</sup> indicate the presence of carbon [28]. The D and G bands centered at 1330 and 1584 cm<sup>-1</sup> indicate the presence of amorphous and graphitic carbon, respectively. The ratio of the intensities of these two signals ( $I_G/I_D$ ) is equal to 1.00, indicating that amorphous carbon and graphitic carbon were formed in the support in very similar proportions. The presence of the iron carbide Fe<sub>3</sub>C in the sample is responsible for the magnetic property (Figure 1).

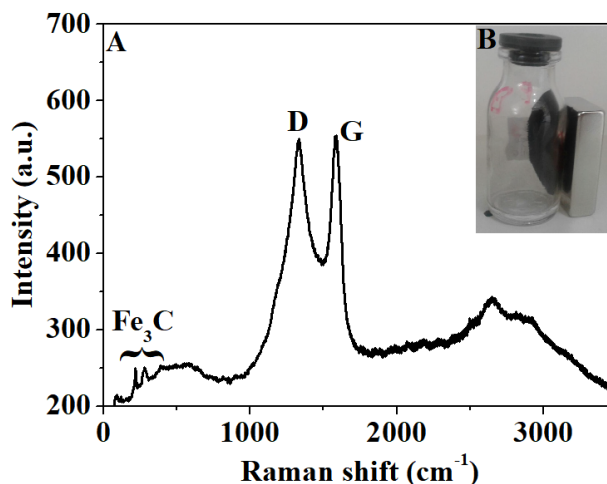


**Figure 1.** Raman spectra for the magnetic carrier C/Fe (A), and photo of the C/Fe being attracted by a magnet (B).

Figure 2 shows the carbon diffractograms obtained from sucrose (C), the C/Fe composite, TiO<sub>2</sub> and the magnetic photocatalysts.

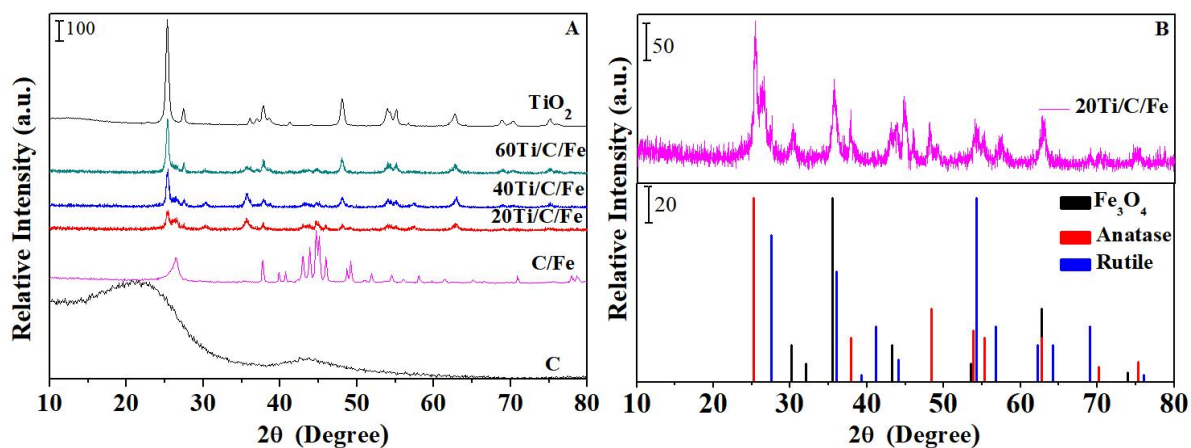


**Figure 2.** Diffractograms of A) C, C/Fe, TiO<sub>2</sub>, and the magnetic photocatalysts, and B) Expansion of 20Ti/C/Fe diffractogram and Fe<sub>3</sub>O<sub>4</sub>, anatase and rutile standards.

In Figure 2A, broad lines are present at 21 and 43° in the carbon diffractogram, confirming the formation of amorphous carbon. Graphitic carbon formation occurred during the thermal treatment of the carbon to form the magnetic support C/Fe ( $2\theta = 26^\circ$  - JCPDS, 0-0640). The diffraction lines also confirm the presence of iron carbide (JCPDS, 34-0001), which was formed by reduction of Fe<sup>3+</sup> present in iron nitrate during the thermal treatment (Equation 1). Heat treatment at high temperatures of char and iron oxide mixtures can result in the formation of metallic iron (Equation 2) [29,30]. This phase might be present in the C/Fe composite due to the high temperature used in its preparation (800°C). However, identifying the corresponding diffraction lines in the diffractogram shown in Figure 2A is difficult, since the Fe signals appear at 44 and 64° (JCPDS, 1-1262), which are values that coincide with the Fe<sub>3</sub>C diffraction lines.



This result corroborates with those obtained by Raman spectroscopy and by Tristão et al. (2015) [26].



In the  $\text{TiO}_2$  P25 diffractogram (Fig. 2B), the diffraction lines confirm the presence of the anatase (JCPDS, 02-0387) and rutile (JCPDS, 01-1292) phases [31,32]. Additionally, the intensity of the diffraction lines of the anatase phase is greater than that of the rutile phase, which confirms that the latter is present at a lower percentage in  $\text{TiO}_2$  P25, as observed by other authors [31,32].

Figure 2B shows that the magnetic photocatalysts have the same phases as those observed in the  $\text{TiO}_2$  P25 diffractogram, proving that this semiconductor is also present in all photocatalyst materials.

Discrete signals appear at 30 and 35°, which indicate the presence of  $\text{Fe}_3\text{O}_4$  (JCPDS, 07-0322) in the magnetic photocatalysts. The formation of  $\text{Fe}_3\text{O}_4$  occurred through the oxidation of  $\text{Fe}_3\text{C}$  during the thermal treatment carried out in an oxidizing atmosphere to support the  $\text{TiO}_2$  on the C/Fe sample, as presented in Equation 3.



In the regions between 43 and 46° in the diffractograms of the Ti/C/Fe photocatalysts, the small intensity diffraction lines suggest the presence of  $\text{Fe}_3\text{C}$  in these samples. The magnetite and iron carbide present in these materials are responsible for the magnetic activity, allowing them to be easily separated from the treated effluent through the action of a magnet.

In Figure 3, the TG and DTA curves obtained for the studied materials are presented.

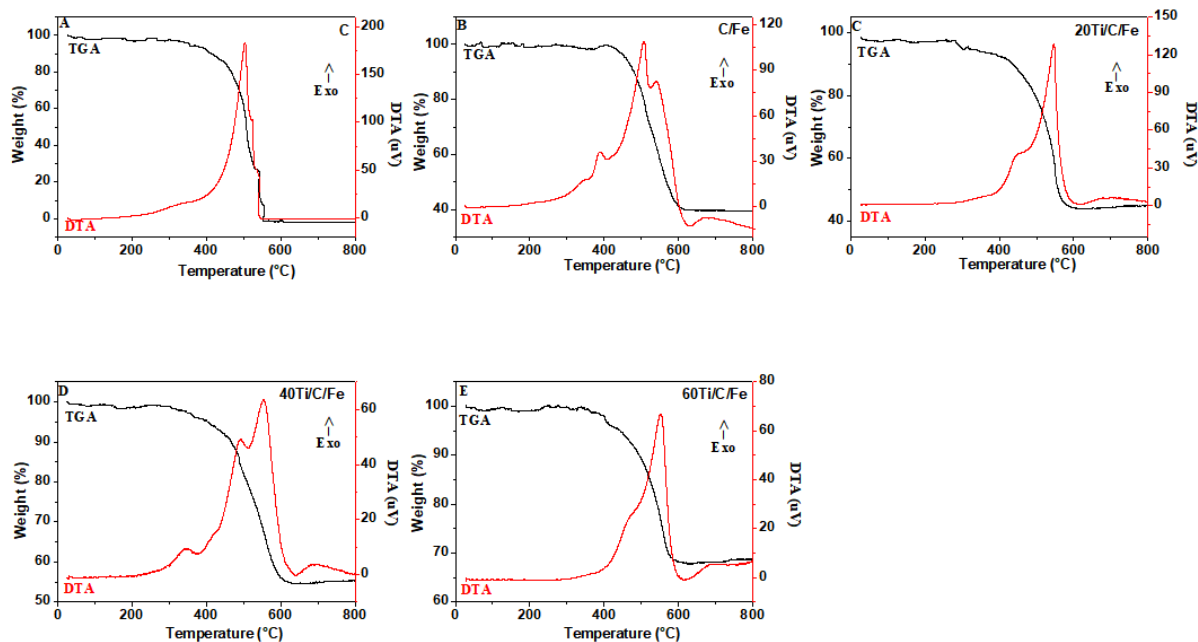


**Figure 3.** TGA and DTA curves obtained for samples A) C, B) C/Fe, C) 20Ti/C/Fe, D) 40Ti/C/Fe and E) 60Ti/C/Fe under O<sub>2</sub> flow.

In the TGA curve of the carbon obtained from sucrose, a weight loss of 94% is observed between 400 and 550°C, which is accompanied by an exothermic signal in the DTA curve. These results are related to the thermal decomposition of char (Equation 4).



In the TGA curve of the C/Fe support, a weight gain (1.25%) can be observed at approximately 400°C, due to oxidation of the iron carbide, leading to the formation of more stable iron oxide phases (Equation 5). In addition, oxidation of carbon to CO<sub>2</sub> also occurs, leading to a weight loss of 58%, and the residual material mainly consists of Fe<sub>2</sub>O<sub>3</sub> [33]. The DTA curve presents strong exothermic events, which are attributed to oxidation of Fe<sub>3</sub>C and carbon.



In the TGA curves of the 20, 40 and 60Ti/C/Fe photocatalysts, weight losses of 52, 42 and 31%, respectively, occur due to the oxidation of the char. Exothermic events are also present in the DTA curves of these materials, which are related to the oxidation of the carbon and the iron phases present in the photocatalysts.

The residue content obtained after heat treatment at 600°C increases in the Fe/C carrier and in the photocatalysts, which indicates that the carbon content in these materials decreases, as the iron and TiO<sub>2</sub> have been incorporated.

The iron and titanium contents were determined by XRF, which enabled the calculation of the amounts of TiO<sub>2</sub> present in the photocatalysts, as shown in Table 1.

**Table 1.** Chemical composition of the photocatalysts obtained from sucrose.

Samples	Fe (%)	Ti (%)	TiO <sub>2</sub> (%)
C/Fe	28.2	0	0
20Ti/C/Fe	17.0	14.6	24.0
40Ti/C/Fe	11.1	22.5	37.5
60Ti/C/Fe	6.1	28.8	48.0

The iron contents obtained for the C/Fe support are different from the theoretical values (17% iron). This can be explained by the presence of moisture and impurities in the sucrose used to obtain the C/Fe support and due to the consumption of this carbon during the reaction to form Fe<sub>3</sub>C (Equation 6).



As a consequence, the iron content in C/Fe and in the photocatalysts is greater than expected. The iron contents decrease with the increase in the amount of TiO<sub>2</sub> used to obtain the magnetic photocatalysts. Although the photocatalyst 60Ti/C/Fe presents low iron content (6.1%), its magnetization is sufficient for it to be separated from the reaction medium by the action of a magnetic field. The TiO<sub>2</sub> contents present in the photocatalysts (calculated from the titanium content) are close to the theoretical values, with the exception of 60Ti/C/Fe. These differences are related to the loss of reagents during the experimental procedures.

Figure 4 shows SEM images for the samples C, Fe/C, 20, 40 and 60Ti/C/Fe.

In the images of the char obtained from sucrose (Figs. 4A and 4B), charcoal blocks with varying size, indefinite shapes and smooth surfaces are observed. The images of the C/Fe support (Figs. 4C and 4D) are similar to those of the char sample, although the presence of small round particles on the surface of the char blocks is noticeable, indicating the presence of iron carbide agglomerates. This result indicates that some of the Fe<sub>3</sub>C was not coated or located in the bulk of the char.

The micrographs of the photocatalysts (Fig. 4E - 4J) show similar morphologies, where char blocks (more regular surfaces) containing smaller round particles distributed on their surface that are certainly TiO<sub>2</sub> agglomerates can be observed. The number of particles present on the surface of the carbon of the photocatalysts is greater than that on the surface of the C/Fe support. These results confirm the presence of TiO<sub>2</sub> in the magnetic photocatalysts. Similar results were obtained in another work from our research group, where SEM images and EDS mapping proved that the particle agglomerates are constituted mainly by TiO<sub>2</sub> [34].

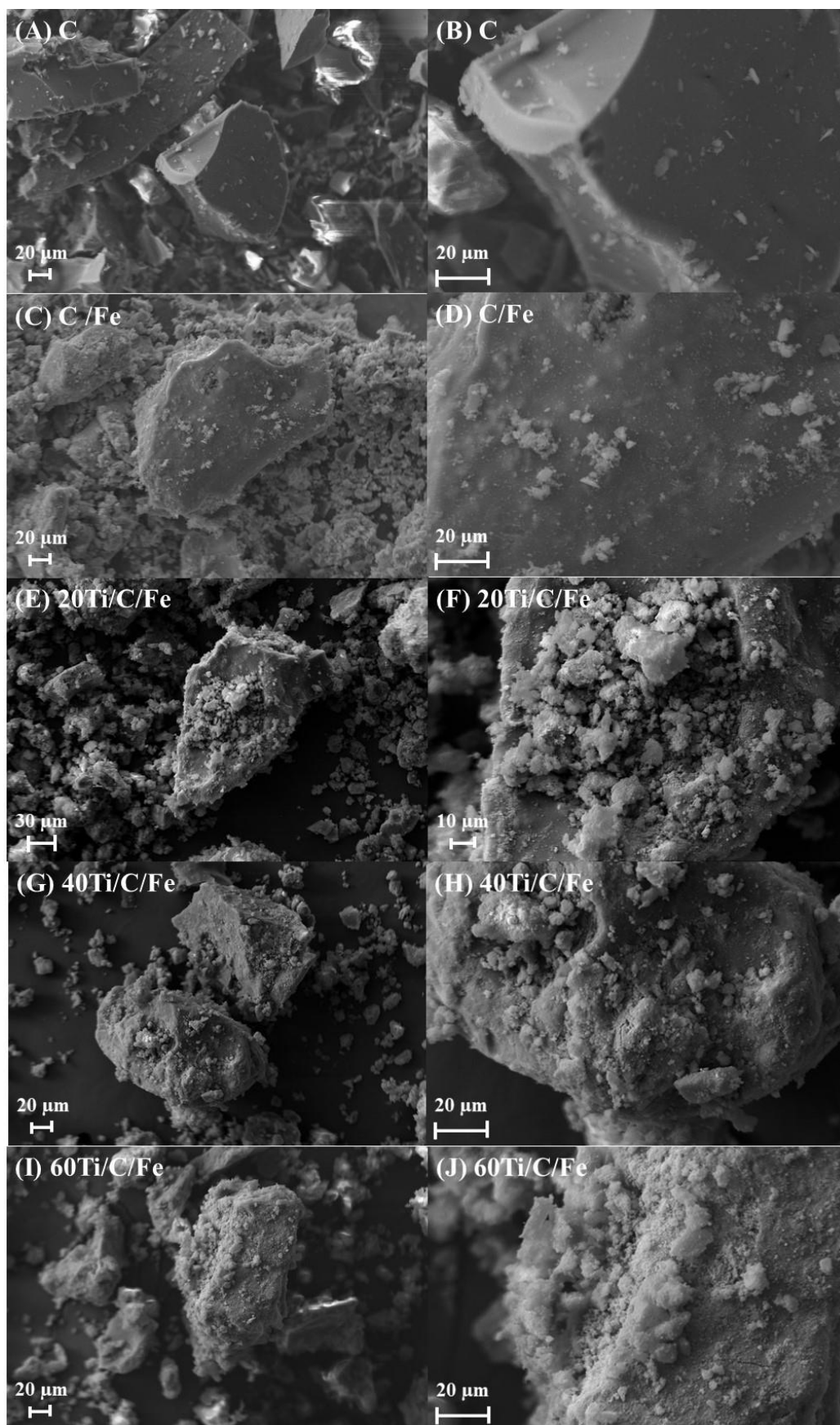


**Figure 4.** SEM images of C, C/Fe and the 20, 40 and 60Ti/C/Fe photocatalysts at 500 and 1500x magnifications.

The surface area obtained for TiO<sub>2</sub> P25 (67 m<sup>2</sup> g<sup>-1</sup>) is close to the values cited in other studies [22,35]. The result obtained for the C/Fe support(183 m<sup>2</sup> g<sup>-1</sup>) is relatively high, suggesting that during the heat treatment, pores formed in the carbonaceous fraction when Fe<sup>3+</sup> and Fe<sup>2+</sup> species were reduced by char (Equations 7 - 9), [36,37].



C/Fe-like composites were obtained by Tristão et al. (2015) and Magalhães et al. (2013) and (2009) [26,29,37] and the surface area values varied between 90 and 158 m<sup>2</sup> g<sup>-1</sup>, which corroborates the results obtained in the present study.

The surface areas for samples 20, 40 e 60Ti/C/Fe were 173, 145 and 129 m<sup>2</sup> g<sup>-1</sup>, respectively. Note that the surface area decreases with the increase of the TiO<sub>2</sub> supported on the C/Fe composite. This effect is related to the filling of the cavities and pores of the carbonaceous fraction with TiO<sub>2</sub> particles, which have a smaller surface area.

Figure 5 shows the N<sub>2</sub> adsorption and desorption isotherms for the studied materials.

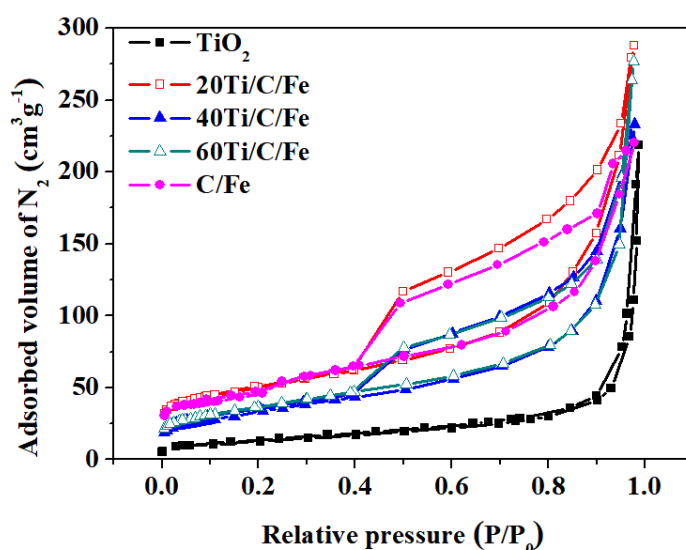


**Figure 5.** N<sub>2</sub> adsorption and desorption isotherms obtained for TiO<sub>2</sub>, C/Fe and 20, 40 and 60Ti/C/Fe.

The isotherms for C/Fe and the 20, 40 and 60Ti/C/Fe photocatalysts can be classified as category IV(a) with H4-type hysteresis, according to IUPAC. This result indicates that these materials are mesoporous, with laminar interparticulas and nonhomogeneous pores. The isotherm obtained for TiO<sub>2</sub> does not show hysteresis and can be classified as type IV(b), which

is also characteristic of mesoporous materials, but with smaller pores compared with the isotherms of the magnetic photocatalysts [38].

Figure 6 shows the diffuse reflectance spectra (A) and the Tauc plot of the transformed Kubelka-Munk function versus the light energy (B).

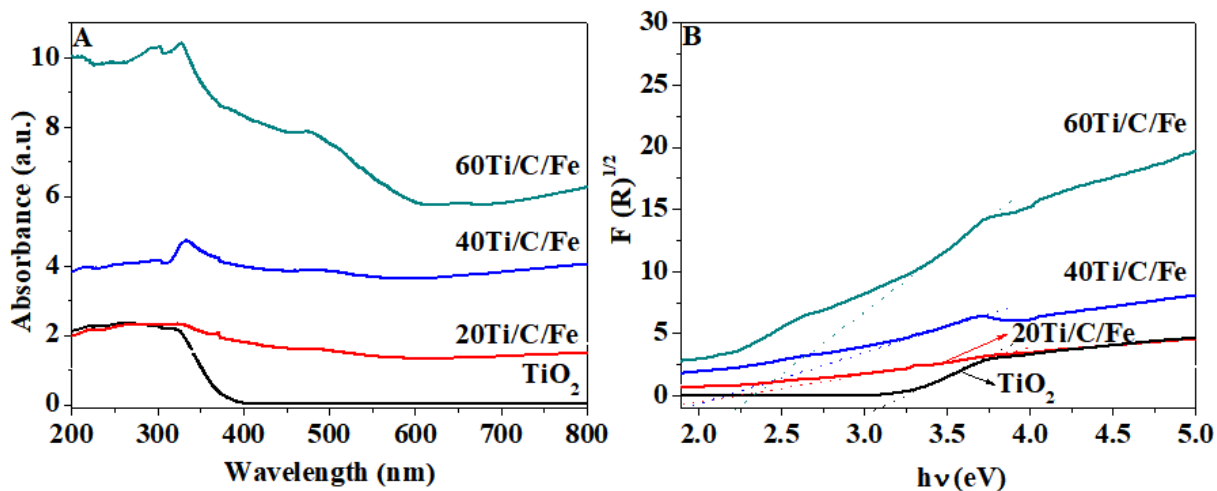


**Figure 6.** The UV-vis absorption spectra of the TiO<sub>2</sub>, 20, 40 and 60Ti/C/Fe materials (A), and the Tauc representation of the transformed Kubelka-Munk function versus the light energy (B).

Figure 6A shows that the TiO<sub>2</sub> absorbs the radiation between 200 and 400 nm, as observed in other studies [39]. This absorption at wavelengths of less than 400 nm is due to the bandgap value of TiO<sub>2</sub> (3.2 eV) [19]. In contrast, the magnetic photocatalysts absorb the radiation in the visible and UV ranges. These results can be explained by the presence of carbon in the photocatalysts [39,40].

The Kubelka-Munk plot (Fig. 6B) was used to obtain the bandgap values of the materials. The values obtained were 3.07, 1.90, 1.97 and 2.23 eV for TiO<sub>2</sub>, 20Ti/C/Fe, 40Ti/C/Fe and 60Ti/C/Fe, respectively. The incorporation of TiO<sub>2</sub> into the magnetic support not only reduced the bandgap of the photocatalysts but also increased the absorption range of these materials. The higher the percentage of C/Fe in the photocatalysts is the smaller the bandgap and the lower the energy required to promote the electrons in the valence band to the conduction band of the semiconductor.

Figure 7 presents the VSM results obtained for the studied samples.

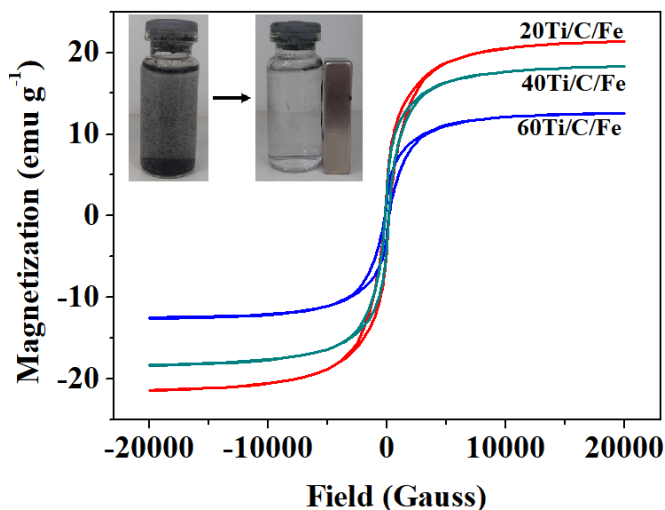


**Figure 7.** Hysteresis loops obtained by VSM of samples 20, 40 and 60Ti/C/Fe and 40Ti/C/Fe photocatalyst dispersed in solution and subsequently attracted by a magnet (Insert).

The saturation magnetization values obtained for the 20, 40 and 60Ti/C/Fe photocatalysts are 22, 18 and 13  $\text{emu g}^{-1}$ , respectively. These values are smaller than those of  $\text{Fe}_3\text{O}_4$  and  $\text{Fe}_3\text{C}$  (55.4 and 118  $\text{emu g}^{-1}$ ) [42,43]. This result is due to the presence of nonmagnetic materials ( $\text{TiO}_2$  and carbon) in the photocatalysts. However, the magnetization presented by the magnetic photocatalysts is sufficiently high to separate them from the reaction medium after the photocatalytic reactions.

### 3.2. Adsorption testes

The contaminants RB5, paracetamol and phenol were used as models to verify the photocatalytic efficiency of the prepared materials. Table 2 presents the percentages of the three contaminant models adsorbed by the magnetic photocatalysts.

**Table 2.** Adsorption percentages of RB5, paracetamol and phenol for the 20, 40 and 60 Ti/C/Fe photocatalysts.

Photocatalysts	Contaminants		
	RB5	Paracetamol	Phenol
	Adsorption (%)		
20Ti/C/Fe	17	18	11
40Ti/C/Fe	14	10	10
60Ti/C/Fe	14	9	8

These results show that under the studied experimental conditions, the adsorption percentages of the three contaminants by the photocatalysts are considered low (8 to 18%). Additionally, adsorption decreases with increasing TiO<sub>2</sub> contents. These results are related to the reduction of the surface areas of the 40 and 60Ti/C/Fe photocatalysts. After 30 minutes the photocatalysts stopped adsorbing the contaminants, showing that the adsorbate/adsorbent system was in equilibrium. Thus, before carrying out the photocatalytic reactions, the photocatalysts were put in contact with the contaminant solutions for 30 minutes to eliminate the interference of the adsorption.

### 3.3. Photocatalytic reactions for degradation of the model organic contaminants

Figure 8 shows the structural formulas of the RB5 (Fig. 8A), paracetamol (Fig. 8B) and phenol (Fig. 8C) molecules, as well as the absorbance spectra of solutions of these contaminants at the beginning (time of 0 minutes) and end of the photocatalytic reactions.

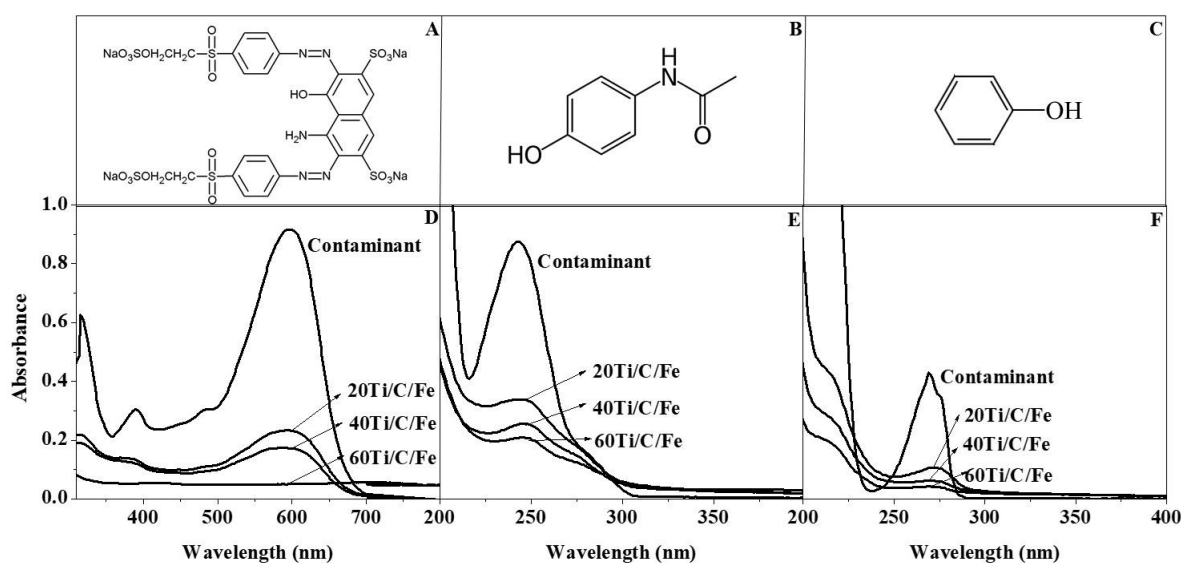


**Figure 8.** Structural formulas of the RB5 (A), paracetamol (B) and phenol (C) molecules, and the UV-vis absorbance spectra for their solutions at the initial (0 minutes of photocatalytic activity) and final photocatalytic (D, E and F) times using the 20, 40 and 60Ti/C/Fe photocatalysts.

The UV-vis absorbance spectrum of the RB5 dye (Fig. 8D) shows a high intensity absorption band at 598 nm, which was used to monitor the discoloration of this contaminant during the photocatalytic reactions. Three other bands of lower intensities, characteristic of RB5, are observed at 310, 400 and 500 nm. During the photocatalytic reactions, the generated radicals react with the RB5 molecules, and when the N=N and C-N bonds of the azo group are



broken, discoloration of the solution occurs, and the intensities of the dye absorption bands decrease (Fig. 8D) [44].

According to Moctezuma et al. (2012) [45] paracetamol (Fig. 8B) shows two characteristic absorption bands at 208 and 243 nm, as shown in Figure 8E. The band at 208 nm corresponds to a  $\pi$ - $\pi^*$  transition, and the band at 243 nm is due to an  $n$  -  $\pi^*$  transition of the C=O group [21]. On the other hand, phenol (Fig. 8C) shows bands at 210 and 269 nm that correspond to  $\pi$ - $\pi^*$  transitions of the aromatic ring. After the photocatalytic reactions using the 20, 40 and 60Ti/C/Fe photocatalysts, the intensities of the absorption bands of the paracetamol and phenol solutions strongly decrease (Figs. 8E and 8F), indicating the degradation of these molecules by the radicals formed during the photocatalytic process.

Figure 9 shows the photocatalytic degradation kinetics of the contaminants RB5 (Fig. 9A), paracetamol (Fig. 9B) and phenol (Fig. 9C) using the photocatalysts prepared in this work.

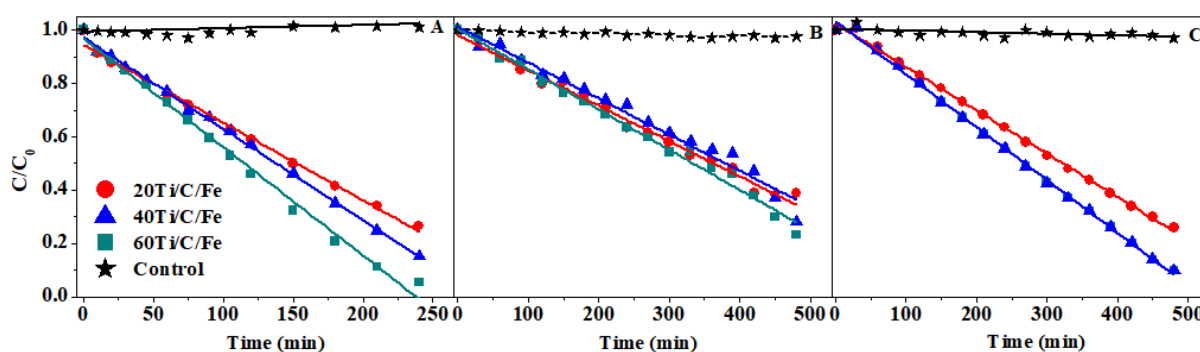


**Figure 9.** Degradation kinetics of RB5 (A), paracetamol (B) and phenol (C) using the 20, 40 and 60Ti/C/Fe photocatalysts.

The results of the control reactions using RB5 dye and phenol showed no significant reduction in concentration during the reaction time, which demonstrates the stability of these compounds when exposed to UV radiation. On the other hand, it is noted that paracetamol underwent c.a 10% degradation due to the photolysis reaction promoted by UV light.

A linear curve is observed in the results obtained during the degradation reactions for the contaminants studied, which suggests pseudo-zero-order kinetics. Thus, the degradation rate constants of the contaminants in the reactions using the photocatalysts were obtained based on the slope of the lines adjusted by linear regression. These results show that the photocatalysts with higher TiO<sub>2</sub> content show higher photocatalytic efficiency in degrading the three studied model contaminant. These results are best observed in Figure 10, which shows the degradation rate constants ( $k$ ) and percentages of degradation and TOC reduction obtained for the RB5 (Fig.

10A), paracetamol (Fig. 10B) and phenol (Fig. 10C) degradation reactions using the 20, 40 and 60Ti/C/Fe photocatalysts.

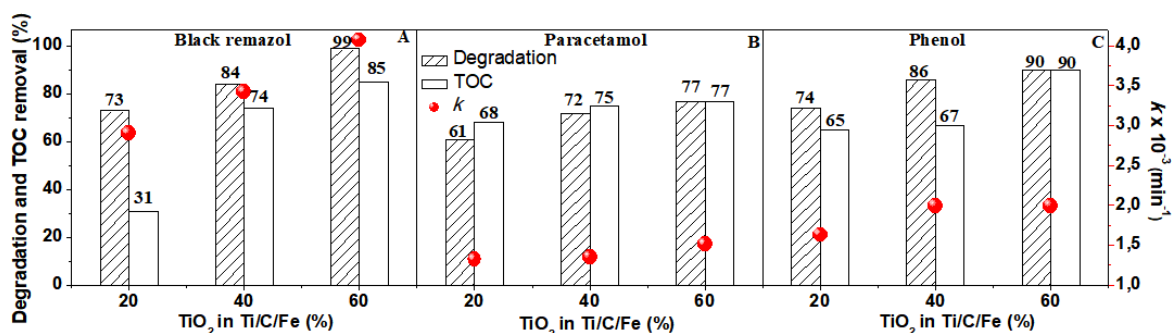


**Figure 10.**  $k$  and percentages of degradation and TOC reduction for RB5 (A), paracetamol (C) and phenol after photocatalytic reactions using 20, 40 and 60Ti/C/Fe.

Figure 10 shows that the higher the TiO<sub>2</sub> content in the Ti/C/Fe magnetic photocatalysts, the higher the values of  $k$  and percentages of degradation and TOC removal in the reactions with RB, paracetamol and phenol. As the surface area of the magnetic photocatalysts decreases with increasing TiO<sub>2</sub> content, the higher photocatalytic efficiency of samples 40 and 60Ti/C/Fe is directly related to the amount of TiO<sub>2</sub>. Considering that the data presented in Figure 10A (degradation of RB5) were obtained for a 240 minutes reaction time and that the other results (Figs. 10B and 10C) were obtained for a 480 minutes reaction time, the RB5 dye is degraded more easily. These results are confirmed by the high  $k$  values for the reactions performed with RB5 in comparison with those obtained for the other reactions. This greater ease of RB5 degradation is certainly related to its greater reactivity.

Similar photocatalysts were prepared by our research group, and the photocatalytic activity for RB5 degradation was investigated [34]. The results obtained were similar to those of the present study, as the photocatalytic activity increased with the supported TiO<sub>2</sub> content, and 71 and 52% efficiency in discoloring and mineralizing the dye, respectively, could be achieved, since the dye has a greater number of reactive sites that can stabilize the •OH radical.

Interestingly, as shown in Figure 10, the TOC removal values for the reactions performed with RB5 are lower than the degradation percentage, whereas for the reactions with paracetamol and phenol, the TOC removal values and degradation percentage are close. These results show that the discoloration (degradation) step of RB5 dye is rapid, while its mineralization is slower. This phenomenon is related to the number of reaction intermediates that form during degradation, as this dye molecule has a high molecular weight (MW = 991.82 g mol<sup>-1</sup>) and the structure complex. In contrast, phenol and paracetamol are smaller molecules

that form fewer intermediates during their mineralization, and, therefore, less competition exists for the hydroxyl radicals formed during photocatalysis.

Figure 11 shows some of the intermediate species that might be formed during a degradation of the studied contaminants.

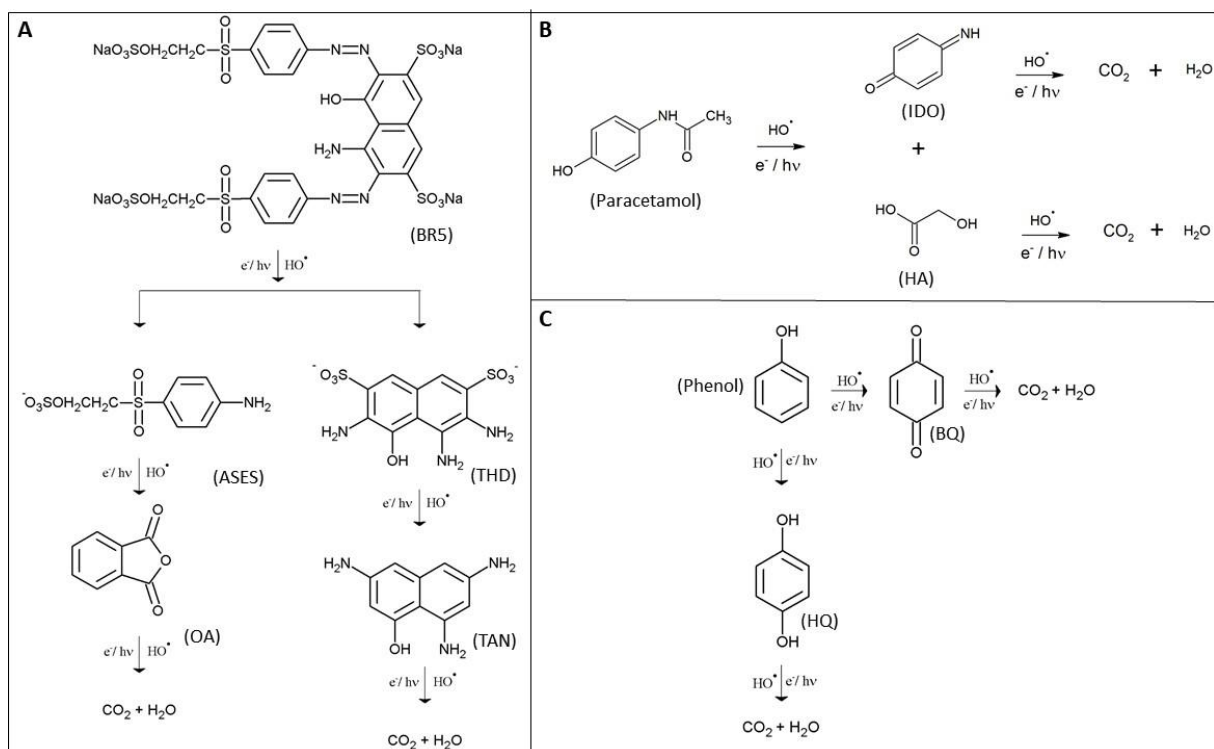


**Figure 11:** Representation of possible intermediates formed during reactions of degradation of contaminants: A) RB5 [46, 47], B) Paracetamol [3, 48, 49], and C) Phenol.

It is noted in Figure 11 (A) that during degradation of RB5 dye, azo bond cleavage occurs, which leads to the formation of 2-((4-aminophenyl) sulfonyl) ethyl sulfate (ASES) and 3,4,6-triamino-5-hydroxynaphthalene-2,7-disulfonate (THD) [46, 47]. Oxalic acid (OA) can form from ASES, which in turn can be mineralized. The cleavage of the C-SO<sub>3</sub> bond of THD forms 3,6,8-triaminonaphthalen-1-ol (TAN). The investigation of the bonds leads to the formation of intermediates that do not have chromophoric groups and, therefore, are colorless. Since this molecule has several active sites can be stabilized faster than paracetamol and phenol, and therefore, its discoloration occurred faster [46, 47].

When paracetamol is attacked by the hydroxyl radical, 4-iminocyclohexa-2,5-dien-1-one (IDO) and 2-hydroxyacetic acid (HA) that are later mineralized (Figure 11B), [3, 48, 49].

Considering other studies in the literature, the phenol is susceptible to oxidation by hydroxyl radicals, forming the main intermediates benzoquinone (BQ) and/or hydroquinone

(HQ), the first step of its degradation. Subsequently, these intermediates break down to form ring-open carboxylic acids, and are mineralized to form  $\text{CO}_2$  and  $\text{H}_2\text{O}$  [3,48,49,50]. BQ and HQ, obtained from HPLC analysis, were formed from the photodegradation of phenol by the studied photocatalysts, (Figure 12).

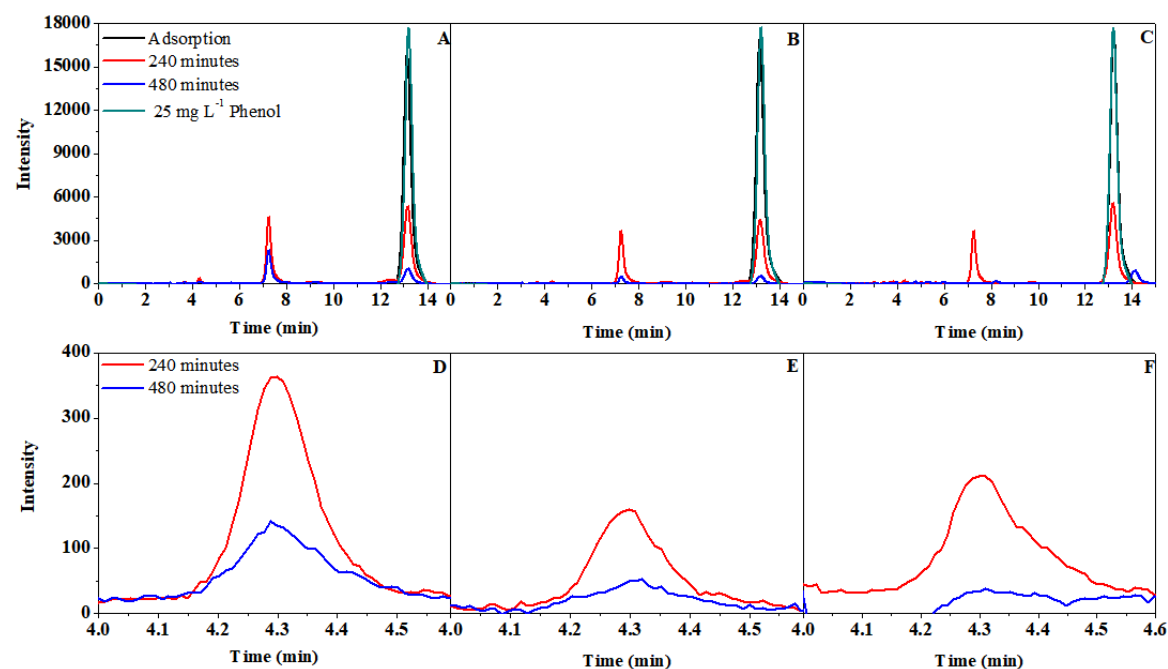


**Figure 12.** Chromatograms of the phenol solution after adsorption and 240 and 480 minutes of photocatalytic reaction using the photocatalysts A) 20Ti/C/Fe, B) 40Ti/C/Fe and C) 60Ti/C/Fe. Charts D, E and F show magnifications (between 4 and 4.6 minutes) of chromatograms A, B and C, respectively.

In all chromatograms, a signal is observed at 13 minutes, corresponding to phenol. The intensity of this signal decreases after adsorption and the 240 and 480 minutes reaction times, which confirms that phenol is being degraded during the photocatalytic reactions. In the chromatogram obtained after 240 minutes of reaction, two new signals located at 4.29 and 7.25 minutes appear (Figs. 12D-12F), which confirm the formation of the intermediates HQ and BQ, respectively, during phenol degradation [50,3,51]. After 480 minutes, the intensities of these signals decrease, confirming that in addition to phenol, the HQ and BQ intermediates are also being degraded by the radicals formed during the photocatalytic reactions. Signals at 7.25 minutes presented greater intensity than that at 4.29 min, which is related to a higher rate of HQ formation during the degradation of phenol [50, 51].

Table 4 presents the degradation data for phenol after adsorption and 240 and 480 minutes of photocatalytic reaction.

**Table 4.** Percentages of phenol degradation obtained based on the relative areas of the chromatograms (Fig. 12) during the reactions using the 20, 40 and 60Ti/C/Fe photocatalysts.

Photocatalyst	Adsorption (%)	Phenol degradation (%)	
		240 minutes	480 minutes
20Ti/C/Fe	10	70	95
40Ti/C/Fe	5	76	96
60Ti/C/Fe	4	69	98

These results show that the efficiency of the magnetic photocatalysts in degrading phenol increases with time and with the amount of TiO<sub>2</sub> present in the photocatalyst. These results corroborate those obtained by UV-vis and TOC analysis for degradation not only of phenol but also of RB5 and paracetamol.

Table 5 shows the catalytic efficiency and experimental conditions for different TiO<sub>2</sub> photocatalysts used to degrade the contaminants RB5, paracetamol and phenol found in the literature and for the materials prepared in the present study.

The photocatalysts presented in Table 5 showed efficiency between 71 to 99% degradation/discoloration of the BR5 dye. The photocatalyst 80Ti/C/RM (TiO<sub>2</sub> supported on the magnetic composite C/RM - reduced red mud coated with char) prepared by our research group [34] presented similar efficiency to the 20Ti/C/Fe prepared in this study. Other data presented in Table 5 are from studies of different authors that used very different experimental conditions, such as initial contaminant concentration, lamp power and type, catalyst mass, solution volume, reactor design, among others. Thus, it becomes difficult to make comparisons regarding the efficiency of these photocatalysts. However, it is noteworthy that practically all the photocatalysts presented in Table 5 have high efficiency to degrade the studied contaminants, where each one was submitted to favorable experimental conditions.

**Table 5.** Catalytic efficiency and experimental conditions of photocatalytic reactions performed for the degradation of RB5, paracetamol, and phenol using photocatalysts 20, 40 and 60Ti/C/Fe and other catalysts found in the literature.

Catalyst	Contaminant (concentration)	Light/power	Photocatalyst Efficiency (%)	Reaction time (min)	Ref.
20Ti/C/Fe	BR5 (40 ppm)	Hg/51 W	73	240	This study
40Ti/C/Fe			84	240	
60Ti/C/Fe			99	240	
80Ti/C/RM	BR5 (40 ppm)	Hg/15 W	71	240	[34]
MANP@TiO <sub>2</sub> MS	BR5 (25 ppm)	UV/300 W	98	90	[52]
20Ti/C/Fe	Paracetamol (30 ppm)	Hg/51 W	61	480	This study
40Ti/C/Fe			72	480	
60Ti/C/Fe			77	480	
TiO <sub>2</sub> (P25)	Paracetamol (50 ppm)	Hg/ 450W	99	90	[53]
50% TiO <sub>2</sub> /Fe <sub>2</sub> O <sub>3</sub>	Paracetamol (50 ppm)	Hg/ 450W	88	90	[53]
Ta-dopedTiO <sub>2</sub>	Paracetamol (35 ppm)	Hg/500 W	80	120	[54]
20Ti/C/Fe	Phenol (25 ppm)	Hg/51 W	74	480	This study
40Ti/C/Fe			86	480	
60Ti/C/Fe			90	480	
BioCl-TiO <sub>2</sub>	Phenol (50 ppm)	Xênon/300 W	43	360	[55]
N-doped TiO <sub>2</sub> anatase/rutile	Phenol (50 ppm)	UV/30 W	99	540	[56]
[FeII(dpbpy) (phen) <sub>2</sub> ]/TiO <sub>2</sub>	Phenol (10 ppm)	Xênon/300 W	97	180	[57]

### 3.4. Sedimentation kinetics and recovery and reuse of the magnetic photocatalysts

Figure 13 shows the sedimentation kinetics of TiO<sub>2</sub> and the photocatalysts in the presence of a magnet.

Figure 13 shows that only 6% of the pure TiO<sub>2</sub> deposited within 30 minutes. In contrast, the tests performed with the magnetic photocatalysts presented excellent results, where reductions of 89, 81 and 76% in the turbidity of the mixtures were observed within only 5 minutes when the 20, 40 and 60Ti/C/Fe photocatalysts were used, respectively.

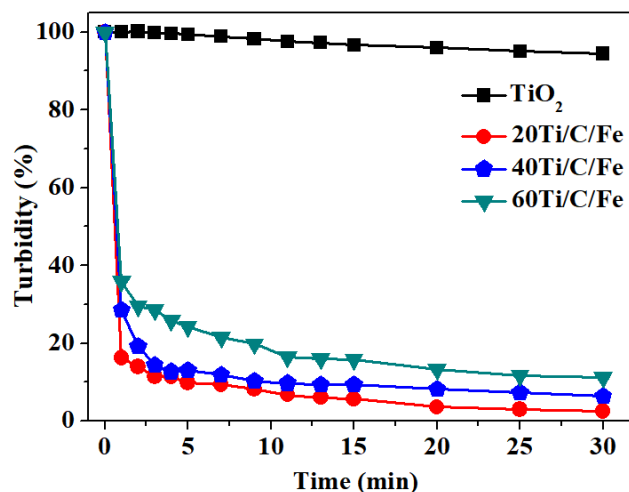


**Figure 13.** Sedimentation kinetics of TiO<sub>2</sub> and the magnetic photocatalysts.

These results corroborate those obtained by XRF and VSM, where the saturation magnetization increases and, consequently, the magnetic separation becomes more efficient with increasing iron content in the photocatalyst.

These results confirm the advantages of incorporating TiO<sub>2</sub> into materials with magnetic properties, which allows its rapid separation from treated effluent in the presence of a magnet.

Figure 14 shows the percentages of the photocatalyst recovery and the RB5 dye discoloration after four reaction cycles.

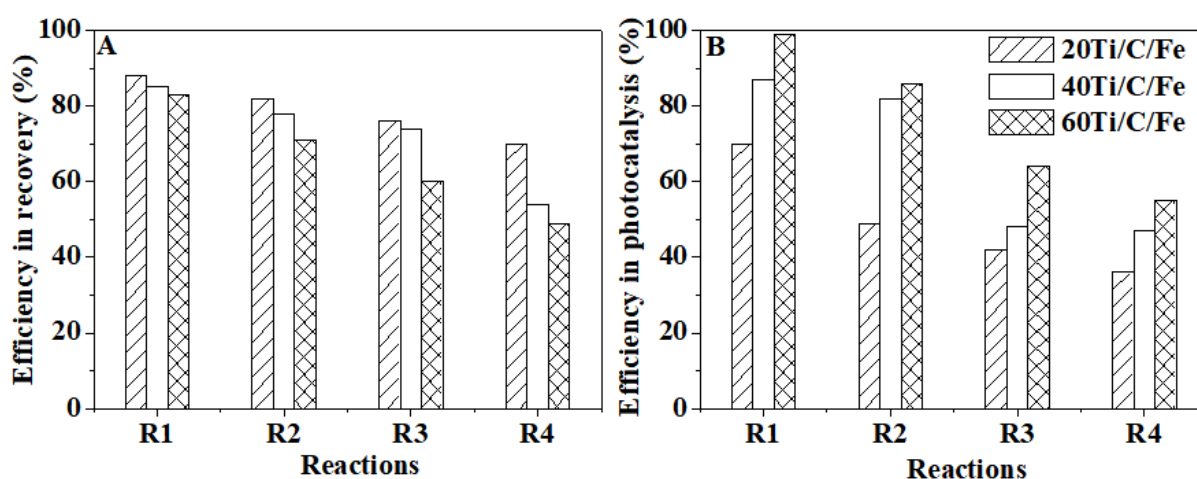


**Figure 14.** Recovery efficiency (A) and photocatalytic efficiency (B) of the magnetic photocatalysts in four photocatalysis reactions.

The photocatalytic recovery and activity decrease with the reuse number. Additionally, the photocatalysts with lower TiO<sub>2</sub> content, which have higher saturation magnetization, are recovered with higher efficiency. After the fourth reaction, 70, 54 and 49% of the 20, 40 and

60Ti/C/Fe photocatalysts, respectively, could be recovered. Regarding the photocatalytic activity, the 60Ti/C/Fe photocatalyst presented higher efficiency in all reuse reactions, and its activity decreased from 99 to 55% after the fourth reaction. However, the photocatalytic activity of the 60 and 40Ti/C/Fe photocatalysts showed a small reduction in reaction 2. These data show that despite the loss of material and photocatalytic efficiency in reuse, the magnetic photocatalysts show recovery and photocatalytic efficiency.

#### 4. Conclusion

The results of the magnetic photocatalyst characterizations proved the presence of TiO<sub>2</sub>, Fe<sub>3</sub>O<sub>4</sub>, Fe<sub>3</sub>C and charcoal, indicating that the photocatalysts could be efficiently obtained, and the saturation magnetization values confirmed the magnetic properties. The photocatalysts presented excellent photocatalytic efficiency in degrading and mineralizing the contaminants RB5, paracetamol and phenol. The sample with the highest amount of TiO<sub>2</sub>, 60Ti/C/Fe, showed the highest activity. The magnetic photocatalysts showed great efficiency in discoloring the dye RB5 during four successive cycles of recovery and reuse tests. The rapid and efficient separation from an aqueous medium and the possibility of reuse simplifies the effluent treatment process and implies reduced operational costs and waste generation, contributing to environmental preservation and sustainability. Thus, the photocatalysts prepared in this study have great potential for scale up and in solar photocatalysis application.

#### 5. Referências

1. M. Wu, L. Li, N. Liu, D. Wang, Y. Xue, L. Tang. Molybdenum disulfide (MoS<sub>2</sub>) as a co-catalyst for photocatalytic degradation of organic contaminants: A review. *Process Saf. Environ. Prot.* 118, (2018) 40–58. <https://doi.org/10.1016/j.psep.2018.06.025>.
2. M. Nadimi, A. Z. Saravani, M. A. Aroon, A. E. Pirbazari. Photodegradation of Methylene Blue by a ternary magnetic TiO<sub>2</sub>/Fe<sub>3</sub>O<sub>4</sub>/Graphene oxide nanocomposite under visible light. *Mater. Chem. Phys.* (2018) <https://doi.org/10.1016/j.matchemphys.2018.11.029>.
3. X. Yang, J. Guo, Z. Zhu, H. Zhang, T. Qi. Chinese Journal of Chemical Engineering Doping effects on the electro-degradation of phenol on doped titanium suboxide anodes. *Chinese J. Chem. Eng.* 26, (2018) 830–837. <https://doi.org/10.1016/j.cjche.2017.12.007>.
4. B. Szczepanik. Applied Clay Science Photocatalytic degradation of organic contaminants over clay-TiO<sub>2</sub> nanocomposites: A review. *Appl. Clay Sci.* 141, (2017) 227–239. <https://doi.org/10.1016/j.clay.2017.02.029>.
5. K. Choi, J. Min, S. Park, B. Joo, J. Jung. Enhanced photocatalytic degradation of trichlorophenol by Fe<sub>3</sub>O<sub>4</sub>@TiO<sub>2</sub>@Au photocatalyst under visible-light. *Ceram. Int.* (2018) 0–1. <https://doi.org/10.1016/j.ceramint.2018.09.104>.



6. S. Ahmed, M. G. Rasul, W. N. Martens, R. Brown, M. A. Hashib. Heterogeneous photocatalytic degradation of phenols in wastewater: A review on current status and developments. *Desalination*. 261, (2010) 3–18. <https://doi.org/10.1016/j.desal.2010.04.062>.
7. R. F. P. Nogueira, W. F. Jardim. A fotocatalise heterogênea e sua aplicação ambiental *Quim. Nova*. 21 (1998) 69–72. <http://dx.doi.org/10.1590/S0100-40421998000100011>.
8. A. Fujishima, T. N. Rao, D. A. Tryk. Titanium dioxide photocatalysis. *J. Photochem. Photobiol., C* 1, (2000) 1–21. [https://doi.org/10.1016/S1389-5567\(00\)00002-2](https://doi.org/10.1016/S1389-5567(00)00002-2)
9. X. Wei, H. Wang. Preparation of magnetic g-C<sub>3</sub>N<sub>4</sub>/Fe<sub>3</sub>O<sub>4</sub>/TiO<sub>2</sub> photocatalyst for visible light photocatalytic application. *J. Alloys Compd.* 763, (2018) 844–853. <https://doi.org/10.1016/j.jallcom.2018.06.031>.
10. A. Papi, G. Byzanski, L. Ruotolo. Photocatalytic Activity and RNO Dye Degradation of Nitrogen-doped TiO<sub>2</sub> Prepared by Ionothermal Synthesis. *Materials Research*. 20, (2017) 628–638. <http://dx.doi.org/10.1590/1980-5373-MR-2016-0837>
11. L. Shi, Y. He, X. Wang, Y. Hu. Recyclable photo-thermal conversion and purification systems via Fe<sub>3</sub>O<sub>4</sub>@TiO<sub>2</sub> nanoparticles. *Energy Convers. Manage.* 171, (2018) 272–278. <https://doi.org/10.1016/j.enconman.2018.05.106>.
12. P. Sun, R. Xue, W. Zhang, I. Zada, Q. Liu, J. Gu, H. Su, Z. Zhang, J. Zhang, D. Zhang. Photocatalyst of organic pollutants decomposition: TiO<sub>2</sub>/glass fiber cloth composites. *Catal. Today* 274, (2016) 2–7. <https://doi.org/10.1016/j.cattod.2016.04.036>.
13. X. Liu, Y. Liu, S. Lu, W. Guo, B. Xi. Performance and mechanism into TiO<sub>2</sub>/Zeolite composites for sulfadiazine adsorption and photodegradation. *Chem. Eng. J.* 350, (2018) 131–147. <https://doi.org/10.1016/j.cej.2018.05.141>.
14. W. Zhang, Y. Li, C. Wang, P. Wang. Kinetics of heterogeneous photocatalytic degradation of rhodamine B by TiO<sub>2</sub>-coated activated carbon: Roles of TiO<sub>2</sub> content and light intensity. *Desalination*. 266, (2011) 40–45. <https://doi.org/10.1016/j.desal.2010.07.066>.
15. Y. Ide, Y. Koike, M. Ogawa. Journal of Colloid and Interface Science Molecular selective photocatalysis by TiO<sub>2</sub>/nanoporous silica core / shell particulates. *J. Colloid Interface Sci.* 358, (2011) 245–251. <https://doi.org/10.1016/j.jcis.2011.02.018>.
16. N. Neghi, M. Kumar, D. Burkhalov. Synthesis and application of stable, reusable TiO<sub>2</sub> polymeric composites for photocatalytic removal of metronidazole. *Chem. Eng. J.* 326, (2017) 29–36. <https://doi.org/10.1016/j.cej.2017.05.087>.
17. A. Manassero, M. L. Satuf, O. M. Alfano. Photocatalytic reactors with suspended and immobilized 2: Comparative efficiency evaluation. *Chem. Eng. J.* 326, (2017) 29–36. <https://doi.org/10.1016/j.cej.2017.05.087>.
18. W. Li, H. Wu. Sodium citrate functionalized reusable Fe<sub>3</sub>O<sub>4</sub>@TiO<sub>2</sub> photocatalyst for water purification. *Chem. Phys. Lett.* 686, (2017) 178–182. <https://doi.org/10.1016/j.cplett.2017.08.046>.
19. M. Li, B. Lu, Q. Ke, Y. Guo, Y. Guo. Synergetic effect between adsorption and photodegradation on nanostructured TiO<sub>2</sub>/activated carbon fiber felt porous composites for

- toluene removal. *J. Hazard. Mater.* 333, (2017) 88–98. <https://doi.org/10.1016/j.jhazmat.2017.03.019>.
20. D. Maučec, A. Šuligoj, A. Ristić, G. Dražić, A. Pintar, N. N. Tušar. Titania versus zinc oxide nanoparticles on mesoporous silica supports as photocatalysts for removal of dyes from wastewater at neutral pH. *Catal. Today.* 310, (2018) 32–41. <https://doi.org/10.1016/j.cattod.2017.05.061>.
21. N. S. Kovalevskiy, M. N. Lyulyukin, D. S. Selishchev, D. V Kozlov. Analysis of air photocatalytic purification using a total hazard index: Effect of the composite TiO<sub>2</sub>/zeolite photocatalyst. *J. Hazard. Mater.* 358, (2018) 302–309. <https://doi.org/10.1016/j.jhazmat.2018.06.035>.
22. J. Krýsa, M. Baudys, X. Vislocka, M. Neumann-spallart. Composite photocatalysts based on TiO<sub>2</sub> – carbon for air pollutant removal: Aspects of adsorption. *Catal.Today*, (2018) <https://doi.org/10.1016/j.cattod.2018.09.027>.
23. Q. Li, K. Ma, Z. Ma, Q. Wei, J. Liu, S. Cui, Z. Nie. Microporous and Mesoporous Materials Preparation and enhanced photocatalytic performance of a novel photocatalyst: Hollow network Fe<sub>3</sub>O<sub>4</sub>/mesoporous SiO<sub>2</sub>/TiO<sub>2</sub> (FST) composite microspheres. *Microporous Mesoporous Mater.* 265, (2018) 18–25. <https://doi.org/10.1016/j.micromeso.2017.12.012>.
24. P. Jana, V. Fierro, A. Celzard. Ultralow cost reticulated carbon foams from household cleaning pad wastes. *Carbon.* 62, (2013) 510–520.
25. M. Lezanska, Pietrzyk, A. Dudek, J. Wtoch. Nitration and reduction route to surface groups of mesoporous carbons obtained from sucrose and phloroglucinol/formaldehyde precursor. *Mater. Chem. Phys.*, 149-150 (2015) 539-552.
26. J. C. Tristão, F. G. Mendonça, R. M. Lago, J. D. Ardisson. Controlled formation of reactive Fe particles dispersed in a carbon matrix active for the oxidation of aqueous contaminants with H<sub>2</sub>O<sub>2</sub>. *Environ. Sci. Pollut. Res.* 22, (2015) 856–863. <https://doi.org/10.1007/s11356-014-2554-z>.
27. I. M. Arabatzis, S. Antonaraki, T. Stergiopoulos, A. Hiskia, E. Papaconstantinou, M. C. Bernard, P. Falaras. Preparation, characterization and photocatalytic activity of nanocrystalline thin film TiO<sub>2</sub> catalysts towards 3,5-dichlorophenol degradation. *J. Photochem. Photobiol. A Chem.* 149, (2002) 237–245. [https://doi.org/10.1016/S1010-6030\(01\)00645-1](https://doi.org/10.1016/S1010-6030(01)00645-1).
28. X. Wang, P. Zhang, J. Gao, X. Chen, H. Yang. Facile synthesis and magnetic properties of Fe<sub>3</sub>C/C nanoparticles via a sol-gel process. *Dye. Pigment.* 112, (2015) 305–310. <https://doi.org/10.1016/j.dyepig.2014.07.021>.
29. C. C. Amorim, M. M. D. Leão, P. R. Dutra, J. C. Tristão, F. Magalhães, R. M. Lago. Chemosphere Use of tar pitch as a binding and reductant of BFD waste to produce reactive materials for environmental applications. *Chemosphere* 109, (2014) 143–149. <https://doi.org/10.1016/j.chemosphere.2014.01.067>.
30. F. Magalhães, M. C. Pereira, J. D. Fabris, S. E. C. Bottrel, M. T. C. Sansiviero, A. Amaya, N. Tancredi, R. M. Lago. Novel highly reactive and regenerable carbon/iron composites prepared from tar and hematite for the reduction of Cr(VI) contaminant. *J. Hazard. Mater.*

- 165, (2009) 1016–1022. <https://doi.org/10.1016/j.jhazmat.2008.10.087>.
31. E. Filippo, A. L. Capodilupo, C. Carlucci, P. Perulli, F. Conciauro, G. A. Corrente, B. F. Scremin, G. Gigli, G. Ciccarella. Efficient, Green Non-Aqueous Microwave-Assisted Synthesis of Anatase TiO<sub>2</sub> and Pt Loaded TiO<sub>2</sub> Nanorods with High Photocatalytic Performance. *Nanomater. Nanotechnol.* 5, (2015) 31. <https://doi.org/10.5772/61147>.
  32. Y. Li, Y. Cai, X. Chen, X. Pan, M. Yang, Z. Yi. Photocatalytic oxidation of small molecule hydrocarbons over Pt/TiO<sub>2</sub> nanocatalysts. *RSC Adv.* 6, (2016) 2760–2767. <https://doi.org/10.1039/c5ra22459d>.
  33. J. Wang, G. Wang, S. Miao, X. Jiang, J. Li, X. Bao. Synthesis of Fe/Fe<sub>3</sub>C nanoparticles encapsulated in nitrogen-doped carbon with single-source molecular precursor for the oxygen reduction reaction. *Carbon.* 75, (2014) 381–389. <https://doi.org/10.1016/j.carbon.2014.04.017>.
  34. L. D. O. Pereira, S. G. De Moura, G. C. M. Coelho, L. C. A. Oliveira, E. T. De Almeida, F. Magalhães. Journal of Environmental Chemical Engineering Magnetic photocatalysts from industrial residues and TiO<sub>2</sub> for the degradation of organic contaminants. *J. Environ. Chem. Eng.* 7, (2019) 102826. <https://doi.org/10.1016/j.jece.2018.102826>.
  35. T. Phongamwong, W. Donphai, P. Prasitchoke, C. Rameshan, N. Barrabés, W. Klysubun, G. Rupprechter, M. Chareonpanich. Novel visible-light-sensitized Chl-Mg/P25 catalysts for photocatalytic degradation of rhodamine B. *Appl. Catal. B Environ.* 207, (2017) 326–334. <https://doi.org/10.1016/j.apcatb.2017.02.042>.
  36. F. Magalhães, M. C. Pereira, J. D. Fabris, S. E. C. Bottrel, M. T. C. Sansiviero, A. Amaya, N. Tancredi, R. M. Lago. Novel highly reactive and regenerable carbon/iron composites prepared from tar and hematite for the reduction of Cr (VI) contaminant. *J. Hazard. Mater.* 165, (2009) 1016–1022. <https://doi.org/10.1016/j.jhazmat.2008.10.087>.
  37. L. N. Paula, L. A. R. Giusto, R. C. R.s Filho, L. R. Castilho, F. Magalhães. Modificação e caracterização do resíduo pó de aciaria elétrica (PAE) para aplicação em reações de redução de cromo (VI). *Quim. Nova.* 36, (2013) 1332–1337.
  38. M. Thommes, K. Kaneko, A. V Neimark, J. P. Olivier, F. Rodriguez-reinoso, J. Rouquerol, K. S. W. Sing. Physisorption of gases, with special reference to the evaluation of surface area and pore size distribution (IUPAC Technical Report). *Pure Appl. Chem.* 87, (2015) 1051–1069. <https://doi.org/10.1515/pac-2014-1117>.
  39. M. A. Fitri, M. Ota, Y. Hirota, Y. Uchida, K. Hara. Fabrication of TiO<sub>2</sub>-graphene photocatalyst by direct chemical vapor deposition and its anti-fouling property. *Mater. Chem. Phys.* 198, (2017) 42–48. <https://doi.org/10.1016/j.matchemphys.2017.05.053>.
  40. A. C. Martins, A. L. Cazetta, O. Pezoti, J. R. B. Souza, T. Zhang. Sol-gel synthesis of new TiO<sub>2</sub>/activated carbon photocatalyst and its application for degradation of tetracycline. *Ceram. Int.* 43, (2017) 4411–4418. <https://doi.org/10.1016/j.ceramint.2016.12.088>.
  42. A. Habibi-yangjeh, M. Mousavi, K. Nakata. Journal of Photochemistry & Photobiology A: Chemistry Boosting visible-light photocatalytic performance of g-C<sub>3</sub>N<sub>4</sub>/Fe<sub>3</sub>O<sub>4</sub> anchored with CoMoO<sub>4</sub> nanoparticles: Novel magnetically recoverable photocatalysts. *J. Photochem. Photobiol. A Chem.* 368, (2019) 120–136. <https://doi.org/10.1016/j.jphotochem.2018.09.026>.

43. G. Adolfo, L. Martinez. Síntese de nanopartículas magnéticas com elevada magnetização de saturação e estabilidade química. (2013)
44. J. Puentes-cárdenas, A. Florido-cuellar, J. Cardona-bedoya, P. Bohorquez-echeverry. Simultaneous decolorization and detoxification of black reactive 5 using TiO<sub>2</sub> deposited over borosilicate glass. *Univ. Sci.* 17, (2012) 53–63. <https://doi.org/10.11144/Javeriana.SC17-1.sdad>.
45. E. Moctezuma, E. Leyva, C. A. Aguilar, R. A. Luna, C. Montalvo. Photocatalytic degradation of paracetamol : Intermediates and total reaction mechanism. *J. Hazard. Mater.* 243, (2012) 130–138. <https://doi.org/10.1016/j.jhazmat.2012.10.010>.
46. M. Bilal, T. Rasheed, M. N. Iqbal, H. Hu, W. Wang. Toxicological Assessment and UV/TiO<sub>2</sub> -Based Induced Degradation Profile of Reactive Black 5 Dye. *Environ. Manage.* 61, (2018) 171–180. <https://doi.org/10.1007/s00267-017-0948-7>.
47. M. El Bouraie, W. S. El Din. Biodegradation of Reactive Black 5 by *Aeromonas hydrophila* strain isolated from dye-contaminated textile wastewater. *Sustain. Environ. Res.* 26, (2016) 209–216. <https://doi.org/10.1016/j.serj.2016.04.014>.
48. N. Rosman, W. N. W. Salleh, A. F. Ismail, J. Jaafar, Z. Harun, F. Aziz, M. A. Mohamed, B. Ohtani, M. Takashima. Photocatalytic degradation of phenol over visible light active ZnO/Ag<sub>2</sub>CO<sub>3</sub>/Ag<sub>2</sub>O nanocomposites heterojunction. *J. Photochem. Photobiol., A.* 364, (2018) 602–612. <https://doi.org/10.1016/j.jphotochem.2018.06.029>.
49. H. Wang, J. Chu, H. Ou, R. Zhao, J. Han. Analysis of TiO<sub>2</sub> photocatalysis in a pulsed discharge system for phenol degradation. *J. Electrostat.* 67, (2009) 886–889. <https://doi.org/10.1016/j.elstat.2009.07.008>.
50. H. Li, J. Ji, C. Cheng, K. Liang. Journal of Physics and Chemistry of Solids Preparation of phenol-formaldehyde resin-coupled TiO<sub>2</sub> and study of photocatalytic activity during phenol degradation under sunlight. *J. Phys. Chem. Solids* 122, (2018) 25–30. <https://doi.org/10.1016/j.jpics.2018.06.012>.
51. A. M. Al-hamdi, M. Sillanpää, T. Bora, J. Dutta. Applied Surface Science Efficient photocatalytic degradation of phenol in aqueous solution by SnO<sub>2</sub>: Sb nanoparticles. *Appl. Surf. Sci.* 370, (2016) 229–236. <https://doi.org/10.1016/j.apsusc.2016.02.123>.
52. K. O. Hamaloglu, E. Sag, A. Bilir, A. Tuncel. Monodisperse-porous titania microspheres and their gold decorated forms as new photocatalysts for dye degradation in batch fashion. *Mater. Chem. Phys.* 207, (2018) 359–366. <https://doi.org/10.1016/j.matchemphys.2017.12.065>.
53. T. F. O, A. Abdel-wahab, A. Al-shirbini, O. Mohamed, O. Nasr. Journal of Photochemistry and Photobiology A : Chemistry Photocatalytic degradation of paracetamol over magnetic flower-like. "Journal Photochem. Photobiol. A Chem. 347, (2017) 186–198. <https://doi.org/10.1016/j.jphotochem.2017.07.030>.
54. L. Rimoldi, D. Meroni, E. Falletta, A. Maria, A. Gervasini, G. Cappelletti, S. Ardizzone. Applied Surface Science The role played by different TiO<sub>2</sub> features on the photocatalytic degradation of paracetamol. *Appl. Surf. Sci.* 424, (2017) 198–205. <https://doi.org/10.1016/j.apsusc.2017.03.033>.
55. D. Sánchez-rodríguez, M. Guadalupe, M. Medrano, H. Remita, V. Escobar-barrios. Journal

- of Environmental Chemical Engineering Photocatalytic properties of BiOCl-TiO<sub>2</sub> composites for phenol photodegradation. *J. Environ. Chem. Eng.* 6, (2018) 1601–1612. <https://doi.org/10.1016/j.jece.2018.01.061>.
56. M. Azuwa, W. N. W. Salleh, J. Jaafar, A. F. Ismail. Photodegradation of phenol by N-Doped TiO<sub>2</sub> anatase/rutile nanorods assembled microsphere under UV and visible light irradiation. *Mater. Chem. Phys.* 162, (2015) 113–123. <https://doi.org/10.1016/j.matchemphys.2015.05.033>.
57. X. Wang, Y. Sun, L. Yang, Q. Shang, D. Wang, T. Guo, Y. Guo. Science of the Total Environment Novel photocatalytic system Fe-complex/TiO<sub>2</sub> for efficient degradation of phenol and norfl oxacin in water. 656, (2019) 1010–1020. <https://doi.org/10.1016/j.scitotenv.2018.11.419>.